UNIVERSITY OF CAPE TOWN

FACULTY OF ENGINEERING AND BUILT ENVIRONMENT

Department of Civil Engineering

An Investigation into the Effects of Asperities on Geomembrane/Geotextile Interface Shear Characteristics

Author: Adeleke Daniel
Supervisor: A/Prof. Denis Kalumba
Co-supervisor: Lita Nolutshungu
Co-supervisor: Johnny Oriokot

A thesis submitted in partial fulfilment of the requirement for the award of the degree of Master of Science in Civil Engineering Specializing in Geotechnical Engineering at the University of Cape Town

[June 2020]

PLAGIARISM DECLARATION

1. Plagiarism is to use another's work and to pretend that it is one's own. I know that plagiarism is wrong.

2. I have used the Harvard convention for citation and referencing. Each significant contribution to and quotation in this report from the work or works of the other people have been attributed and has been cited and referenced.

3. This report is my own work.

4. I have not allowed and will not allow anyone to copy my work with the intention of passing it off as his or her own work.

Signature: Signed by candidate Date: 10th June 2020

Student Name: Adeleke Daniel

DEDICATION

TO

My mum, Mrs Ayo Adeleke, siblings, Oluwasegun, and Damilola Adeleke.

Above all, my heavenly Father, GOD ALMIGHTY and my Lord JESUS CHRIST; my surest foundation.

ACKNOWLEDGEMENTS

This research was made possible not by one individual, but a community of supporters and well-wishers. First and foremost, I am grateful to my supervisor; A/Prof. Denis Kalumba, and co-supervisors; Lita Nolutshungu and Johnny Oriokot. They provided the environment needed to dream new ideas and to innovate in the laboratory. Also, their knowledge, guidance, and positive criticism were essential to the completion of this work.

I acknowledge the robust financial support from the MasterCard Scholarship Foundation at the University of Cape Town (UCT) towards this Master's degree. Special gratitude to Ms Carol Ojwang, Mr Xolani Mboka, Mr Riyaadh Fakier, Ms Insaaf Isaacs, and Mrs Jean Alfeld.

Furthermore, I would like to thank the Geosynthetic Institute (GSI) for accepting me into the institute's fellowship based on this research and the problem it addresses. Much appreciation goes to Ms Jamie R. Koerner for allocating funds to support this study.

On the technical side, I am grateful to Mr Hardie and Mr Oriokot of AKS Lining Systems (Pty) Ltd, and Fibertex South Africa (Pty) Ltd, respectively, as they wilfully donated and transported the geosynthetics materials used in this work to the UCT Geotechnical Laboratory.

Also, special acknowledgement goes to A/Prof. Alejandro Martinez and Mr Justin Talkington of the University of California Davis, USA for offering to assist with the geomembrane surface roughness measurements. Their interest and enthusiasm for this research are highly appreciated.

The laboratory testing carried out in this work would have been deprived of technical support if the assistance of Mr Noor Hassen, Mr Tahir Mukaddam, Mr Charles Nicholas, Mr Elvino Witbooi, Mr Christopher, and Mr Swayiza Masimthembe, of the Civil Engineering laboratory, were withdrawn. A special thanks to you for the continuous support.

My experience at UCT would be incomplete without my colleagues. Much appreciation to Charles Sikwanda, Monica Damane, Shade Muluti, Jason Venter, Mapekula Lunga, Dr Laxmee Sobhee-Beetul, and Faridah Chebet, for every captured moment during my stay.

Finally, my gratitude goes to my family, relatives, friends, acquittances and the Redeemed Christian Fellowship (RCF) as well as the Redeemed Christian Church of God (RCCG) Latter House Parish for their support and encouragement during my stay in Cape Town.

ABSTRACT

Geomembranes are often utilized as fluid barriers in geotechnical applications such as landfills. Due to their relative impermeability and chemical resistance characteristics, they are usually used alongside other geosynthetics like geotextiles in landfills to constitute base, side-slope, and cover liner systems. Uniquely, within the side-slope liner composite system, which consists of multiple geosynthetics interfaces, the geomembrane/geotextile (GMB/GTX) interface is known to have relatively low shear strength. In an effort to mitigate sliding failure occurrence at the GMB/GTX interface, asperities have been incorporated into GMB manufacturing to increase the shear characteristics. Presently, many GMB with various asperities properties is now available because of asperities proven advantage. Challengingly, only a few studies have substantiated and quantified the importance of varying asperities properties (height, density, and shape) on the GMB/GTX interface. Therefore, this study was aimed at investigating the effects of asperities variation on GMB/GTX interface shear characteristics and mechanism, as well as to identify the asperity parameters combination which optimizes the GMB/GTX interface shear strength.

The GMB/GTX interface shear tests were conducted according to ASTM D5321, under saturated conditions with the "305 mm by 305 mm" direct shear box at applied normal stresses; 25 kPa to 400 kPa. In this research, the two common geotextile polymers (polypropylene and polyester) in South Africa were used at the GMB/GTX interface. Also, the geomembranes used had their asperity height varied from 0 mm to 2.02 mm, while the asperity density and shape were varied from 0 to 663 spikes per 10000 mm^2, and conical to hook-cone asperity shape, respectively.

GMB/GTX interface shear results showed that with a 70 % increase in the geomembrane asperity height at constant asperity density, friction angle increased by 25 %. Also, an average increase of 25 % in the friction angle was observed as asperity density was doubled at constant asperity height. However, the friction angle was not significantly affected by changes in asperity shape from conical to "hook-cone" shape. Therefore, among identified asperities and roughness features, asperity height together with surface roughness affect the GMB/GTX interface shear parameter more dominantly. These outcomes present a better explanation of the "fibre/asperity" interaction at the GMB/GTX interface and identified asperity properties which optimised surface interaction. The optimised interaction produces efficient shear mechanism that would ultimately lead to a stable and durable landfill liner system.

RESEARCH OUTPUT

Different sections of the study described in this thesis have been published or presently been reviewed as listed in the following articles.

Adeleke, D; Kalumba, D; Nolutshungu, L; & Oriokot, J. 2021. Laboratory investigation of asperity concentration effects on geomembrane/geotextile interface shear characteristics. Abstract accepted for the 20th International Conference on Soil Mechanics and Geotechnical Engineering, Sydney 2021.

Adeleke, D; Kalumba, D; Nolutshungu, L; Oriokot, J.; & Martinez, A. 2021. The influence of asperities and surface roughness on geomembrane/geotextile interface friction angle. Under review to be submitted to the International Journal of Geosynthetics and Ground Engineering.

Adeleke, D; Kalumba, D; & Hardie, P. 2019a. Effects of asperities on the geotextile-geomembrane interface shear characteristics. In 13th Australia New Zealand Conference on Geomechanics. H.E. Acosta-Martínez & B.M. Lehane, Eds. Perth, Western Australia: Australian Geomechanics Society. pp 699–703.

Adeleke, D; Kalumba, D; & Oriokot, J. 2019b. Asperities effect on polypropylene & polyester geotextile-geomembrane interface shear behaviour. In E3S Web of Conferences. V. 92. 5. DOI: 10.1051/e3sconf/20199213017.

TABLE OF CONTENTS

LIST OF FIGURES

LIST OF TABLES

LIST OF EQUATIONS

NOTATIONS AND ABBREVIATIONS

The abbreviations used in this dissertation were standard acronyms recommended by the International Geosynthetics Society (IGS). All abbreviations and symbol used in the text are listed below with their respective meaning. More so, S.I units convention were used to represent quantities of known dimensions.

Symbols

A_v	Asperity volume
H:h	General and hazardous waste landfills
H:H	Hazardous waste landfills
R	Line roughness
S	Surface roughness
a, q, s, and z	Average, root-mean-square, surface and maximum roughness subscript
S_x	Asperity spacing in the assumed horizontal axis
S_y	Asperity spacing in the assumed vertical axis
δ	Interface friction angle
c_a	Apparent adhesion

Abbreviations

3D	Three-dimensional
ABS	Acrylonitrile butadiene styrene
ASTM	American Society of Testing and Materials
CAB	Cellulose acetate butyrate
CBR	California bearing ratio
CCL	Compacted clay liners
CoR	Coefficient of regression
CSPE	Chlorosulphonated polyethylene
DWAF	Department of water affairs and forestry
FoS	Factor of safety
GCD	Geo-composite drains

GCE	Geocells
GCL	Geosynthetic clay liners
GFO	Geofoam
GGR	Geogrids
GMB	Geomembranes
GMB-S	Smooth geomembranes
GMB-T	Textured geomembranes
GNT	Geonets
GPP	Geopipes
GSY	Geosynthetics materials
GTX	Geotextiles
GTX - PET	Polyester geotextile
GTX - PP	Polypropylene geotextile
HDPE	High-density polyethylene
IRD	Initial rate of disposition
LD	Large displacement
LEM	Limit equilibrium method
LLDPE	Linear low-density polyethylene
LVDT	Linear vertical displacement transducer
NP	Needle-punched
NPNW	Needle-punched nonwoven
MD	Machine direction
MRD	Maximum rate of disposition
PA	Polyamide
PB	Polybutylene
PD	Percentage difference
PE	Polyethylene
PET	Polyester
PP	Polypropylene

PVC	Polyvinylchloride
RMS	Root-mean-square
SANS	South African National Standard
SDR	Shear displacement rate
SEM	Scanning electron microscope
UV	Ultraviolet
VFPE	Very flexible polyethylene
VLDPE	Very low-density polyethylene
XMD	Cross-machine direction

Units

°	Degree
"	Inches
°C	Celsius degree
cm	Centimetre
cm/sec	Centimetre per second
g/cm	Gram per centimetre
g/cc	Gram per cubic centimetre
g/m^2	Gram per unit area
hr	Hour
kg or g	Kilograms or grams
kN	Kilonewtons
kN/m^2	Kilonewtons/ per unit area
kN/m^3	Kilonewtons/ per unit area
kPa	Kilopascals
Ibs	Pounds
mm^3/mm^2	Cubic millimetres per unit area
mm^2	Square millimetres
mm	Millimetres

m	Metres
min	Minutes
m/s	Metre per second
mm/min	Millimetres per minutes
N	Newtons
s	Seconds
sec^{-1}	Per second
T	Tonnes
T/day	Tonnes per day

1. INTRODUCTION

1.1. Background of study

According to DWAF (1998a), landfills are a cost-effective, ancient, and efficient method of disposing of waste in developing countries. With strict regulations in place, landfills are designed and built to accommodate the highest possible waste within a given area with minimal environmental contamination. The high level of quality control required in landfill operations has triggered the extensive use of selected materials' technical advantages. For instance, materials used in landfills should have superior hydraulic performance, physical properties, mechanical characteristics, and easy installation procedure. (McCartney *et al*., 2009).

Over the years, a significant challenge in landfills design and management is leachate build-up (i.e. collected liquid at the bottom of a landfill). Historically, leachates in landfills were prevented from percolating to the groundwater layer by a compacted clay liner (CCL). An observed setback to this over time is the quick formation of cracks in the CCL layer, especially during thermal contraction (Karademir, 2011). Since soil has a thermal coefficient of contraction, which is three times higher than that of steel, as reported by Karademir (2011), the continuous crack formation in clays would eventually lead to groundwater contamination from leachate seepage. In order to mitigate contamination and environment risk, geosynthetics such as geomembranes (GMB) were introduced as a relatively impermeable layer and barrier to prevent further pollution of groundwater and acts as a critical components of modern landfill designs and containment system (Bhatia & Kasturi, 1996; Orebowale, 2006).

Geosynthetics (GSY) are planar products manufactured from "polymeric" material and are used with soil, rock, or other geotechnical engineering-related material as an integral part of a human-made project and structure (Zornberg and Christopher, 2007). Common examples of geosynthetics include geotextiles (GTXs), geomembranes (GMBs), geogrids (GGRs), geosynthetic clay liners (GCLs), geonets (GNTs), geocells (GCEs), geocomposite drains (GCDs), geofoam (GFOs) and geopipes (GPPs). Furthermore, due to their vast applications in groundwater control and containment system, geosynthetics have a vibrant and growing market.

Geomembranes, which are polymeric sheets with low hydraulic conductivity, find utilisations as vertical, horizontal, and inclined barrier systems in projects involving groundwater remediation

and control, and waste containment. There are two general categories of geomembranes based on their manufacturing processes; these are calendered and extruded. Also, as regards to polymer classification; different types of geomembranes have been manufactured. However, according to Zornberg & Christopher (2007), high-density polyethylene (HDPE) geomembrane, due to its high tensile properties and low strain levels is the most widely used geomembranes in landfill applications. Likewise, geotextiles are porous engineered textile materials that are an integral component of landfills liners. Their utilization in the separation, filtration, drainage, protection and reinforcement functions is partly due to their relative fibre smoothness. For instance, in landfills, GTX act as a protection layer for GMB against aggressive puncture and abrasion (Bacas *et al*., 2011). There are three main classes of geotextile, namely, nonwoven, woven and knitted geotextile.

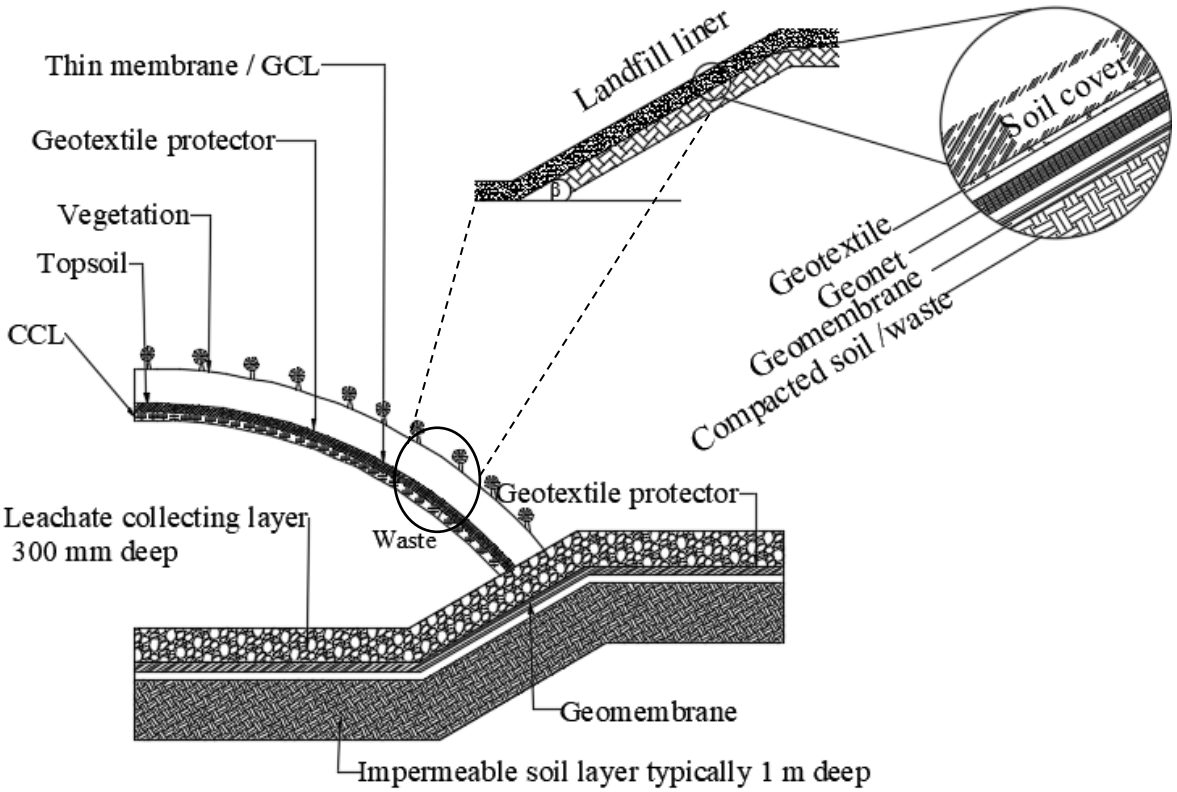

Figure 1-1: Typical cross-section of the base, side-slope and cover liner system in landfill systems (after Textile Center of Excellence, 2019)

An integral part of landfills design is the liner system, and they are usually made up of a series of elements, as shown in Figure 1-1. Generally, the class of a proposed landfill determines the type, number, and sequence of liner components required (DWAF, 1998a). For instance, single and double composite liner systems are used for municipal solid waste containment and

hazardous waste landfills, respectively, and they have liner constituent consisting of different geosynthetics and soil layers. Largely, landfill liners are categorized into basal, side-slope and capping liner system, where the basal and side-slope liners are in direct contact with the earth at the foundation of the landfill while capping liners are installed during the closure phase of the landfill (Zornberg & Christopher, 2007).

1.2. Problem statement

The stability of waste containment facilities is dependent on the liner system interactions between the geosynthetics and soil layer, particularly at the side-slope. At times, interaction at the interface could be of low shear strength, as was the case with the Kettleman Hills landfill, where shear stresses generated from static or dynamic loads and waste decomposition, became insufficient (Byrne, 1992). Eventually, the low shear stress resulted in sliding failure that caused groundwater contamination, air pollution, and adverse health effects. Therefore, an accurate shear strength characterization for possible interfaces present in the side-slope liner is a condition for durable design (Walsh *et al*., 2009; Bacas *et al*., 2011). In a typical landfill liner, possible single geosynthetics interface include GMB/GCL, GCL/CCL, GMB/GTX, and GTX/GCD (Bhatia & Kasturi, 1996). However, studies by Bergado *et al.*, (2006), Xuede (2008), and Bacas *et al*., (2015b) identified GMB/GTX interface as an interface with lower frictional resistance and shear strength (i.e. "critical interface"). Thus, this critical interface was the focus of this study.

The interaction between smooth GMB and other geomaterials such as geotextiles often produced low shear strength for landfill designers. Moreover, in response to increasing the shear resistance at the smooth GMB interfaces, geosynthetics manufacturers have occasioned to the inclusion of texturing/asperities to the GMB surfaces. As a result, textured geomembranes have asperities of diverse shapes, density, and height. However, an investigation into the different asperities effects on the GMB/GTX interface shear resistance has not been fully studied. As only a few studies by Yesiller (2005), Adesokan & Blond (2018), and Robbe-Valloire *et al.*, (2018) researched the influence of asperity height on the GMB/GTX interface, while only limited studies by Fowmes *et al.*, (2017) and Zaharescu (2018) investigated asperity density and shape. Therefore, this study was undertaken to contribute to the understanding of the GMB/GTX interface shear responses as asperity parameters were varied.

1.3. Research objectives

The main aim of the study was to investigate the influence of different GMB asperity properties on the GMB/GTX interface shear characteristics. In order to accomplish this, several objectives were established. These included the following:

- To evaluate the relationship between geomembrane asperity height and GMB/GTX interface shear parameters.
- To evaluate the effect of asperity density on GMB/GTX interface shear characteristics.
- To evaluate the influence of asperity shape and volume on the GMB/GTX failure envelope.
- To describe/ evaluate GMB surface roughness and its effects on the GMB/GTX interface shear mechanism.

1.4. Scope and limitations of research

This thesis focused only on the experimental investigation of asperities effects on GMB/GTX interface shear characteristics, although other numerous geosynthetics interfaces are present in landfill liners. At the GMB/GTX interface, only HDPE geomembrane and non-woven geotextiles (polypropylene and polyester) were examined. Also, the considered GMB had asperity height ranging from 0.0 mm to 2.02 mm and asperity density ranging from 0 to 663 spikes per 10000 mm^2. Furthermore, the direct shear device used in this research had dimension, maximum shear displacement, and maximum applied stress of "305 mm x 305 mm", 75 mm, and 450 kPa, respectively. Thus, larger dimensions, displacement and applied stress were not considered. Also, as at the time this work, only geosynthetics specimen available from manufacturers were used, simply because the random variation of GMB asperity parameters for academic purposes involve severe technical and economic consequences.

1.5. Thesis overview

Chapter One introduced the research topic followed by background information. Also, the problems of concern and the identified gaps were stated, which provided the motivation for conducting this study. The relevant literature on previous studies and other areas of importance concerning the research-topic were presented in Chapter Two. Chapter Three detailed the experimental procedures for the large direct shear, geosynthetics specification, asperities

measurement and classification, as well as sample preparation. Chapter Four presented and discussed the result of the different asperities parameters on the geomembrane/geotextile interface shear behaviour and concluded with the research findings. Lastly, in the Fifth Chapter, research conclusions were extracted from the main findings, and future research recommendations were given.

2. LITERATURE REVIEW

2.1. Introduction

This chapter presents a review of studies that focused on geosynthetics interface shear characteristics and controlling factors. It begins with the assessment of solid waste management, landfilling, and typical landfill components. This is followed by a brief introduction into geosynthetics and their application in landfill liners, particularly geomembranes and geotextile. Also, the physical properties of geomembranes such as asperities, roughness, and thickness, and shear equipment as well as interface testing conditionings in previous researches, were examined. Lastly, at the end of the chapter, a summary of the discussion of the findings was presented.

2.2. Solid waste and waste management

Solid waste refers to solid unwanted material which does not have immediate use at the point of generation (Chandrappa & Bhusan Das, 2012). Moreover, if improperly handled, solid waste can adversely affect and pollute the environment, hence, the need for waste management. According to Fronti (1994), solid waste management consist of five primary components; namely generation, storage, collection, transportation, and disposal.

The generation of waste is the phase where unwanted substances are discarded. The phase characterised by the temporary retention/storage of the discarded item storage phase is termed "storage". Afterwards, accumulated wastes are obtained from different sources and mobilized to a disposal site (Fronti, 1994). The final phase of solid waste management is waste disposal.

Over the years, methods ranging from burning to dumping into the sea have been developed for effective solid waste disposal operations. However, according to Fronti (1994), four methods which are burying (landfilling), composting, burning (incineration), and recycling has been frequently utilized as waste disposal techniques in developing countries. Although all four methods are commonly applied, landfilling is undoubtedly a more popular solution for solid waste disposal in these countries (Fronti, 1994).

2.3. Landfills

Typically, landfills are designated site allotted by environmental agencies for the disposition of waste on land directly or in excavations as shown in Figure 2-1 (Berardino, 2017). Over the

years, landfilling is credited to be the most economical and convenient form of waste disposal, as a result, in South Africa and globally, over 95 % and 85 % of the generated waste, respectively, are disposed of in landfills (DWAF, 1998a). Traditionally, with emphasis on disposal methods, design, and operations, landfills are classified into an open dump, basic landfill, engineered landfill, and bioreactor landfill. In this study, engineered landfills were focussed on, as they protect the environment with the use of geosynthetics, which is in contrast, to open dumps and basic landfills. Whereas concerning bioreactor landfills, their applications are mainly in industrial gas production, decomposition and microbiological activities (Berardino, 2017).

Figure 2-1: Designated area of waste disposal (Romano Disposal Services, 2018)

2.3.1. Types of engineered landfills

Engineered landfills, according to DWAF (1998b), are characterized based on the recognized inherent qualities such as the type of generated waste, the waste stream size, the type and quantity of leachate produced.

2.3.1.1 Classification of engineered landfills based on the waste type

DWAF (1998b), grouped wastes into two categories, namely general and hazardous wastes. General waste, due to their composition, does not pose a significant danger to the environment and can be disposed of on any permitted landfill. Whereas, even in low concentrations, hazardous waste can only be disposed at designated sites, as they pose dangers to the environment and its inhabitants. Examples of general wastes include domestic, commercial, industrial and construction rubble. While organic, inorganic, and oily wastes are examples of hazardous wastes.

Hazardous wastes' degree of toxicity is dependent on its inherent chemical characteristics, which in turn determines the amount of treatment needed and disposal requirements. According to SANS 10228 (2012), all hazardous waste are clustered into nine classes depending on the assigned hazard rating. Hazard rating value ranges from 1 to 4, where 1 and 4 represent a high hazard and low hazard scenarios, respectively. Therefore, all landfills are classified into two types according to the waste's designed hazard rating. These are H: H landfills and H:h landfills; where H: H landfills accept all hazardous waste and H:h landfills can only accept general and low hazardous waste (DWAF, 1998b).

2.3.1.2 Classification of engineered landfills based on the waste stream

The design of a landfill according to physical size is mostly dependent on the amount of waste expected to flow into the landfill during its operational life. Landfill operational size is reliant on the daily rate of waste deposition and the size of the population served. This classification focuses on the waste stream size, operation, and maintenance requirement. Landfills are classified based on the estimated "Maximum Rate of Deposition (MRD)" (DWAF, 1998b). MRD can be calculated from the initial rate of deposition (IRD) as shown in Equation 2-1.

$$\mathrm{MRD} = (\mathrm{IRD})((1 + \mathrm{d})^{\mathrm{t}})$$

Equation 2-1

where IRD = initial rate of deposition of refuse on-site in T/day

d = forecasted annual development rate based on population growth rate in the area served by the landfill

t = years since deposition started at IRD

MRD = maximum rate of waste deposition after t years, expressed in tonnes per day

Table 2-1: Landfill class sizes (DWAF, 1998b)

Landfill size categories	Maximum rate of deposition (MRD) (Tonnes per day)
Communal, C	C < 25
Small, S	25 < S < 150
Medium, M	150 < M < 500
Large, L	L > 500

Depending on the calculated MRD value, waste landfills are divided into four categories, as shown in Table 2-1, namely; communal, small, medium, and large categories. Where MRD falls within a range, it is recommended to select a class based on the maximum value.

2.3.1.3 Classification of engineered landfills based on significant-leachate generation potential

According to DWAF (1998a), landfills can be classified based on the capacity to generate significant leachate and the need for leachate management. Although most landfills can potentially generate periodic leachate in extremely wet weather conditions, the installation of leachate management systems such as underlines drains and removal systems, are only landfill design requirements when there is the possibility for significant leachate generation that could adversely affect the environment. This classification system identifies the potential for leachate generation and subsequently recommend the leachate collection and treatment system. The landfill leachate generation potential is dependent on the site water-balance, where water-balance is directly related to rainfall, evaporation, waste moisture content and water flow into the waste body.

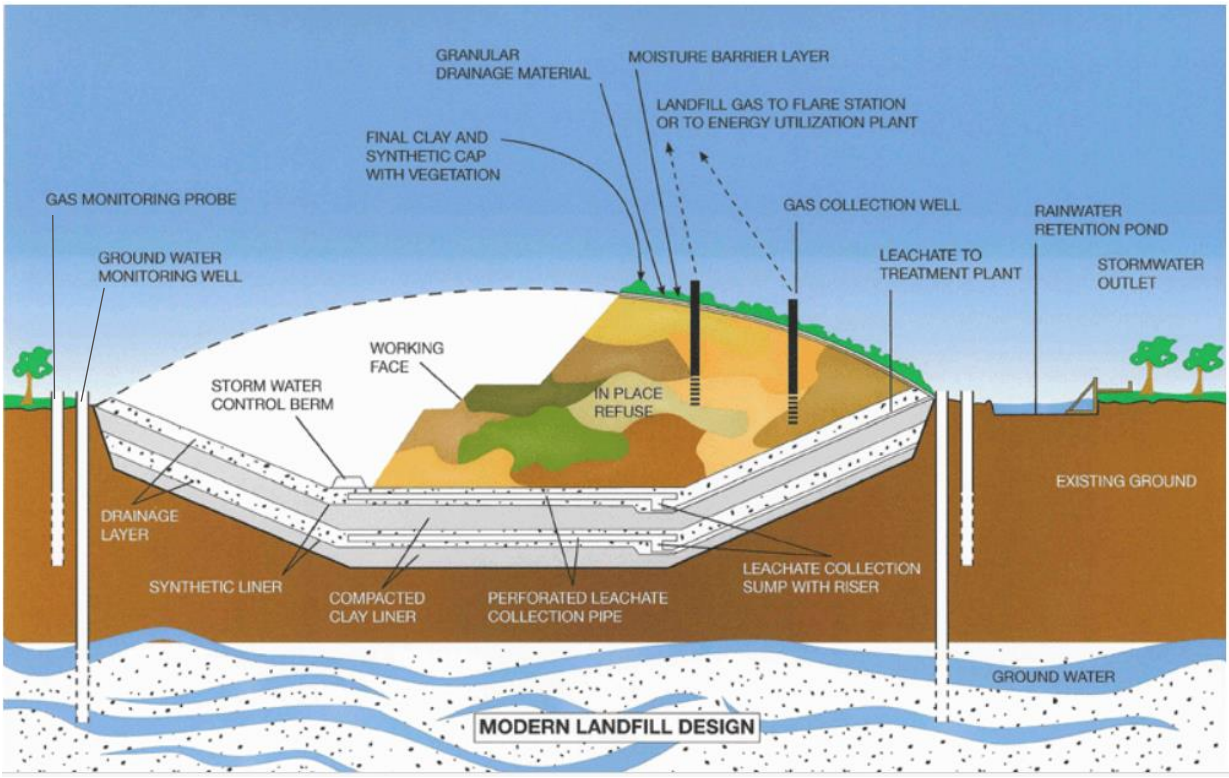

Figure 2-2: Typical components of modern landfill design (CSIR, 2000)

2.3.2. Typical landfill component

According to Oriokot (2018), conceptual and technical phases are the two-part of any landfill design process. During the conceptual design phase, the geometric design and other planning are executed. While the technical design, which is based on the conceptual design, includes detailed specifications of materials, measurement and procedures, as well as complete drawings of the systems required for the landfill to be functional (DWAF, 1998a). As illustrated in Figure 2-2, functional landfills, among other components, consist of the following; leak detection and collection system, leachate treatment plants, surface water drainage, groundwater monitoring well, geocomposite drainage layer, landfill gas monitoring probe, gas collection and extraction system, compacted clay layer, basal and side liner system, capping liner system and liner anchor trench. Geosynthetics find application in many landfill components, especially, at the basal, side slope and capping liner system (Ross, 2009). This literature review focused on the application of geosynthetics at the landfill liner system, as some landfill failures have occurred as a result of the low interfacial strength at the liner.

2.3.3. Landfill liner

Landfill liner is a layer of natural or synthetic materials with low permeability, situated in waste containment facilities to prevent environmental contamination. Traditionally, before the discovery and use of geosynthetics, landfill liners consisted of compacted soil or clay layers. Currently, geosynthetics, because of their hybrid and superior qualities, have found application in landfills at basal, side-slope, and capping liner, as illustrated in Figure 2-3. In this review, because of the tendency to slide, liner system application was focused on the side-slope liner.

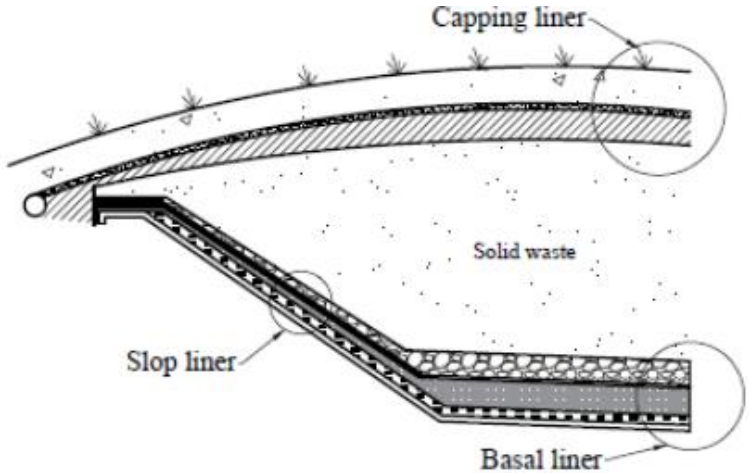

Figure 2-3: Three-component of an engineered landfill liner system (after Oriokot, 2018)

Landfill liners can either consist of single or composite liners, in which geosynthetics and soil are placed above or below waste materials. The single and composite liner consists of a one-layer barrier system and multiple layer barrier systems, respectively (Chrysovergis, 2012). Historically, liner systems were composed of single liner systems of compacted clay. Whereas, modern liner systems use composite liners that consist of compacted clay liner (CCL) overlaid with geosynthetics such as geosynthetics clay liner (GCL), geomembranes (GMB), and geocomposite drain (GCD). Also, landfill liner composition is dependent on the accommodated waste-type, i.e. general or hazardous waste, project-specific conditions and country's environmental agencies. Thus, general waste and hazardous waste landfills contain different liner system. For instance, Figure 2-4 shows a typical hazardous and general waste basal liner system, according to the DWAF (1998b).

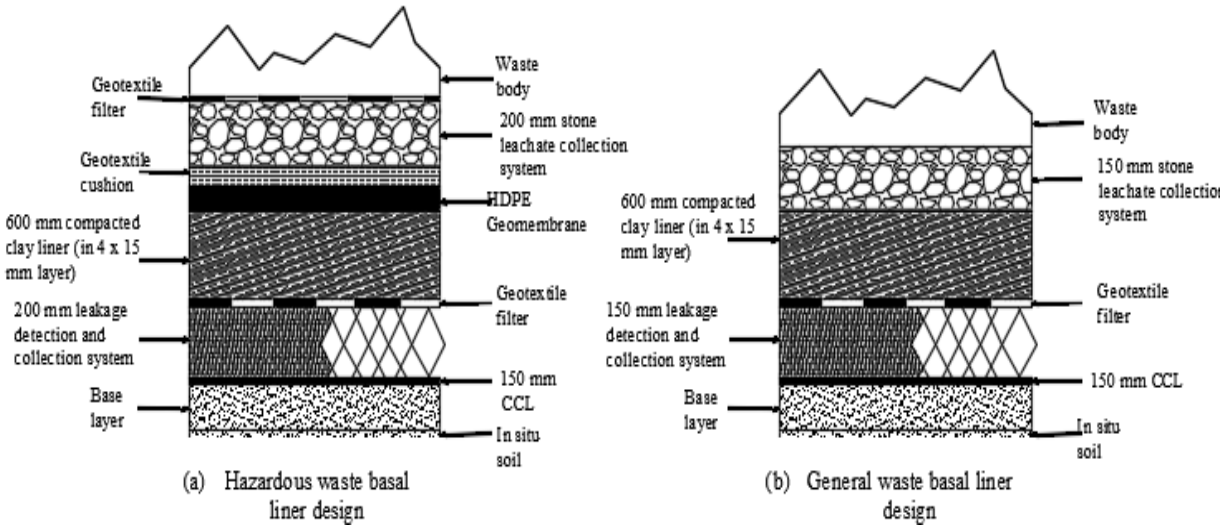

Figure 2-4: Landfill baseliner system for (a) hazardous waste (b) General waste (after DWAF, 1998b)

2.4. Geosynthetics

Geosynthetic consists of two syllabi; explicitly geo- and -synthetics, where “geo” represents earth, ground or soil, and “synthetics” represent chemically manufactured products that model natural behaviour/characteristics (Oriokot, 2018). According to ASTM D4439 (2018), geosynthetics are a planar product manufactured from polymers, where polymers are substance with molecular structure built-up from chemically bonded numerous smaller and similar units (monomers). Examples of polymers are polyamide (PA), polyethylene (PE), polypropylene (PP), polyester (PET), polyvinyl chloride (PVC), polybutylene (PB), acrylonitrile butadiene styrene

(ABS), cellulose acetate butyrate (CAB), and Chlorosulphonated polyethylene (CSPE) (Oriokot, 2014; Buthelezi, 2017).

According to the Textile Center of Excellence (2019), geosynthetics are classified into permeable and impermeable geosynthetics. Permeable geosynthetics are geotextiles and, geotextile-related products such as geo-mesh, geonets, geocells, geogrids, geo-pipes, geofoams, whereas impermeable geosynthetics comprise of geomembranes and geosynthetics clay liner (GCLs). Also, the properties and functions of geosynthetics vary considerably due to the employed manufacturing technique and additives (Zornberg & Christopher, 2007). Common examples of additives include stabilizers, antioxidants, carbon black, pigment, plasticisers and fillers.

2.4.1. Geosynthetics functions

According to Robert *et al.*, (2005), geosynthetics primary functions includes separation, filtration, drainage, barrier, protection, and reinforcement function, as well as surface erosion control and marine function. However, this review focused on functions like barrier and protection where geomembrane asperities have significant effects.

Liquid barrier layer – Geosynthetics, as shown in Figure 2-5, can act as a relatively impermeable membrane to prevent gases and leachate from percolating into the environment over the estimated service life of the structure (Shukla & Yin, 2006; Chrysovergis, 2012). The surface characteristics (asperities) of the geosynthetics can increase the interaction between the geosynthetics, as well as the stability of the slope.

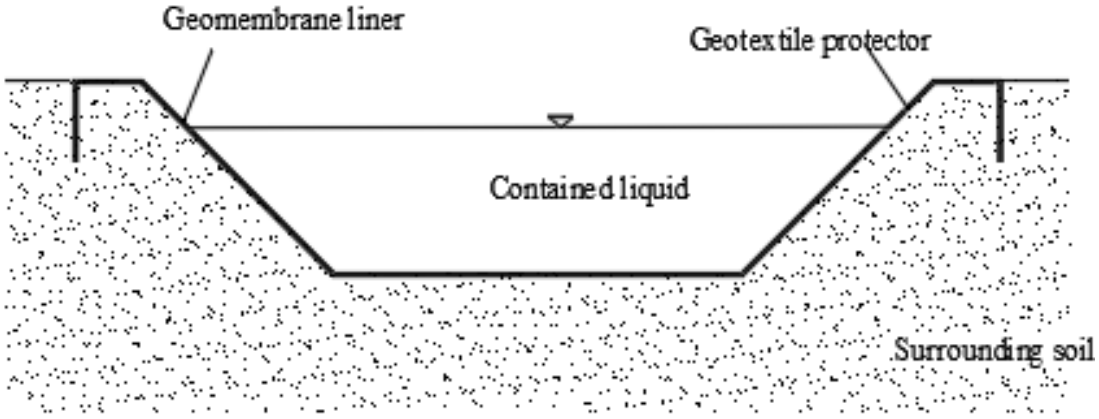

Figure 2-5: Geosynthetics liquid-barrier function (after the Textile Center of Excellence, 2019)

Protection layer – In landfill applications, geosynthetics placed before or above materials can perform a protective function as it reduces or distributes stresses and strains transmitted to the protected material (see Figure 2-6). This action helps to minimize the damage potential of the

geotechnical system (Shukla & Yin, 2006). For instance, in landfills, geotextiles due to its high puncture resistance and easy installation find application as a protection layer for HDPE geomembrane liner on side slopes (Sikwanda, 2018).

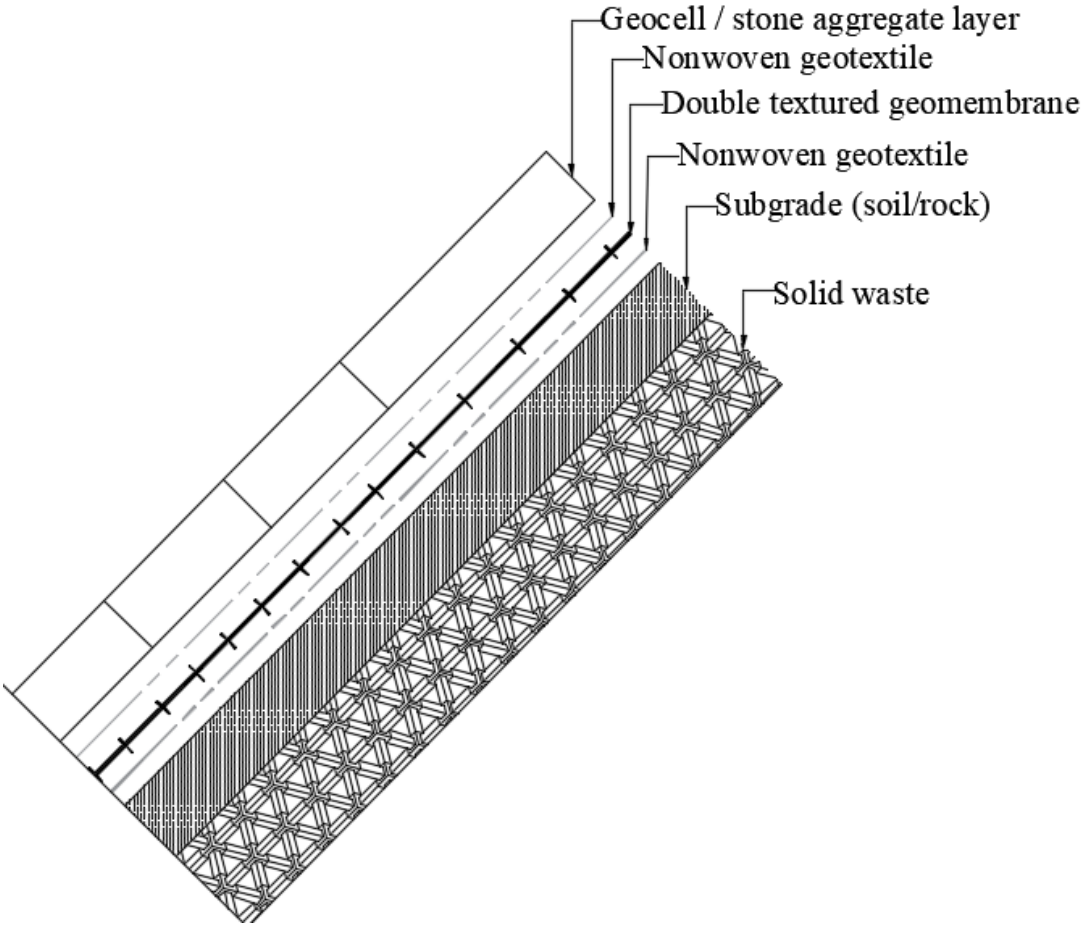

Figure 2-6: Protection layer function of geosynthetics (after Foye, 2011)

Besides the primary functions which characterize the mentioned geosynthetics, they sometimes possess additional secondary function(s) (Zornberg & Christopher, 2007). For instance, geotextiles (GTXs) whose primary function is "protection" can perform an extra function as a drainage layer.

2.4.2. Geotextiles

Geotextiles are permeable engineered textile materials placed within or near a structure to improve its performance (ASTM D4439, 2018). Manufacturing of geotextiles is centred on five principal fibre types, namely monofilament, multifilament, staple fibre yarn, slit film monofilament and slit-film multifilament. In the production process, these fibres are manufactured into fabrics which include woven, nonwoven, stitched or knitted as illustrated in

Figure 2-7 below. Woven geotextiles are produced by interlacing two or more sets of fibres, filament, and tapes at right angles. They find usage in applications involving fine particles.

Figure 2-7: Basic fabric manufacturing choices (a) Woven monofilament, calendered (b) Woven multifilament, (c) Woven slit (split) film (d) Nonwoven needle punched, (e) Nonwoven heat bonded (All images have a magnification of X30) (Koerner, 2005)

Nonwoven geotextiles are sheet manufactured from oriented staple filaments, which were mechanically, thermally or chemically bonded into a flexible web. They can vary in thickness and pigmentation, as shown in Figure 2-8 below. According to Oriokot (2018), nonwoven geotextiles account for approximately 80 % of geotextiles applications in geotechnical engineering, as they are appropriate options for geo-structures laid with granular materials. Also, in scenarios requiring higher strength, nonwoven geotextiles are more preferred as they exhibit more ductile responses in comparison to woven types (Karademir, 2011).

Figure 2-8: Typical non-woven geotextile with varying thickness and pigmentation

Knitted geotextiles are produced by interloping one or more fibres or filaments. Also, stitch-bonded geotextiles, as the name implies, are formed by stitching fibres or yarns together (Nanak, 2012).

2.4.3. Geomembranes

Geomembranes are geosynthetics with substantially low permeability (10^{-11} to 10^{-12} cm/sec) whose properties depend on the polymer composition and manufacturing technique (ASTM D4439, 2018). In engineering applications, geomembranes are used in different projects such as mining (e.g. liners for tailing dam), and landfills (e.g. water, liquid and gas containment barriers). Depending on the polymer used in production, geomembranes are divided into different

categories, namely; CSPE, CPE, PP, PVC, HDPE, LDPE, and VFPE geomembranes. However, recent landfills projects in Southern African have mostly utilized HDPE because of its high chemical resistance, long-term durability, and high strength (Hardie, 2018). On the contrary, HDPE possesses weak puncture resistance, a high thermal expansivity and high-stress cracking, which must be considered in its usage (Sikwanda, 2018).

HDPE geomembranes may have a smooth or textured finish, as illustrated in Figure 2-9. Notably, both geomembranes have been used in different applications requiring low permeability, high chemical and ultraviolet resistance. The main difference between them is that smooth geomembrane is more applicable in level grounds where frictional resistance is not required, whereas textured geomembranes are more suitable for high shear strength application. Irrespective of usage, geomembranes should have a minimum thickness of 0.75 mm; however, to facilitate welding in field scenarios, HDPE geomembranes should have at least 1.5 mm thickness (Zaharescu, 2018).

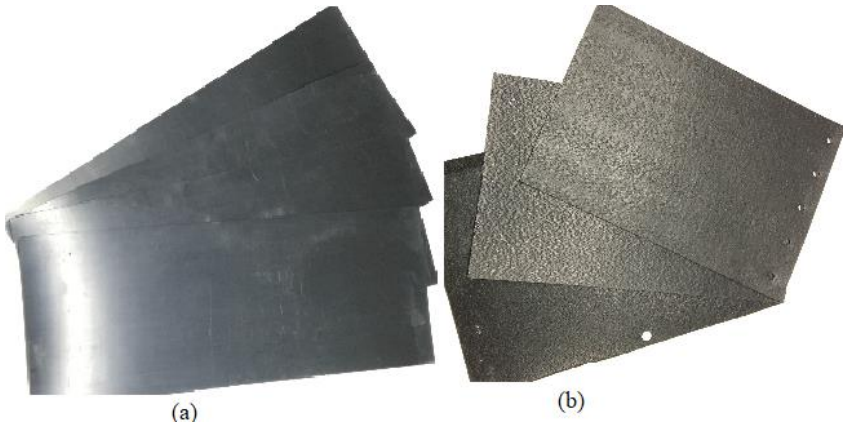

Figure 2-9: Geomembranes surface view (a) Smooth; (b) Micro-textured; blown film

Textured geomembrane manufacturing is an intricate process that begins with the production of polymers and ends with the finished geomembranes sheets transported to site (Zaharescu, 2018). There are two categories of geomembranes based on the manufacturing processes in South Africa; namely, calendered and extruded geomembranes.

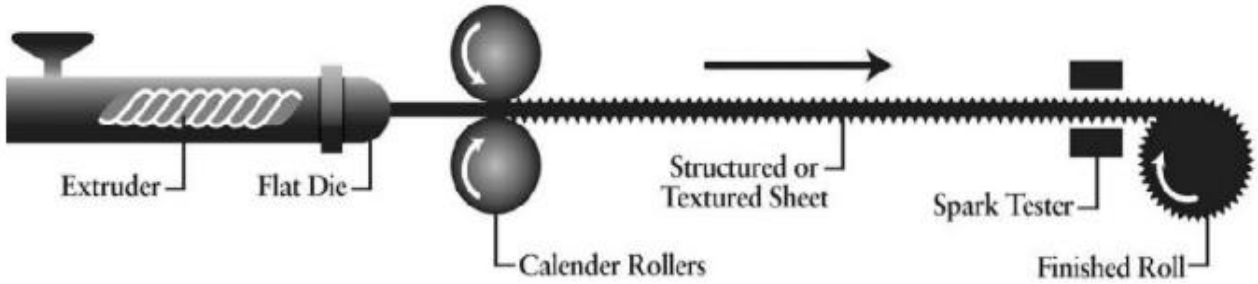

Figure 2-10: Schematic of calendered geomembrane manufacturing process (AGRU, 2020)

Calendered geomembranes are formed by working and flattening a hot/molten viscous formulation between two counter-rotating rollers immediately after exiting the die lips, as shown in Figure 2-10. The properties of the resulting membrane sheet are dependent on the characteristics of the roller (see Figure 2-11).

Figure 2-11: Calendered geomembrane textured products

Extruded geomembranes are manufactured by melting a polymer resin, or chips, and forcing the molten polymer through a die using a screw extruder. The process of extrusion is facilitated by applying molten extrudate together with nitrogen gas (blowing or foaming agent) through a small extruder (see Figure 2-12). The textured surface is created as the nitrogen gas expands and opens towards the cooling extrudate product surface. This process creates a rough surface with varying and smaller asperity height, alteration in thickness, non-uniform area coverage, and small stress crack resistance, therefore, its application could be limited (Zaharescu, 2018).

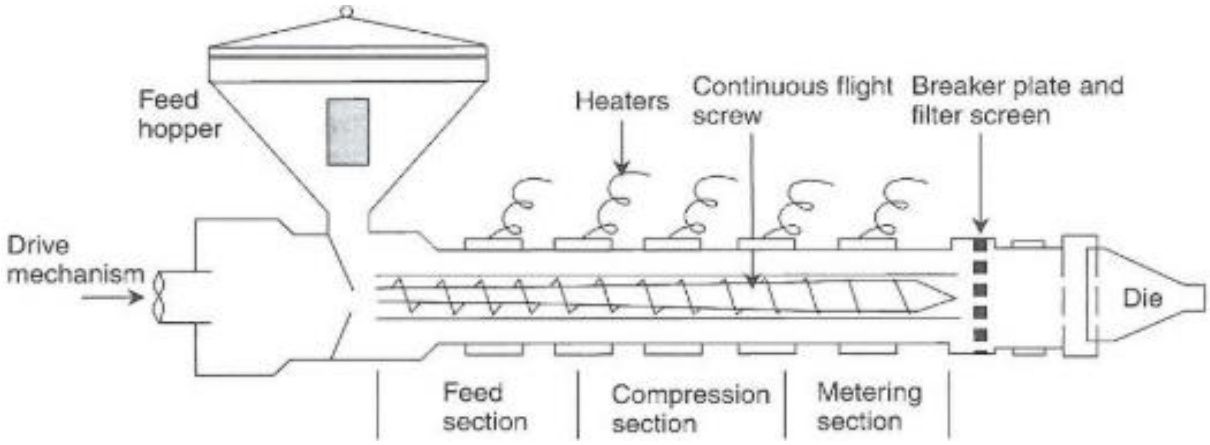

Figure 2-12: Schematic of "flat die extruded" geomembrane manufacturing process (Jeon & Kim, 2018)

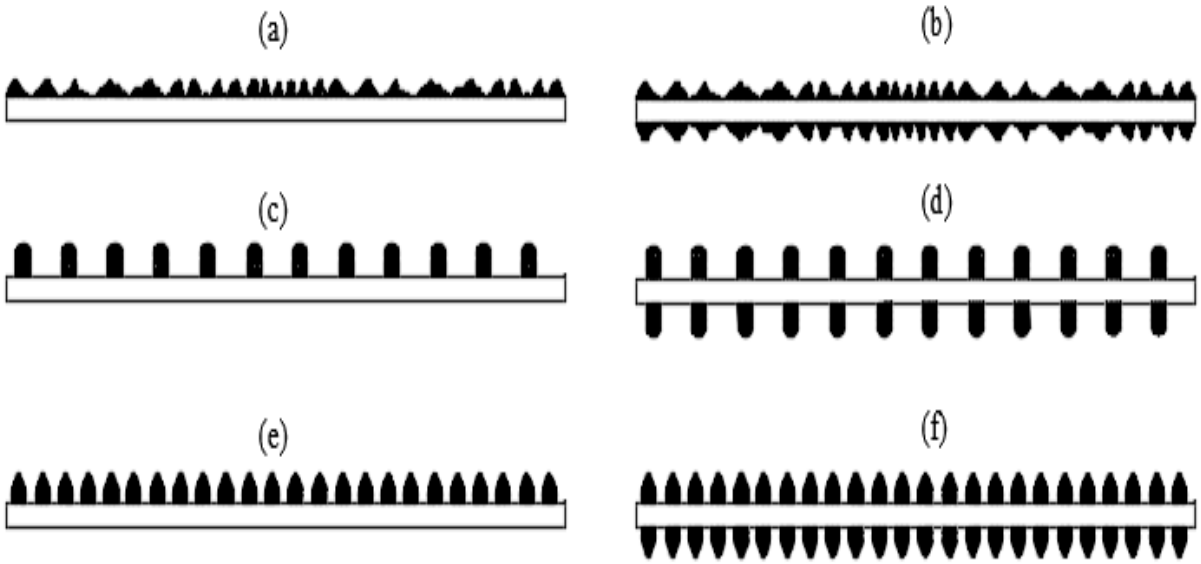

Figure 2-13: Sectional view of geomembrane surfaces; (a) Flat-die extruded mono-textured (b) Flat-die extruded double-textured (c & e) Calendered mono-textured (d &f) Calendered double-textured

Textured geomembranes, either mono-textured or double-textured (see Figure 2-13 a-f), allow higher fibre interaction between the adjacent materials and produces improved interface strength. Figure 2-13 a & b are products of the flat-die extrusion manufacturing process, while Figure 2-13 c - f represent products fabricated using the calendering manufacturing process. It is important to note that the calendering process can produce membrane sheets with different asperity height, shape and spacing, as shown in Figure 2-13 c & e. Each of the different geomembrane types has different interfacial shear as well as mechanical and durability properties when interfaced against another geomaterial. Thus, in order to ensure the safe and stable design of geomembranes as a composite system in conjunction with other geosynthetic materials, it is important to characterize the surface properties which inturn affects engineering behaviour and developed interface shear mechanism (Karademir, 2011). These, among other vital reasons, have necessitated the need to investigate the influence of geomembrane surface properties variation on the resulting interface strength (Blond & Elie, 2006)

2.5. Geosynthetics interface in landfill liner system

The placement of geosynthetics with similar or dissimilar properties adjacent to each other in a landfill liner often results in a zone of interaction. This zone of interaction is called an “interface”. During the service life of landfills, there is a high probability of relative displacement occurring at the interface. The mode and rate of displacement at the interface are primarily influenced by

the presence and degree of discontinuities, and the surrounding conditions (stress). Also, the order of geosynthetics placement in a landfill liner affects the relative displacement at the interface. For instance, the interface and the corresponding interface movement would be different for various landfill classes as well as single and double composite liner systems (Karademir, 2011).

Most innovative applications of geosynthetics have been attributed to geosynthetics composite systems; this is because they result in an advantageous combination with better physical, mechanical, and hydraulic properties than "individual" geosynthetics solutions (Karademir, 2011). Often, because of the resulting low shear strength at a weak interface, interactions between geosynthetics in field applications can develop a slip surface rapidly at the weak interface. Thus, among other significant factors, the critical interface is a significant determinant in defining the liner system strength and overall geo-structure stability (Karademir, 2011). For instance, from studies by Bergado *et al*., (2006), Xuede (2008), and Bacas *et al*., (2015b) on weak interface identification, the shear interactions between geotextiles, geomembranes, GCLs and sands were identified to be of low interfaces shear strength.

Studies by Hebeler *et al.*, (2005), Orebowale (2006), Rawal and Saraswat (2011), and Bacas *et al*., (2015a) indicated that the mechanical surface properties such as surface roughness and hardness of the counter-face materials often influence the shear characteristics available at the weak interface, and possibly reduce the potential for sliding failure occurrence. Therefore, it is necessary to thoroughly examine the properties of the materials at the weakest interface that could affect the interface shear stress-displacement response (Dove & Frost, 1999).

2.5.1. Critical and non-critical landfill liner interface

Interface shear strength of the geosynthetics alongside the slope and height of waste containment facilities can influence the stability of multiple layer landfill lining systems (Bergado *et al*., 2006). The term used to describe the interface liner degree of stability is "criticality", meaning that some interfaces are more critical than others. For instance, of the numerous identified non-hazardous and hazardous landfills project located at Sa Kaeo Province, Thailand, interfaces between smooth geomembrane/geotextile, a geomembrane/GCL, and smooth geomembrane/CCL were identified as critical interfaces. The friction angle at these critical interfaces ranges from 6.5° to 9.5°and 6.5° to 10.5° for wet and dry conditions, respectively

(Bergado *et al*., 2006). Also, from the series of geosynthetics interface shear tests that have been conducted at the Geotechnical Engineering Laboratory of the University of Cape Town, geomembrane/geotextile, and geomembrane/GCL interfaces have been considered to have low shear strength, with 19° and 11° friction angle, respectively. Similarly, according to Hsuan & Koerner (1998), Xuede (2008) and Bacas *et al*., (2015a), the interface created through the incorporation of geomembrane material into geotextile was discovered to generate a potential plane of weakness within the system along which failure occurred. Therefore, critical interfaces such as geomembrane/geotextile interface are interfaces where the friction angle is low; hence, this interface is described in the next section.

2.5.2. Geomembrane/geotextile interface

Studies by Mitchell *et al*., (1990), Fox & Thielmann (2014) and Lajevardi *et al*., (2018) have indicated that the geomembrane/geotextile (GMB/GTX) interaction is of crucial concern in geosynthetics application. In practical applications, two scenarios of GMB/GTX interface exist. The first is the geotextile immediately above a geomembrane liner serving as a protection layer, while the other is a geomembrane layer above a geotextile surface in a GCL. The category of geotextile in recurring use is the non-woven geotextile, while the HDPE geomembrane is one of the three predominantly utilized geomembranes in engineering applications (Chrysovergis, 2012).

Non-woven geotextiles are characterized by porous and fibrous materials that are randomly oriented along their filaments and often acts as a discrete material. The fibrous materials usually vary in terms of spatial distribution, curvature, orientation, size, and mass density. In contrast, geomembranes are “continuum surface” materials with properties such as tensile strength, hardness, surface roughness, and chemical constituent, which determines its behaviour. The utilization of different geosynthetics with varying physical and mechanical properties can impact the interaction and performance at the GMB/GTX interface (Dove & Frost, 1999). Therefore, knowing and understanding the factors controlling shear strength-displacement behaviour at the GMB/GTX interface is essential towards improving the interface strength (Karademir, 2011).

2.5.3. Interface stability in landfill liner

According to DWAF (1998a), contemporary landfills with steeper slopes, excessive loading conditions, significant leachate levels, and complex geometries must consider liner interface

stability along the geosynthetics before construction. Geosynthetics interface stability are required because findings by Bouazza (2002) identified that the landfill liner stability was largely influenced by the shear interaction between geosynthetics and adjacent materials. Also, the stability check helps to identify the type of failure and probability of failure. Typical failure scenarios include circular rotational, non-circular, translational, wedge, and compound slip failures.

Summary of landfill failure case studies provided by Stark (1999) identified that the translational and rotational failure are the two primary modes of failure in a landfill, with the former having a high occurrence rate than the latter. Furthermore, Buthelezi (2017) mentioned that the initiation of the failure could either occur within the waste stream or at the liner system. Therefore, slope stability analysis for a landfill would include cross-sections and plan views for the critical slope conditions that may occur during operation, filling, lateral expansion, closure, and post-closure of the landfill (Stark, 1999). Most importantly, because slope length can increase during landfill expansion, many stability analyses focus solely on the slope cross-sections. This is because, from the cross-sections, the interface with the highest potential to slip is identified through its corresponding calculated FoS.

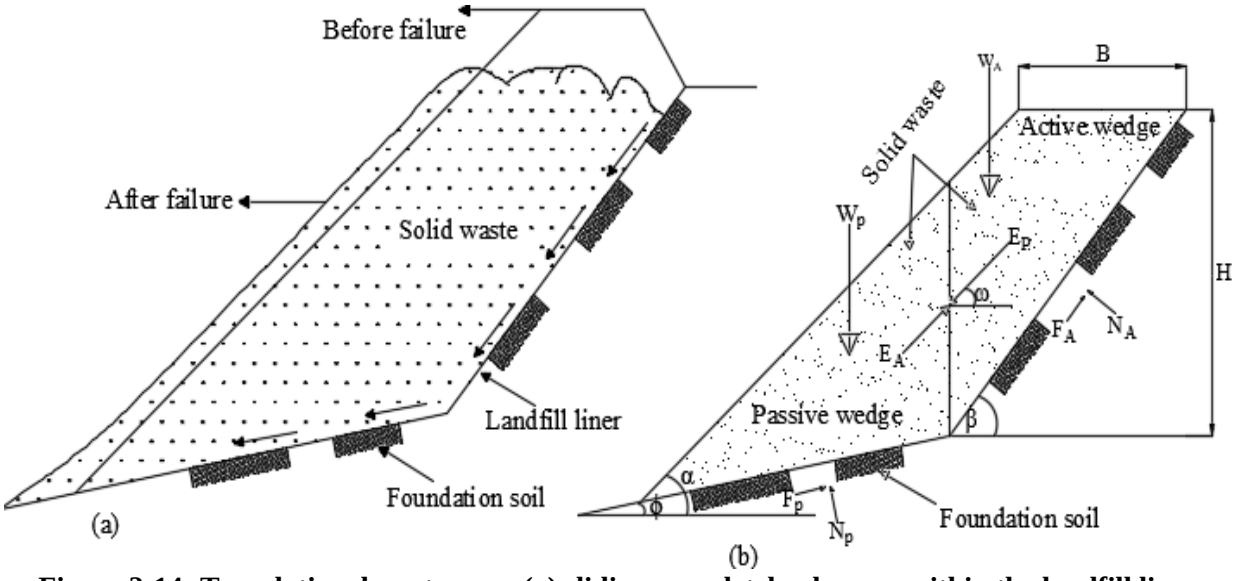

Figure 2-14: Translational waste mass (a) sliding completely along or within the landfill liner system (b) forces acting on two adjacent wedges of the waste mass (Qian *et al.*, 2003)

Various analytic methods such as limit equilibrium (LEM) and stress analysis have been proposed for assessing slope failures in landfills. However, the method that estimates a representative factor of safety (FoS) value in which waste strength is not exceeded within the

waste mass is the two-part wedge limit equilibrium method (Qian *et al*., 2003). It is important to note that this method is more applicable to translational failure analysis (see Figure 2-14a).

Figure 2-14b shows the two-part wedge method that was derived by Qian *et al*., (2003) and subsequently used to calculate FoS of the waste stream against possible translational failure. The two-part wedge consists of an active and passive wedge, where the active wedge can trigger failure because it lies adjacent to the side slope. Whereas the passive wedge tends to resist failure, as it lies on the foundation or liner system (Qian *et al*., 2003).

Translational failure model is illustrated in Figure 2-14b, where N_A and N_P are the normal forces acting at the bottom of the active and passive wedges, W_A and W_P are the weights of the active and passive wedges, F_A and F_P are the frictional forces acting at the bottom of the active and passive wedges, B is the top width of the waste mass, and H is the height of the back slope. The active and passive frictional forces (F_A and F_P) can be obtained from the corresponding total apparent cohesive forces (C_A and C_P) and interface friction angle (δ_a and δ_p). Also, with respect to the wedge geometry, α, β, and θ represent front slope angle, back slope angle, and landfill cell subgrade angle, respectively. The interface between the active and passive wedges is paramount to ascertain the probability of failure. For instance, if the average shear stress on the interface is greater than the average shear strength of the waste at the interface, translational failure could occur (Qian *et al*., 2003).

Qian *et al*., (2003), established the force equilibrium equations from the active and passive wedges force equilibrium. The resulting FoS is mathematically expressed as given in Equation 2-2: Also, depending on the input parameters (apparent cohesion and friction angle), minimum, average, or maximum FoS value would be obtained. In this study, FoS_{min} was selected as it represents the worst-case scenario. The expressions for the input parameters are presented by Equation 2-2 through Equation 2-11.

$$FoS_{min} = \frac{-b \pm \sqrt{b^2 - 4ac}}{2a}$$

Equation 2-2

where a, b, and c were quadratic functions used to simplify the force equilibrium equations. The functions were determined as follows:

$$a = W_A.sin\beta.cos\theta + W_P.cos\beta.sin\theta$$

Equation 2-3

$$b = (W_A.tan\delta_p + W_P.tan\beta).sin\beta.sin\theta - (W_A.tan\delta_a + W_P.tan\delta_p).cos\beta.cos\theta - C_A.cos\theta - C_P.cos\beta$$

Equation 2-4

$$c = -\begin{bmatrix}(W_A.cos\beta.sin\theta + W_P.sin\beta.cos\theta).tan\delta_a.tan\delta_p \\ +C_A.sin\theta.tan\delta_p + C_P.sin\beta.tan\delta_a\end{bmatrix}$$

Equation 2-5

Also, the values of W_A, W_P, C_A, and C_P can be computed using the following equations:

When,

$$B < \frac{H}{tan\beta}$$

$$C_A = c_a \frac{H}{sin\,\beta}$$

Equation 2-6

$$W_A = 0.5.\gamma_{sw}.\frac{H^2}{tan\beta} - 0.5.\gamma_{sw}.\left[\frac{H}{tan\beta} - B\right]^2.tan\alpha$$

Equation 2-7

$$C_P = c_p\left[\left(H - \frac{H}{tan\beta} + B.tan\alpha\right) + (cos\theta.tan\alpha - sin\alpha)\right]$$

Equation 2-8

$$W_P = 0.5.\gamma_{sw}.\left[\left(\frac{H}{tan\alpha} - \frac{H}{tan\beta} + B\right)^2.\frac{tan\alpha.tan\theta}{tan\alpha - tan\theta} + \left(\frac{H}{tan\alpha} - \frac{H}{tan\beta} + B\right)^2.tan\alpha\right]$$

Equation 2-9

When,

$$B \geq \frac{H}{tan\beta}$$

$$W_A = 0.5.\gamma_{sw}.\frac{H^2}{tan\beta}$$

Equation 2-10

$$W_P = 0.5.\gamma_{sw}.\left[\left(\frac{H}{tan\alpha} - \frac{H}{tan\beta} + B\right)^2.\frac{tan\alpha.tan\theta}{tan\alpha - tan\theta} + H\left(B - \frac{H}{tan\beta} + \frac{0.5H}{tan\alpha}\right).tan\alpha\right]$$

Equation 2-11

It is important to note that obtaining a suitable FoS in the translational failure analysis, among other factors, is mainly dependent on the shear characteristics (c_a, geomaterial apparent cohesion; δ_a, active-interface friction angle; and δ_p, passive-interface friction angle) at the interface with the "lowest shear strength", which in this case is GMB/GTX interface. The corresponding cohesion (c_a) and friction angle (δ_a & δ_p) can be determined from laboratory shear testing.

2.6. Geosynthetics interface characteristics and measurement

The ambient conditions within a waste containment facility are prone to changes before and after waste disposal and during landfill operations. Friction at the liners is an essential property of dynamic characteristic which should be accurately measured since it directly influences the mechanical and stability properties of the landfill side-slopes liner system (Karademir, 2011). Every interface created in a landfill liner from geosynthetics and natural material interaction possesses a unique shear strength value (derived from friction angle and cohesion), and in-turn follows a given shear mechanism (Sikwanda *et al.,* 2019).

2.6.1. Geosynthetics interface shear characteristics

In situ stresses acting on geosynthetics liners most often subject the materials to different modes of failure. Although field conditions in landfill liners are complex and situation-dependent, the material interaction and shear failure mechanism developed during the service life of the landfill can be predicted from the observation and analysis of laboratory testing results. Examples of geosynthetics failure modes in field application include rotational, shear, translational and pull out failure. However, based on studies by Cen *et al.*, (2018) and Datta *et al*., (2018), shear and translational failures are the predominant types of geosynthetics failure that occurs at GMB/GTX interface and in landfill side-slope liners. Shear failure referred to the formation of surface rupture at peak shear stresses and followed by a reduction in shear stress with an increase in displacement (Goodman, 1989). The interfacial failure mechanism is the micro-mechanical description of the shear failure that occurs at the interface. The mechanism of shear failure is dependent on the equipment used, surface properties, applied normal stresses (see Figure 2-15 below), and test conditions. The shear characteristic (strength) at an interface is the resistance to shear stresses between two or more adjacent materials, and it can be characterized by peak or residual shear strength criterion. The interface failure envelope is defined in terms of two interface shear

parameters which are the interface friction angle representing its inclination in the shear stress-normal stress space, and adhesion representing the intercept of the failure envelope with the shear stress axis.

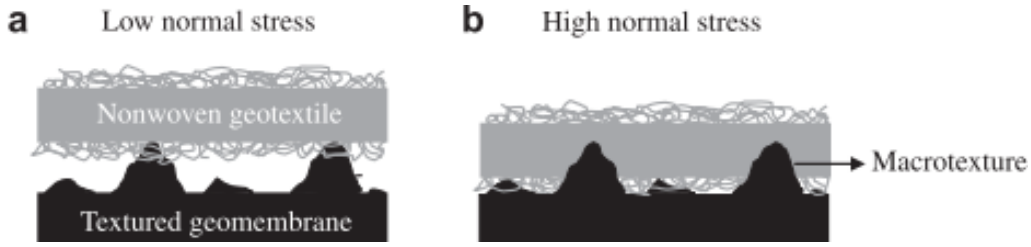

Figure 2-15: Interaction mechanism between nonwoven geotextile and textured geomembranes at different normal stresses (Hebeler *et al*., 2005)

Failure envelopes can either be linear, multi-linear (e.g. bilinear or trilinear), or non-linear (curvilinear) and may pass through the origin or otherwise (i.e. zero cohesion or non-zero cohesion intercept). The linear envelope is considered the most uncomplicated relationship between shear and applied stress. In contrast, multi-linear and curvilinear gives an advanced relationship between the stresses, and their envelope consists of two or more-line segment with an abrupt or gradual change in friction angle, where the degree of nonlinearity is affected by the applied stresses and surface properties (Giroud *et al*., 1993; Fox & Stark, 2009).

2.6.2. Major interface shear measurement device

Over the years, the experimental procedure has been one of the most reliable approaches to quantitatively and intensively study the behaviour at any geosynthetics interface (Jorge & Christopher, 1999; Rouncivell, 2007; Sikwanda, 2018). Generally, the experimental procedures include laboratory tests, field tests (i.e., in-situ test and field monitoring), numerical modelling, or a combination of approaches (Chenggang, 2005). For an experimental procedure in the laboratory to be the true representative of site conditions, different aspects of shear testing conditions of geosynthetics must be thoroughly understood and adjusted to suit the site conditions.

As a result, various devices have been developed to represent site-specific conditions, to determine shear characteristics, and to investigate the variables affecting geosynthetics interface shear strength. Usually, the geosynthetics interface shear strength is significantly controlled by the mechanisms of normal and shear load application, specimen size, and specimen confining method for the shear device (Zornberg & McCartney, 2009). Some conventional shear devices

include the direct shear device, the pull-out test, the ring shear device, and the tilt table, though the result from each shear testing device can differ from one another (Orebowale, 2006).

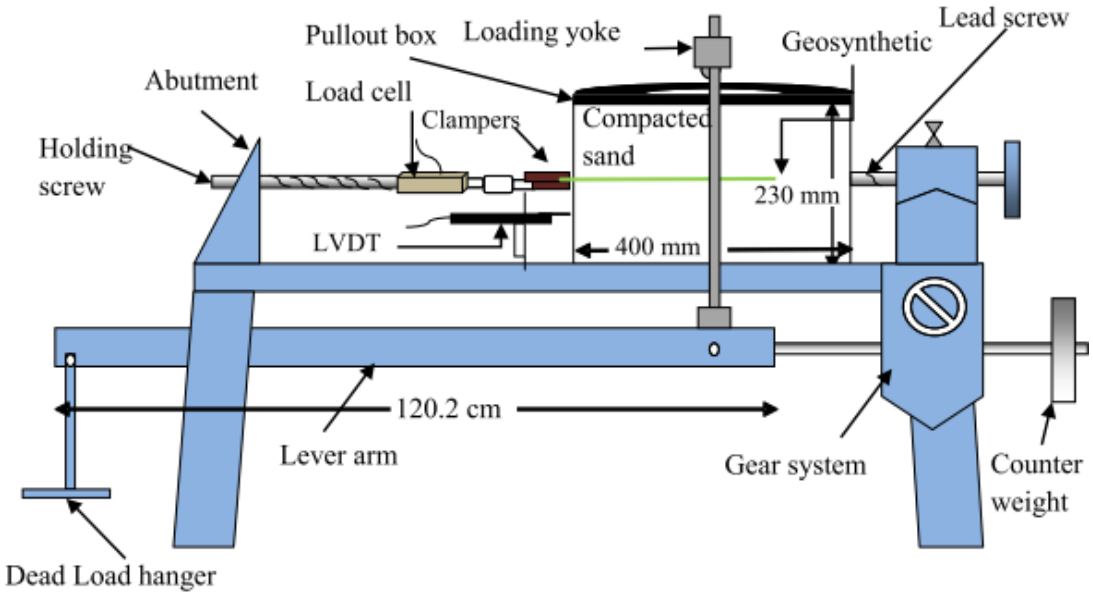

Figure 2-16: Pull-out shear machine (Prashanth *et al*., 2016)

Firstly, the pull-out test was designed to model the friction between soil and geosynthetics as it is suitable for simulating the friction and interlocking effect. Although the value of cohesion and friction angle are usually slightly smaller than values from other devices, their results are quite similar. The pull-out shear machine and specimen configuration are shown in Figure 2-16. During testing, the specimen is sheared between a horizontal stainless-steel pull-out plate and the floor of the test chamber. Volume change of the geosynthetics specimen and pore pressures at the interface can be measured during hydration and shearing stage using the thin stainless-steel needle embedded in the pull-out plate (Triplett & Fox, 2001).

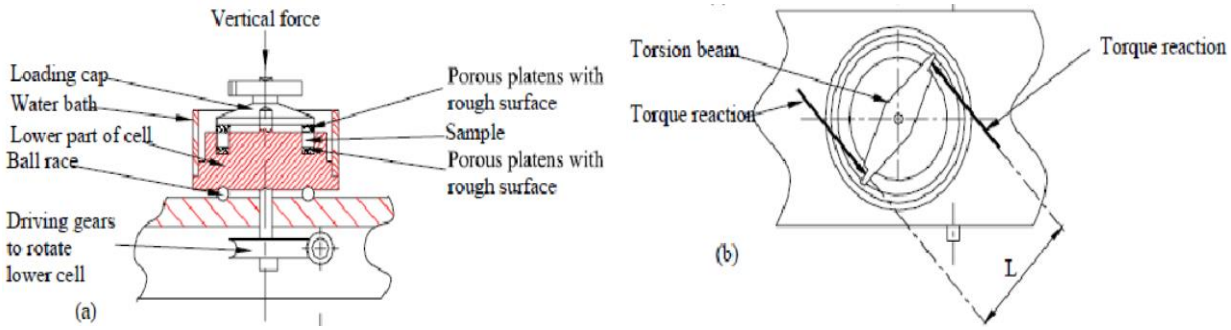

Figure 2-17: Ring shear device schematic (a) cross-section (b) plan section (Osano, 2009)

The ring shear device, like the one shown in Figure 2-17, has been used by researchers to assess the friction mobilized at the geosynthetics interface (Russell *et al*., 1998; Fox, Stark & Swan,

2008; Eid, 2011). With this device, settlement can be monitored with a dial gauge connected to a transducer during consolidation. The ring shear can accommodate normal stress and shear stress up to 1000 kPa and 500 kPa, respectively, with unlimited displacement. Also, another advantage of the ring shear is that it has a constant shear plane. Most tests conducted with the device would be fully drained due to the large displacement it can accommodate; hence, ring shear is not used to measure pore water pressure at the interface (Orebowale, 2006).

The tilt table devices are used to mobilize interface shear and normal stress through gravity. The specimen rests on a rigid board inclined at an angle that can be increased at a specific rate until failure occurs, as shown in Figure 2-18. It can accommodate a larger specimen than most other shear testing equipment and is well suitable for creep investigations. However, the applied normal stresses are limited to 50 kPa, and post-peak stresses are not measured because as the tilting angle increases loading conditions on the failure surface become increasingly non-uniform (Rouncivell, 2007).

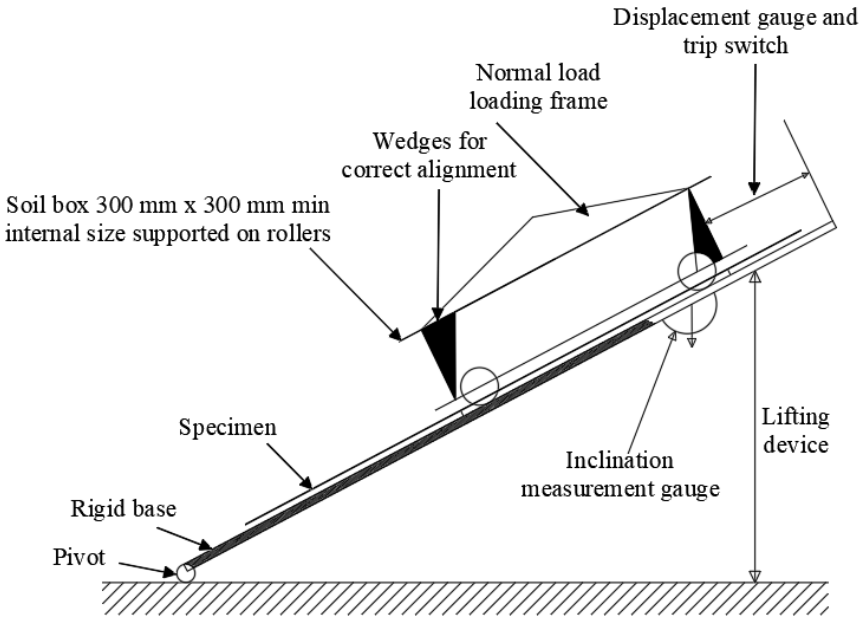

Figure 2-18: Illustration of a tilt table device (after Orebowale, 2006)

The direct shear test is used to model friction between soils and geosynthetics interface. Some identified variations in direct shear devices include variations in the top and bottom box sizes, changes in box designs and shear displacement as well as different loading systems (Orebowale, 2006). Studies by Triplett & Fox (2001), Fox & Stark (2009), and Choudhary & Krishna (2016) show that direct shear test is relatively explicit and its result quite comparable from laboratory to

laboratory. The stress-displacement relationship and shear strength parameters of the interface can be obtained graphically (Chenggang, 2005).

2.6.3. Large direct shear device

Many investigations on interface shear by researchers such as Fox *et al.*, (1997), McCartney *et al.*, (2002), and Bacas *et al.*, (2015a), were carried out using the large direct shear device mainly because of its broad acceptance by the geosynthetics community. Also, the ASTM D5321 recommended that geosynthetics or soil interface shear strength should be determined by the direct shear device, with a minimum dimension of 300 mm or 15 x d_{85} of the coarser soil or whichever is higher.

The large direct shear box works on the same principle as the conventional small direct shear test for soils, as it depends on the horizontal force applied to the specimen, which is needed to induce movement and ultimately a shear failure on the horizontal plane. According to Zornberg & McCartney (2009), larger shear boxes with sizes of 305 mm x 305 mm are explicitly used for geosynthetics testing to accommodate a representative amount of internal reinforcements within the specimen and minimize boundary effects from specimen confinement. Also, the ease of specimen preparation and availability has been identified as a further practical advantage of using direct shear devices over other options.

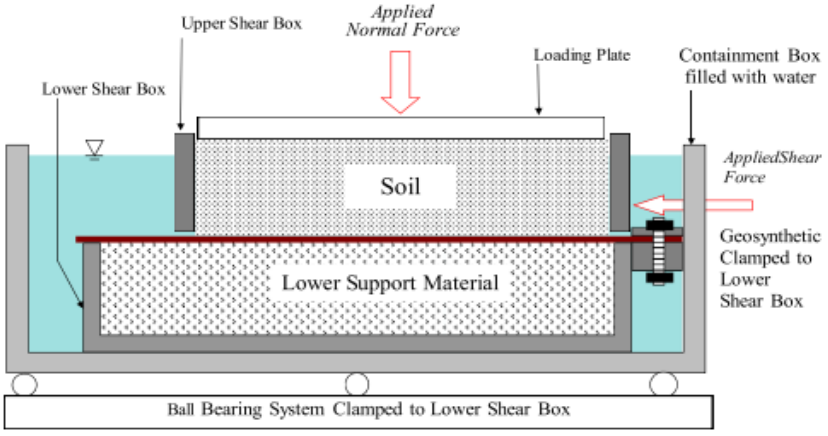

Figure 2-19: Schematic diagram of the direct shear test configuration (Stark *et al.*, 2015)

Most large direct shear devices, as schematically shown in Figure 2-19, typically allow shear displacements of 50 to 75 mm. The large displacements provide a constant area during shearing (with minimal system error), which was impossible with small shear boxes (Karademir, 2011). Often, the bottom box is 50 to 75 mm longer (in the direction of shearing) than the top box in the

shear device. Also, the large direct shear device permits the acquisition of large-displacement interface strength values. Large-displacement shear strengths of the specimen are defined as the shear strength measured at displacements sufficient to achieve converging shear stress which is similar to the actual representation of the residual strength (Hebeler *et al*., 2005).

Irrespective of the type and configuration of the interface shear testing device, commonly used direct shear devices have horizontally and vertically mounted linear variable differential transducers (LVDT), which measure the lateral and vertical displacement, respectively. Also, the device contains a horizontally and vertically mounted load cell attached under the loading frame to monitor shear resistance and confining force, respectively. The load cells are balanced when in contact with the steel ball placed above the top shear box, the steel ball aid in preventing moment and eccentric forces from occurring in the system during shearing (Karademir, 2011).

2.7. Review of factors affecting geomembrane/geotextile interface shear behaviour

It is essential to thoroughly evaluate the characteristics of the materials at the GMB/GTX interface in order to understand the behaviour and to identify factors controlling the shear stress development (i.e. shear strength parameters). Some of the frequently mentioned influencing factors of the GMB/GTX shear parameter are listed in the following sections.

2.7.1. Geomembrane surface roughness

Geomembrane surface roughness, amongst other factors such as tensile strength, modulus and surface hardness, and loading conditions are identified as primary contributors to geosynthetic interface shear strength and dilative shear behaviour (Alzahrani, 2017).

According to Thomas (1999), surface roughness is defined as the surface irregularities and undulations which are acquired on the surface during the manufacturing process. To describe geosynthetics surface property, the surface roughness and topography are usually measured. Consequently, different profiling methods and instruments such as LVDT, stylus and laser profilometer have been devised and used by Dejong (2001), Frost *et al*., (2002), and Karademir (2011) to measure surface roughness. The choice of profiling methods depends on the research purpose and surface properties been assessed. Depending on the profiling equipment, a quantity is recorded to represent the roughness of the material.

Karademir (2011), measured surface roughness using a Taylor-Hobson stylus profilometer, where the geomembrane was placed on a separate flat table to minimise disturbance and waviness during measurement. After which topographies measurements were performed with the profilometer in a direction perpendicular to the shearing motion. According to Karademir (2011), textured geomembranes surface roughness (Rs) often enhance geosynthetics interface shear properties, where Rs is defined as the ratio of actual surface area to the projected surface area. Table 2-2, proposed by Dove & Frost (1996) classified geomembranes based on their Rs ranges. The surface indentation/interaction observed when soil or geosynthetics interacts with a textured, or smooth geomembrane is related to the measurement of the geomembrane surface roughness.

Table 2-2: Geomembrane roughness classification (Dove & Frost, 1996)

Textural Descriptor	Rs Range
Smooth	1.00 – 1.10
Slightly Textured	1.10 – 1.35
Moderately Textured	1.35 – 1.60
Heavily Textured	> 1.60

Textured geomembranes interacting with other geosynthetics or soil usually produce a corresponding shear characteristic. However, of the many possible geosynthetics interfaces, GMB/GTX interface sometimes exhibits a low interface shear strength (Foye, 2011), hence, the need for its improvement. Research by Frost and Lee (1990) into the behaviour at GMB/GTX interfaces showed that the roughness of the textured geomembrane is integral to the development of interface shear strength. In support of the argument, McCartney *et al.*, (2009) conducted an experiment on the GMB/GTX interface and among many influencing factors identified, surface roughness and manufacturing process exhibited a significant impact on the result.

Roughness and textures are quantified to determine the shearing and failure mechanisms occurring at the interface. For instance, smooth GMB/GTX interfaces shear test conducted by Adeleke *et al.*, (2019) revealed that its primary shearing mechanism was “sliding with less resistance” at the interface. Conversely, for roughed textured geomembranes, the shearing mechanism was “sliding with more resistance (ploughing)” which resulted in higher interface friction angles. Also, the experiment reported by Karademir (2011) on interface shear tests between four types of GMB and seven types of woven or nonwoven GTX, stated that the geomembrane surface roughness controls the GMB/GTX interface friction angle. Similarly, from

the series of interface shear tests between nonwoven geotextiles and textured geomembranes conducted by Kim (2006), Bacas *et al.*, (2011) and Bacas *et al.*, (2015a) at normal stress levels ranging up to 450 kPa, revealed that there was a corresponding change in peak interface strengths as surface roughness was varied, see graphical summary presented in Figure 2-20.

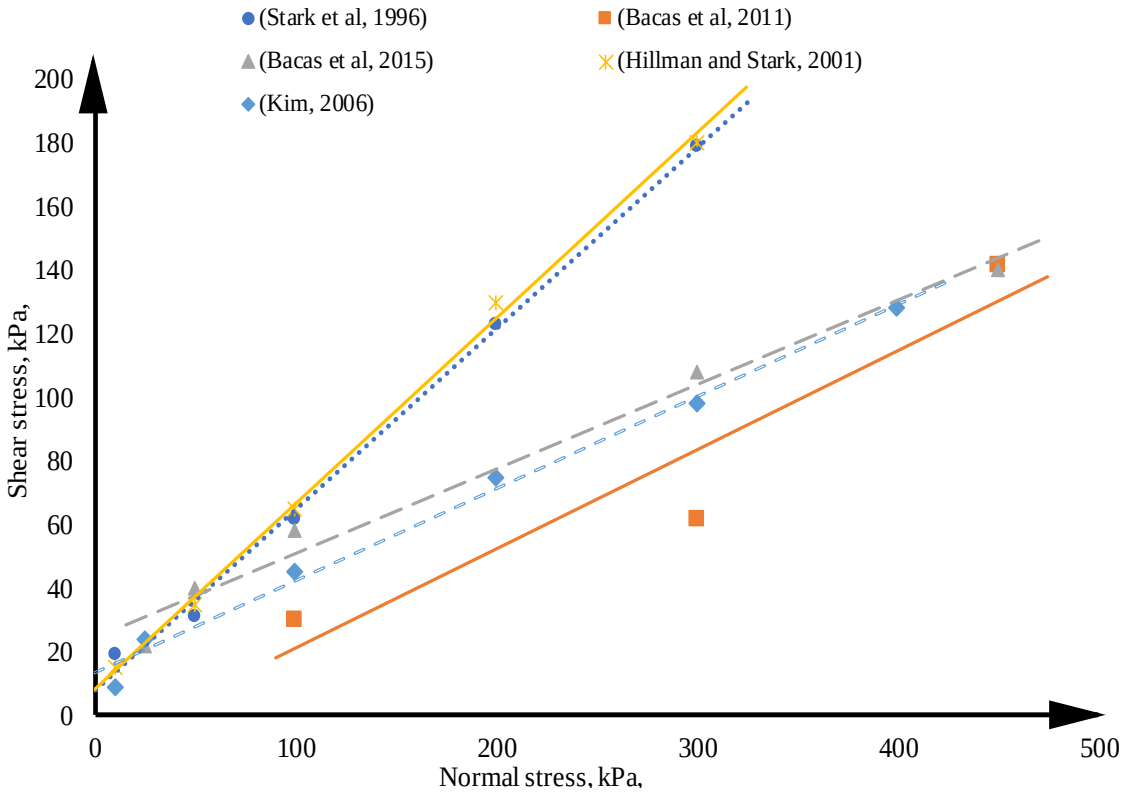

Figure 2-20: Failure envelopes for various textured GMB/GTX interfaces

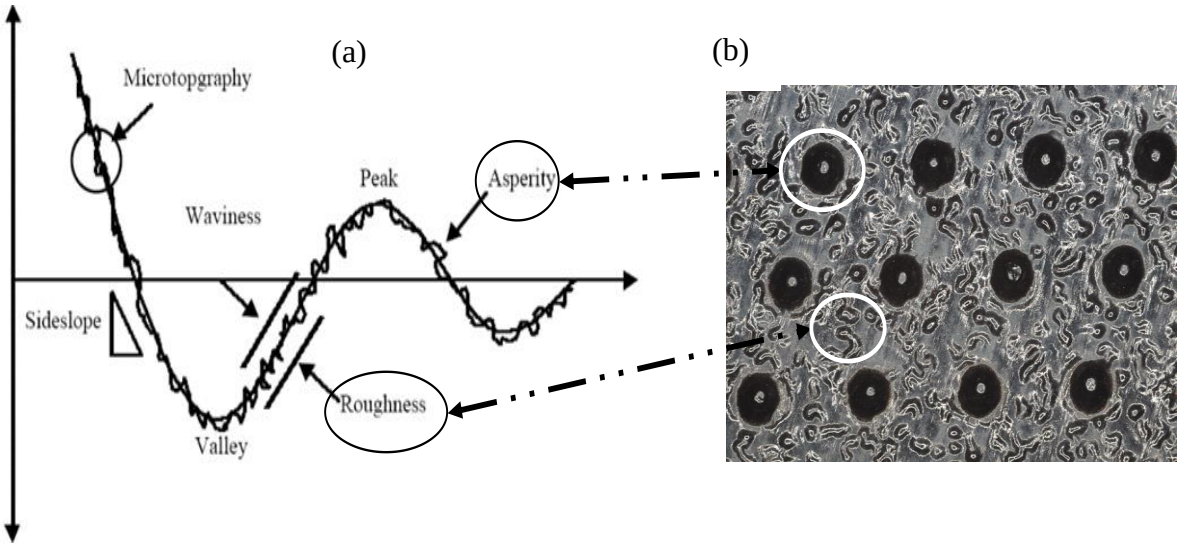

Figure 2-21: (a) Surface topography terminologies (b) X50 magnification of typically textured geomembrane (after Karademir, 2011)

In order to understand the role of surface roughness on interface shear properties, Dove and Frost (1996) further identified that the surface roughness of material should be subdivided into two categories, namely: macro-topography and micro-topography features. The macro-topography features are features quite visible to the human eye while the micro-topography features are visible only with the aid of an electronic magnifying instrument. The micro-topography features as shown in Figure 2-21b (with X50 magnification), are relatively confined to localized irregularities on the material surface. Conversely, macro-topography features are pronounced variations that have a more significant contribution to the quantitative measurement of roughness. Also, a summary from previous research on the effect of roughness on different geosynthetics interfaces was presented in Table 2-3. These studies carried out on textured geomembranes with recorded surface roughness show a substantial increase in shear strength (Frost & Lee, 1990; Stark *et al*., 1996). It is important to note that though the increase in Rs values often results in increased friction angle, heavy texturing with "above critical" Rs value can cause pulling out and raking of the geotextile filaments, and consequently, friction angle reduction (see Table 2-3).

Bacas *et al.*, (2015a), referenced in Table 2-3, analysed the differences between the various geomembrane roughness patterns interfaced with nonwoven needle-punched geotextile through the plot of interface shear strength against shear displacement. The geomembrane roughness (Rs) was measured with the aid of stylus profilometer, and the average value was recorded. It was observed from the study that the interface shear strength from the interaction of three nonwoven geotextiles and five geomembranes presented similar values independent of Rs pattern at normal stress lower than 50 kPa. However, at normal stress higher than 50 kPa, regular texturing (calendered geomembrane) showed more considerable interface shear strength and strain-softening behaviour than irregular texturing (flat-die extruded geomembrane).

2.7.2. Geomembrane asperity properties

Asperities are individual projections of polymer that extend above the main surface of a textured geomembrane (ASTM D7466, 2015). They are surface properties used to quantify the degree of roughness of a geomembrane surface and are characterized by their height, concentration, spacing and pattern (Yesiller, 2005). Asperity concentration is the number of individual polymer projections per given area. Table 2-3 clearly shows that roughness effects on shear strength have

Table 2-3: Summary of the effect of roughness on the geosynthetic interface by several authors

Author	Shear device size	SDR (mm/min)	Normal stress (kPa)	Hor. Disp. (mm)	Interface tested	Roughness (Rs)	Peak friction angle (^{0})	Peak adhesion (kPa)
(Frost & Lee, 1990)	102 mm x 102 mm	2	50 - 150	80	GMB/GTX	1.7	22.5	2.5
(Hebeler *et al.*, 2005)	102 mm x 102 mm	5	0.4 – 312	80	Coextruded GMB/GTX	1.28	30.4	9.5
(Kim, 2006)	102 mm x 102 mm	1	10 - 400	80	GMB/GTX	Not reported	29.05	14.57
(McCartney *et al.*, 2009a)	(not reported)	0.1	97 -482	75	GCL / GMB	Not reported	17.2	33.5
(Bacas *et al.*, 2011)	300 mm x 300 mm	5	25 - 450	50	GMB/GTX	Not reported	26.72	0
(Karademir, 2011)	100 mm x 100 mm	1	10 - 400	60	GMB/GTX	0.13	31.8	0
(Frost *et al.*, 2012)	102 mm x 102 mm	0.25	100– 300	80	Sand / GMB	1.4	40	Not reported
(Bacas *et al.*, 2015a)	300 mm x 300 mm	5	25 – 450	50	GMB/GTX	1.0	27	17.8
(Chai & Saito, 2016)	200 mm x 200 mm	1	50 - 100	33	GMB/GTX	1.28	26.72	0

been investigated in some existing literature. However, a more detailed investigation into the properties of asperities and its influence on the geosynthetics interface shear characteristics was observed to be limited, as 70 % of the studies in Table 2-3 did not consider asperity effect on the geosynthetics interface. The study by Bacas *et al.,* (2015a) on asperities effects on geosynthetics interface revealed that shearing nonwoven geotextile against textured geomembrane (with closer asperities) yielded a better result than interfaces with farther asperities. However, interfaces with extremely close asperities produced little or no improvement, as the surface tends to become uniform. Also, from the study, the smaller values of interface friction angle corresponded to the interface with little or no asperity height. Also, geomembranes with asperity height greater than 1 mm were identified with greater peak strength and post-peak interface strength loss. The behaviour was due to the interlock interaction between the geosynthetics and high capacity damage to the geotextile fibre, respectively. Bacas *et al.*, (2015a), concluded that geomembrane asperities together with geotextile-type are essential factors that can quantify the interlocking and the interbedding (hook and loop) factors at the interface, where the hook-loop interaction is a known method used for quantifying geosynthetic interface performance.

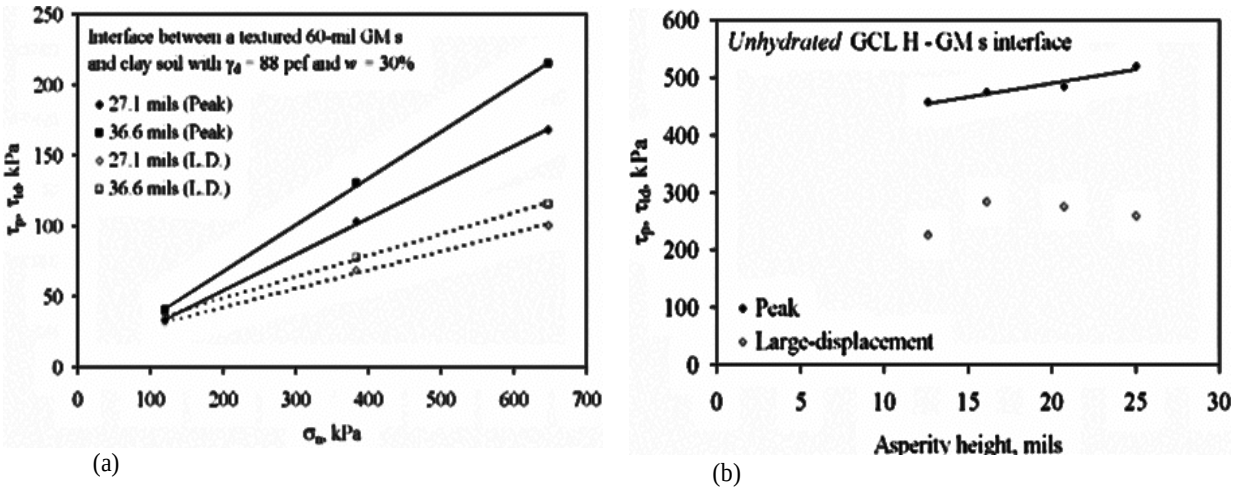

(a) (b)

Figure 2-22: Effect of asperity height on (a) soil - GMB (b) GCL- GMB, interface shear strength (McCartney *et al.*, 2005)

Additionally, Fowmes *et al*., (2017), conducted a series of investigations to vary the asperity shape parameters such as standard spiked and hooked asperity, to vary the asperity density, i.e. the number of asperities on the sheet, and lastly, to vary the asperity height. It was reported that greater asperity height resulted in better interlock at the interface between the geomembrane and geotextile, as well as higher peak shear stresses due to the hook-loop interaction. Results from

the direct shear testing revealed that asperities with hooks gave a reasonable increase in shear strength even at low normal stresses. Also, the reduction of asperities spacing by approximately 30 % resulted in an approximately 10 % increase in peak shear strength at low normal stresses. Also, when asperities height was increased by 60 %, the interface peak shear strength recorded at low normal stresses was increased by 6.7 % (Fowmes *et al.*, 2017).

Similarly, studies by Triplett & Fox (2001), McCartney *et al*., (2005), and Blond & Elie (2006) indicated that textured geomembrane asperities have a significant impact on interface shear strength properties. Specifically, Blond and Elie (2006), conducted over 100 shear test comprising geomembranes with seven different asperities, four different geotextiles, clayey soil and sand, in order to identify the relationship between interface shear test and geomembrane asperity height. In agreement with Blond and Elie (2006), McCartney *et al.*, (2005) found that despite the high variableness of geomembrane asperity heights, it is a good indicator of the peak shear strength of geomembrane/geomaterial interfaces (see Figure 2-22 a & b), as the peak shear strength was observed to increase linearly with increase in asperity height. Although it suggested that for some interface, there exists an optimized asperity height beyond which increases in shear strength becomes minimal. For instance, Blond and Elie (2006) observed that most interface shear property remain reasonably constant after the threshold asperity height (0.51 mm) was reached.

2.7.3. Mass density and thickness of geosynthetics

Highly reliant on the purpose of use and manner of application in the field, geosynthetics are produced by manufacturers with different mass densities and thicknesses measured in g/m^2 and mm, respectively. The thickness of geosynthetics like geotextile contributes to the magnitude of the peak as well as post-peak shear strength that develops at the geomembrane/geotextile interfaces (Karademir, 2011). For instance, Stark *et al.*, (1996) conducted shear tests on HDPE geomembrane/nonwoven geotextiles interface, with the geotextile having different mass densities of 270 g/m^2 and 540 g/m^2 (i.e. mass per unit area). It was recorded that at normal stresses less than 100 kPa, there were negligible differences between both peak and large displacement (LD) failure envelopes.

On the contrary, at normal stresses greater than 100 kPa, there was a notable difference from the failure envelope of the thinner geotextile with lower mass density in contrast to thicker geotextile

with greater mass density. The thinner geotextile with lower mass density yielded a higher peak failure envelope than the thicker geotextile with more significant mass density (see Figure 2-23). The explanation for this anomaly was that the thicker geotextile with higher mass density allowed the easy removal of some filaments from the fibre when sheared at higher normal stresses. It was, therefore, recommended that for a basal and side-slope liner system, a lower mass density is more appropriate. Whereas for capping systems application, it was recommended that either lower or higher mass density is suitable. Additionally, the LD strengths obtained were comparable, and there was almost no difference especially at very high-stress levels greater than 250 kPa, this was attributed to the fact that geotextile filaments were being pulled out or torn after the large shear displacement required to achieve the LD strength condition (Karademir, 2011).

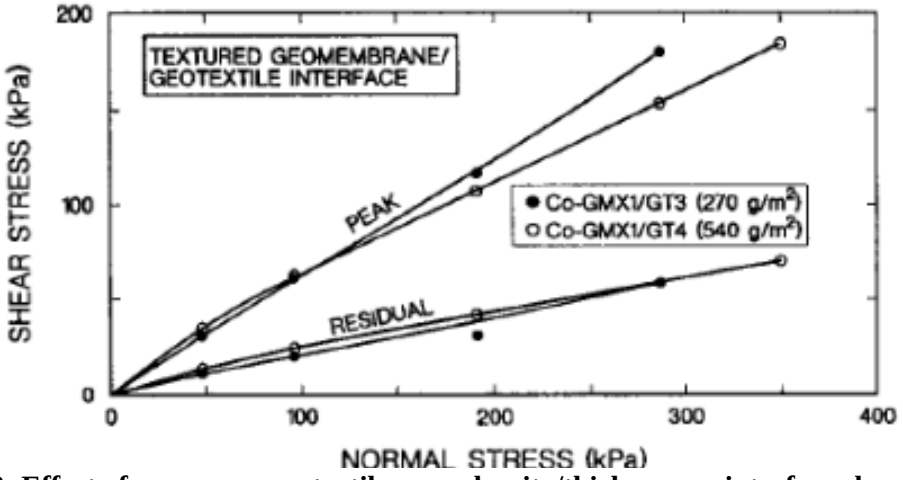

Figure 2-23: Effect of nonwoven geotextile mass density/thickness on interface shear resistance (Stark *et al.*, 1996)

2.7.4. Applied normal stress

Hebeler *et al.,* (2005) carried out a series of shear tests over normal stresses ranging from 0.4 kPa to 312 kPa on the geomembrane/geotextile (GMB/GTX) interface and reported the results to capture the variations of the interface shear behaviour to applied normal stresses (see Figure 2-24). The documented results provided clarity into the interaction mechanisms and the development of interface shear response over the range of normal stress levels at the textured GMB/GTX interface. Over the range of normal stresses tested, the shear stress – horizontal displacement response was directly proportional to the applied normal stress. Also, the structured geomembrane/needle punched nonwoven (NPNW) geotextile composite system and the coextruded geomembrane/NPNW geotextile composite system exhibited a linear peak strength envelope, and a non-linear as well as linear residual strength response. Conversely, both co-

extruded and structured textured geomembrane interfaces exhibited similar non-linear post-peak (pseudo-residual) interface shear strength trends as a function of increasing normal stresses (Karademir, 2011).

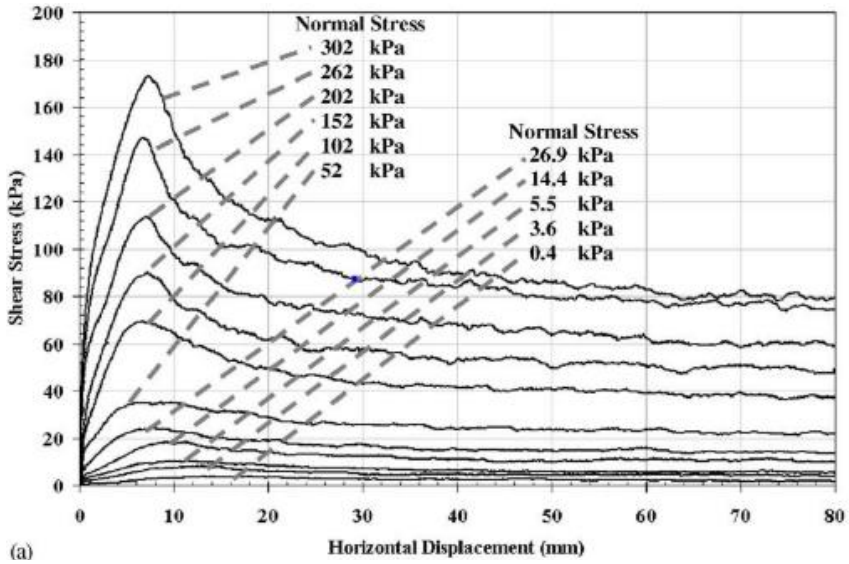

Figure 2-24: Direct interface shear results of HDPE geomembrane against nonwoven geotextile specimens at different normal stresses (Hebeler *et al.*, 2005)

Similarly, Stark *et al.*, (2015) emphasized that the identification of the critical interface in a multi geosynthetics interface is dependent on a couple of factors such as normal stress, geomembrane type, test procedure and manufacturing technique. The normal stress was recognized as a superior factor in exposing the critical interface.

2.7.5. Geosynthetics reinforcement and polymer type

McCartney *et al.,* (2009) reported a geosynthetic-interface experiment conducted over a few years using ASTM testing standard procedures. The number of results in the database allowed the quantification of the impact of geomembrane-type on the geosynthetic interface shear strength to be evaluated. The study examined the shear behaviour of the different geosynthetic interface as the geomembrane polymers were varied. The geomembrane polymers investigated were high-density polyethylene (HDPE), linear low-density polyethylene (LLDPE), very low-density polyethylene (VLDPE), and polyvinyl chloride (PVC) geomembrane. From the study, it was identified that the geomembrane flexibility for the different interfaces tested under normal stresses less than 50 kPa played a sensitive role to the development of interface shear strengths at the woven and nonwoven GCL/textured geomembrane interface (McCartney *et al.*, 2009). Specifically, less flexible geomembrane (e.g., HDPE geomembrane) were found to have lower

interface shear strength (24 kPa) than more flexible VLDPE geomembrane (27 kPa). Similarly, Zornberg and McCartney (2009) indicated that geomembrane with more flexible polymers is posed to have a higher peak shear strength than stiffer geomembrane.

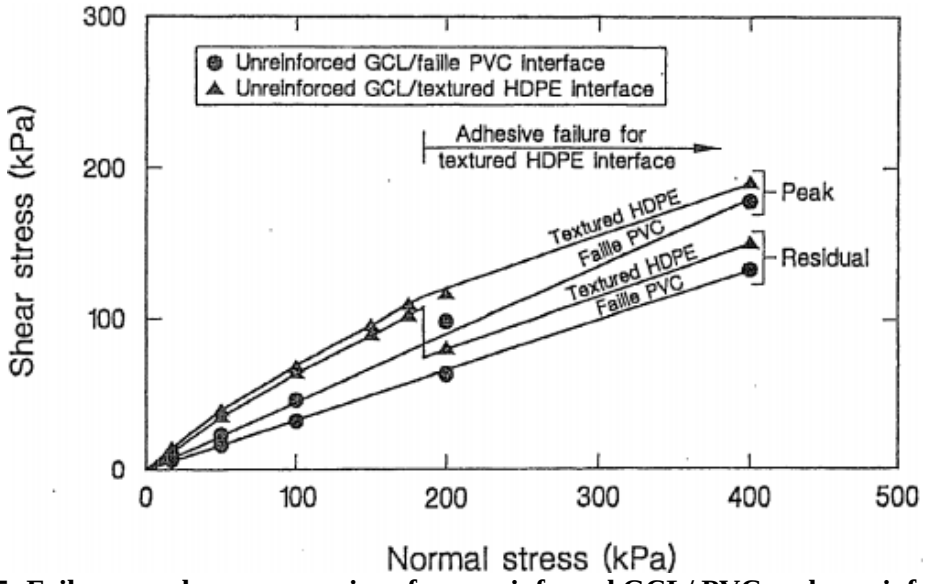

Figure 2-25: Failure envelopes comparison for unreinforced GCL/ PVC and unreinforced GCL/ HDPE interfaces (Hillman & Stark, 2001)

In a separate study, Hillman & Stark (2001), presented shear stress versus normal stress relationship curves for the unreinforced GCL/ PVC and unreinforced GCL/ HDPE interfaces. It was evident that textured HDPE geomembrane interface exhibited a marginally higher shear strength than PVC geomembrane interface, particularly at normal stresses less than 175 kPa, as shown in Figure 2-25. The difference was attributed to the exerted pressure by the HDPE geomembrane asperities into the dry bentonite layer of the GCL.

2.8. Geomembrane asperities

Geomembranes are manufactured thin, flexible thermoplastic or thermoset polymeric used in environmental and structural applications. They have been used in dams construction since 1959, shortly after their invention (Jianxia, 2012). Initially, the manufacturing of geomembrane was solely on smooth sheet production (see initiation stage of Figure 2-26), however, as the areas of applications increases, modification of the geomembranes surface characteristics (texturing) was required to meet environmental demands. Over the years of incorporating texturing on geomembrane surfaces, essential parameters such as asperity shape, height, concentration, spacing (machine direction and cross-machine direction), and configuration have been devised

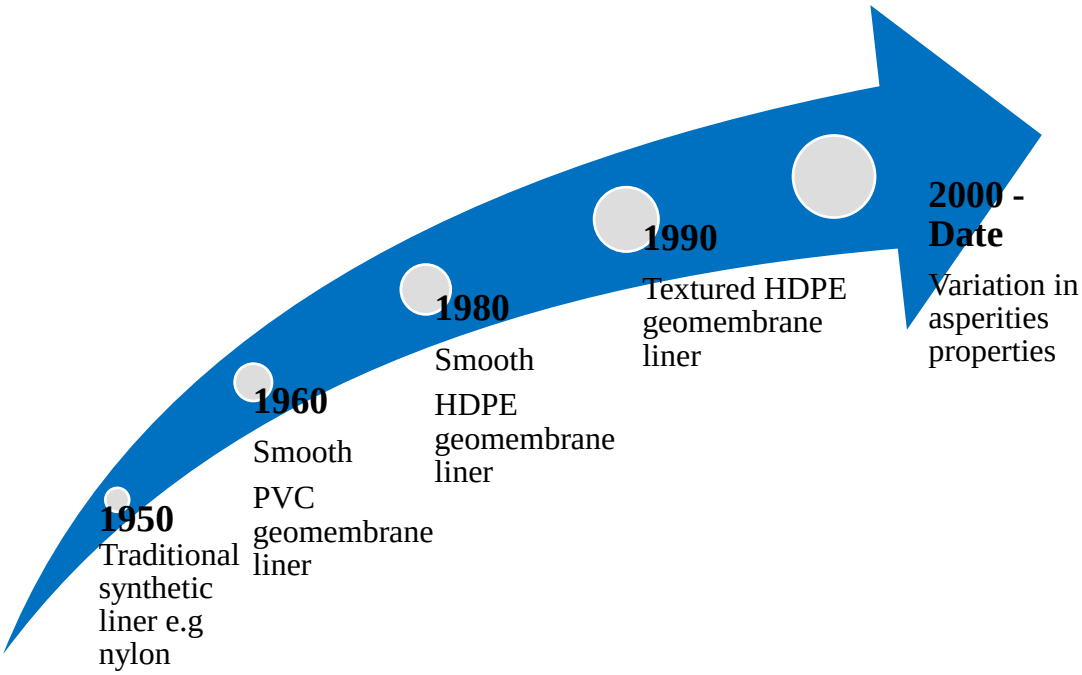

Figure 2-26: Evolution of geomembrane application in history

by researchers such as Bacas *et al.*, (2015a) and Fowmes *et al.*, (2017), and geosynthetics manufacturers have utilised them to describe their products asperity properties, see illustration in Figure 2-27. Due to the importance of asperities to hook and loop interaction at geosynthetics interface, it is recommended that these parameters should be precisely measured using standard devices and methodology (Yesiller, 2005).

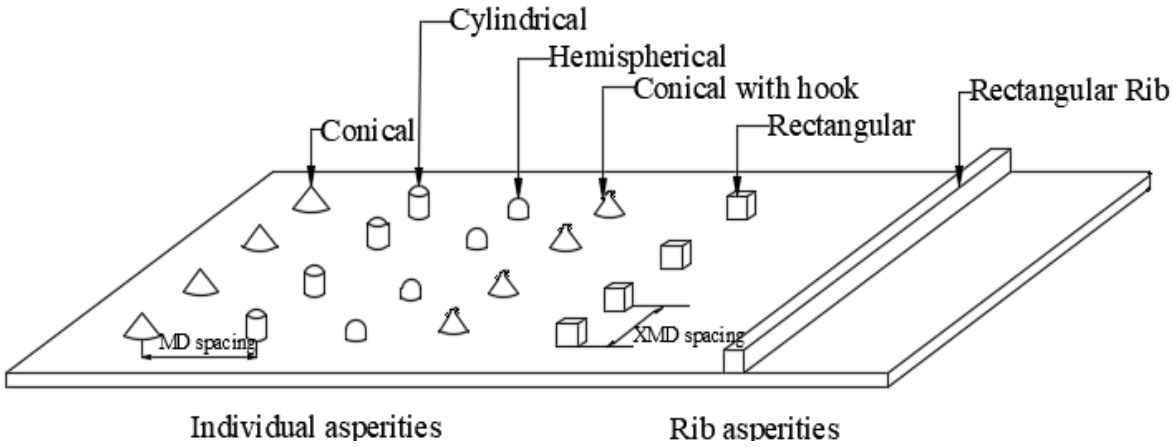

Figure 2-27: Common geomembrane asperities. (after Fowmes *et al.*, 2017)

2.8.1. Geomembrane asperities functions and applications

The inclusion of asperities to geomembrane surfaces have caused their applications to extend to new engineering disciplines. The functions of the asperities on the geomembrane surface can be grouped into four categories, namely drainage, friction, slope stability, and anchor functions.

- Drainage function: In geosynthetic applications, the spacing between adjacent asperities/spikes can act as a flow path in scenarios of insufficient drainage potential. The asperities on the surface can cause an artificial decrease in the required drainage force. This asperity function is recommended in applications susceptible to excessive pore water pressure build-up, as they assist in the system drainage operations. It is important to state that the drainage flow rate would be proportional to the asperities geometric properties.
- Friction function: This category of asperities function is solely for improving the shear resistance at the resulting interface between textured geomembrane and counter faced geomaterial. According to Bacas *et al.*, (2015a), among other factors, the asperity spacing, shape and height of the asperities are a crucial factor in the development of interface frictional resistance.

(a) (b)

Figure 2-28: (a) Co-extruded geomembrane (b) GMB Tunnel applications (AKS Lining Systems, 2020)

- Slope stability function: The combination of the drainage and friction function ultimately increases the interface shear resistance, which in turn positively affects the stability of slopes (side-slope of landfills). The drainage function aids the removal of present water particles (which can induce sliding) and the friction function reduces sliding potential.
- Anchor function: In recent tunnelling/sewage drainage construction, geomembranes have been applied together with concrete structures, see Figure 2-28. This combination often helps to increase the design life of the concrete structure through the inclusion of geomembranes' durability property. It is important to note that the geomembranes asperities due to their geometric features are required to hold the geomembrane and concrete in-place throughout the tunnel design-life.

2.8.2. Advantages and disadvantages of asperities in geomembrane

Asperities, from studies by Blond & Elie (2006), Fowmes *et al.*, (2017), and Adesokan & Blond (2018), were identified as a major determinant of the geosynthetics interface shear characteristics. Some of the recognized advantages are as follows;

- Asperities aid the development of shear strength.
- They can act as a drainage channel to reduce water pressure build-up.
- They can increase stability in applications involving slope liner.

Contrarily, some disadvantages as regards asperities application have been recognized, they include;

- Asperities, depending on properties and application, can cause excessive wear and tear to adjacent (weak) materials during interactions.
- Installation/welding operations of GMB with asperities may become complex.
- Also, in applications involving maintenance, asperities can make cleaning difficult.

2.8.3. Asperities effects on mechanical and durability properties of geosynthetics

2.8.3.1 Creep and asperities

According to Karademir (2011), creep is a time-controlled deformation process, that occurs at given stress which is often less than the material's strength. Creep behaviours are categorized into three groups; namely, primary, secondary and tertiary creep. The creep mechanism, irrespective of the category, is primarily controlled by the applied stress and interface properties. Another factor to be considered in geosynthetics creep behaviour during a shear test is the "shear displacement rate (SDR)". For instance, when polymeric materials are axially loaded at a relatively slow shear rate, they deform through rearrangement of atoms as well as distortion/increase of lengths and angle of atomic chemical bonds until fracture or failure occurs (Osswald, 2003; Karademir, 2011). It is important to note that the extent of creep strain is dependent on the type of polymers at the geosynthetics interface. For instance, there is a pronounced creep impact with HDPE geomembrane asperities on the mechanical properties of the GMB/GTX interface than PVC geomembrane (Mosawi, 2013).

2.8.3.2 Failure mechanism and asperities

Failure mechanism in geosynthetics, such as fracture and shear, occurs as a result of different relative movement in the geosynthetics structural polymers and surface asperities. According to Karademir (2011), fracture failure can be caused by slippage of the monomer chain in the polymers. Also, Kim (2006), mentioned that the geomembrane/geotextile shear failure mechanism are grouped into five stages, where the stages are due to changes in geomembrane (GMB) asperities and geotextile (GTX) fibre structure as shear displacement rate increases. Stage 1 was described by initial compression of GTX with the GMB asperities and was followed by geotextile-stretching through the interlocking of GMB asperities (Stage 2). Stage 3 comprises of geotextile-dilation and geotextile-fibre sliding over GMB texture until failure occurs. At stage 4, GTX filaments rearrangement occurred, and the strong interlocking shear strength was released. Lastly, Stage 5 was distinguished by the failure and degradation of geomembrane texture and geotextile filament, respectively.

2.9. Summary of the literature

This chapter has provided comprehensive background information and review of previous studies on GMB/GTX interface shear characteristics and behaviour. It also considered the effects of different factors such as asperities and other geomaterial characteristics on the GMB/GTX interface strength, as findings identified it as among the weakest “critical” interface in a composite landfill liner. Also, some useful supporting graphs and tables from past research were included to supply a qualitative and quantitative estimate of the factors affecting shear resistance.

Although several studies have been carried out on the GMB/GTX interfaces shear, gaps and questions in areas related to material properties (asperities) and polymer comparison were identified, as most of the previous studies did not extensively consider geomembrane asperity and geotextile polymer details. Also, it was identified that less literature was currently available on asperities variation and its effect on the GMB/GTX interface. As such, studies are needed to investigate the effects of asperities on the GMB/GTX interface and to provide details of the shear and wear behaviour at various normal stress. Therefore, this research was undertaken to provide a better understanding of asperity interaction and would recommend asperity parameters that would enable landfills design engineers to create stable side-slope liner system.

3. RESEARCH MATERIALS AND METHODOLOGY

3.1. Introduction

This chapter describes the materials, implemented methods, and detailed experimental procedures utilized in this research. The geosynthetics utilized in this investigation were geotextiles and geomembranes, and the interface between them constitutes the most critical interface of an engineered landfill liner system (Bergado *et al*., 2006). To ensure that the critical interface tests were conducted according to internationally recognized standards, a large direct shear device, as per ASTM D5321 (2014) and DWAF (1998a) recommendation, was used to measure the interface shear parameters. The chapter concluded with a summary of the tests program and measures adopted to ensure result consistency.

3.2. Research materials

3.2.1. Geotextiles

Non-woven geotextiles were utilized in this research, as they were more applicable to landfill liners and often exhibit a higher friction angle than woven geotextile (Hardie, 2018; Oriokot, 2018). The "F-400M SA" and "400M SA" geotextiles manufactured by Fibertex South Africa (Pty) Ltd in Johannesburg, South Africa were adopted in this study; the former was called "fibertex" geotextiles while the latter was termed "betatex". The symbol "M" and "SA" in the product code indicated that the geotextiles were not heated-bonded calendered and manufactured in South Africa, respectively, while "400" represented its mass density (Fibertex, 2017). Other physical, mechanical, hydraulic, and durability properties of both geotextiles as provided by Fibertex are given in Table 3-1.

The "F-400M SA" and "400M SA" geotextiles had a thickness of 3 mm and 3.4 mm, respectively. These geosynthetics were selected because although they differed in thickness and other material properties, they both have a similar mass density of 400 g/m^2. The mass density of 400 g/m^2 was selected because according to Stark *et al.,* (1996), relatively low mass density geotextiles were preferred than geotextiles with a high mass density (1000 g/m^2) as they often yield higher peak shear, particularly at stresses higher than 100 kPa. Therefore, the selected mass density (400 g/m^2) and the applied stresses range are more likely to allow for greater interface shear strength in a typical landfill liner condition. In addition, the selected 400 g/m^2 mass density

geotextile were readily available and widely used as a protection layer for geomembranes in landfill applications in South Africa (Kiptoo *et al.*, 2017).

Table 3-1: Fundamental geotextile properties (after Fibertex 2017)

Properties	Test methods	Units	GTX-PP (Fibertex)	GTX-PET (Betatex)
Mass per unit area	SANS 9864:2013	g/m^2	400	400
Thickness	SANS 9863:2013	mm	3.4	3.0
Tensile strength	SANS 1525:2013	kN/ m^2	25/28	20/20
Static puncture strength (CBR)	SANS 1223:2013	N	4500	3000
Elongation at break	SANS 1525:2013	%	>50	>40
Dynamic cone drop	SANS 13433:2013	mm	8	17
UV stability	ASTM D4355	%	70	70
Permeability	SANS 11058:2013	m/s	0.04	0.03
Permittivity	SANS 11058:2013	sec^{-1}	0.85	0.68
Pore size	SANS 12956:2013	µm	70	70

The dark grey fibertex geotextiles produced from virgin polypropylene (PP) fibres could be utilized in specific and general applications. Also, it should be noted that the light yellowish-brown betatex geotextiles manufactured from recycled polyester (PET) fibres are best applied in conditions with no specification and/or domestic applications (Fibertex, 2017b). According to Fibertex (2017a), the material specification for fibertex geotextile "F-400M SA" was "polypropylene (PP) staple fibre, needle-punched nonwoven geotextile, with a tensile strength of 25 kN/m^2, 4.5 kN static puncture resistance". Betatex geotextile (400M SA), on the contrary, was specified as "polyester (PET) staple fibre, needle-punched nonwoven geotextile, with a tensile strength of 20 kN/m^2, 3 kN static puncture resistance".

Due to nonwoven geotextile engineering properties, both polypropylene and polyester geotextiles have been used as the protection layer for geomembranes against piercing material movement in identified geotechnical engineering projects such as Vlakfontein Landfill Site in Vereeniging, Holfontein H:H Landfill in Gauteng, and Sasol Secunda Fine Ash Dams 6 (Oriokot, 2018). Nonwoven geotextile engineering properties are attributed to the fibre-fibre bonding process, the addition of UV stabilizer and the spatial arrangement of filaments (Karademir, 2011; Fibertex, 2017a) Polypropylene geotextile (GTX- PP) has extended design life of over 100 years; however, recycled polyester (GTX-PET) has a reduced design life, and according to Greenwood

(2015), this could be 5 – 10 years depending on the site-specific conditions. It is important to note that GTX-PP possesses higher toughness value than GTX-PET, as observed from the dynamic cone drop measurement in Table 3-1 (Osswald, 2003).

Microscopic images of GTX- PET and GTX- PP (Figure 3-1 a & c) were acquired at the Electron Microscope Unit of the University of Cape Town (UCT) to show the microstructural composition of the materials. In order to acquire the imaging, a representative sample of recommended dimension (15 mm x 15mm) was obtained from each supplied roll of the geotextiles. The samples were subsequently subjected to 500 times magnifications using the "Tescan MIRA3 RISE SEM microscope".

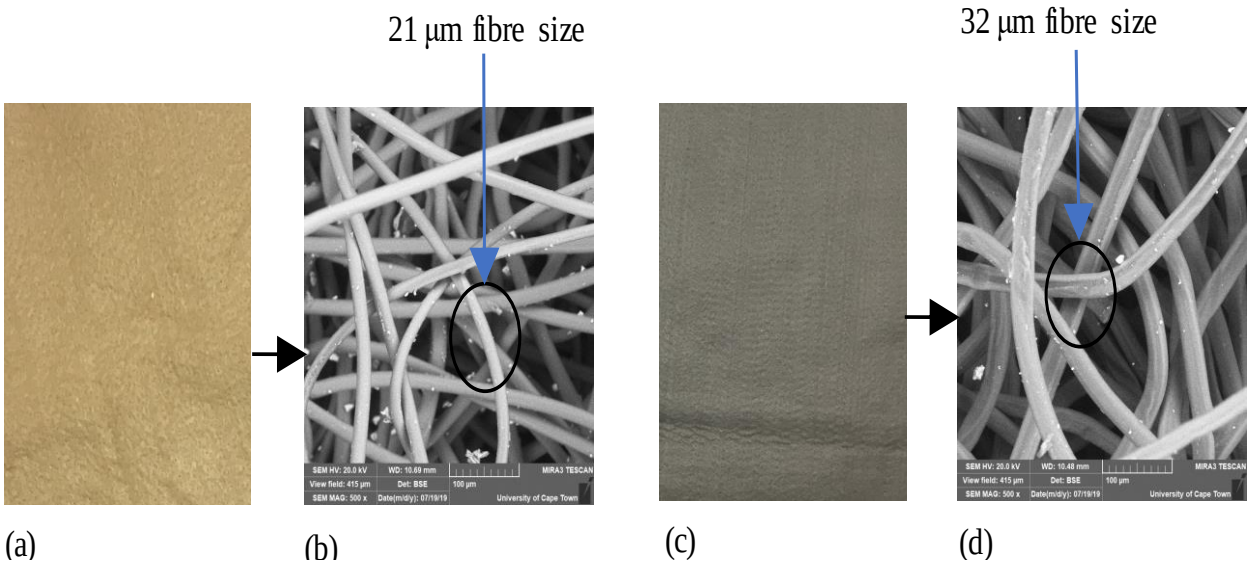

Figure 3-1: Surface and microscopic view of selected geotextile: (a) GTX-PET (b) GTX – PET fibre (X 500) (c) GTX-PP (d) GTX – PP fibre (X 500)

In general, the geotextiles consisted of spatially curved filament (polymer molecules), which were randomly oriented and distributed in the polymer configuration (Karademir, 2011). The orientation and arrangement of the geotextile fibres were dependent on the manufacturing process, individual fibre characteristics (material type, stress-strain properties, and physical properties), and the environment (load applied). The fibre arrangements observed for the geotextiles are shown in Figure 3-1 b & d. Notably, it was observed from the imaging that polyester geotextile (GTX-PET) has a relatively small size (21 µm) and tightly clustered filaments. Contrarily, the filaments in polypropylene geotextile (GTX-PP) were relatively big in size (32 µm) and loosely clustered. The microscopic views given in Figure 3-1 allowed different filaments diameter measurement to be taken. From the recorded measurements, the average fibre diameters were thus calculated, as labelled in the figure.

3.2.2. Geomembrane

Two categories of HDPE geomembrane (GMB) were adopted in this study, namely; flat die extruded smooth and calendered textured geomembrane. The calendered textured geomembranes were selected to investigate the effects of asperity on the geomembrane/geotextile interface shear parameter over other geomembrane-type. This is because an accurate and experimental determination of its surface asperity properties is possible. Also, with calendered geomembranes, texturing over 3 mm can be achieved, and they find frequent industrial applications (Hardie, 2018).

Table 3-2: Geomembranes principal properties and their test method (AKS, 2018)

Material label	Properties	Units	Min average value	Test method
*GMB – S	Formulated density	g/cc	0.94	ASTM D1505
	Thickness	mm	2	ASTM D5199
	Puncture resistance	N	640	ASTM D4833
	Carbon black	%	2.5	ASTM D4218
	Tear resistance	N	249	ASTM D1004
*GMB – T	Formulated density	g/cc	0.94	ASTM D7466
	Thickness	mm	2	ASTM D5994
	Puncture resistance	N	534	ASTM D4833
	Carbon black	%	2.5	ASTM D4218
	Tear resistance	N	249	ASTM D1004

*GMB – S represents smooth geomembrane, as GMB – T denotes textured geomembrane

The smooth geomembrane (GMB-S); i.e. the absence of texturing, acted as the control experiment in this study. Both the smooth GMB (GMB-S) as well as the textured geomembranes (GMB-T), were manufactured by AKS Liner Systems (Pty) Ltd in Cape Town, South Africa. The products were factory-made from HDPE resin under controlled conditions and international specification of GRI – GM13 (Koerner & Koerner, 1999; AKS, 2018). Relevant material specifications such as thickness, formulated density, percentage of carbon black, and tear and puncture resistance, as obtained from AKS Liner Systems were incorporated in Table 3-2 above. Since the introduction of texturing to geomembranes, different surface textures have become available. Hence, it is imperative to distinguish one geomembrane from another. In order to accomplish this differentiation, asperity parameters such as asperity height, density, inclination, and spacing were measured. The detailed description of each asperity parameter is presented in Figure 3-2.

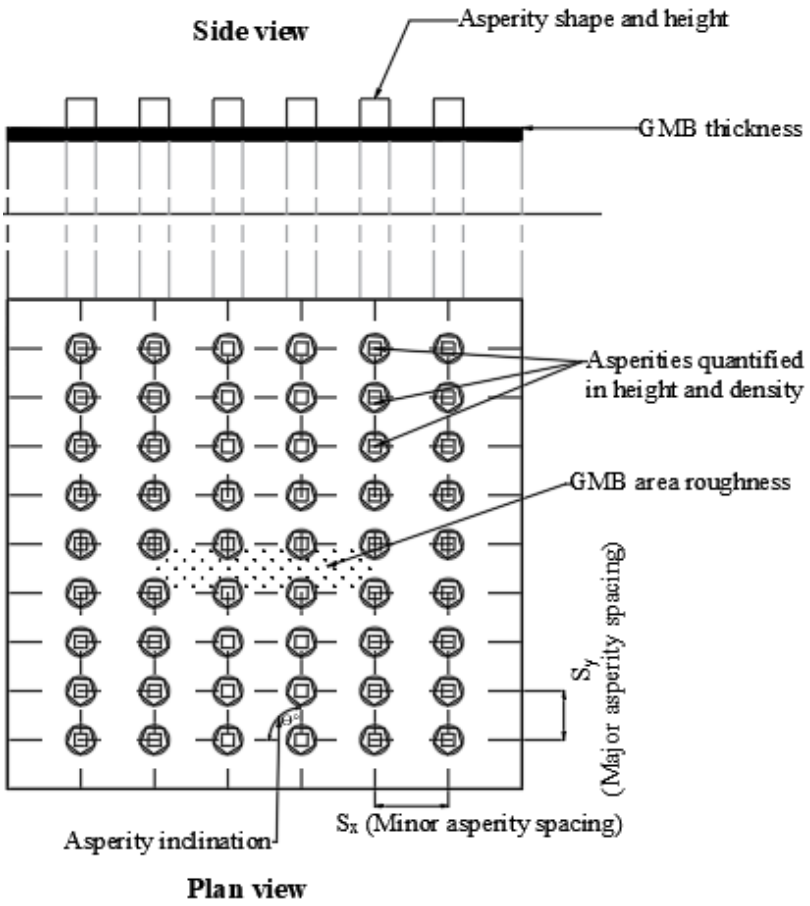

Figure 3-2: Detailed view of geomembrane asperity parameters

Geomembrane asperity parameters of interest in this investigation were asperity height, density, spacing, volume, shape, inclination, and configuration, as depicted in Figure 3-2. In this study, all textured GMBs used had average surface asperity heights ranging from 0.70 mm to 2.02 mm, while their asperity densities ranged from 211 to 663 spikes per 10000 mm^2. Also, the asperities spacing in the abscissa (x-axis) and ordinate (y-axis) had a minimum and maximum spacing of 4.34 mm and 9.76 mm, respectively. It should be noted that the x-axis and y-axis corresponded with the cross-machine direction (XMD) and machine direction (MD), respectively. The asperity inclination, which is the measured angle between the x-axis and y-axis ranged from 56.5° to 75.3°. The aerial configuration of asperity arrangement in the machine direction on the geomembrane surface was either inclined or straight. The summary of measured asperity parameter for all GMB is provided in Table 3-3. Also, the pictorial view of all geomembrane surfaces is presented in Figure 3-3.

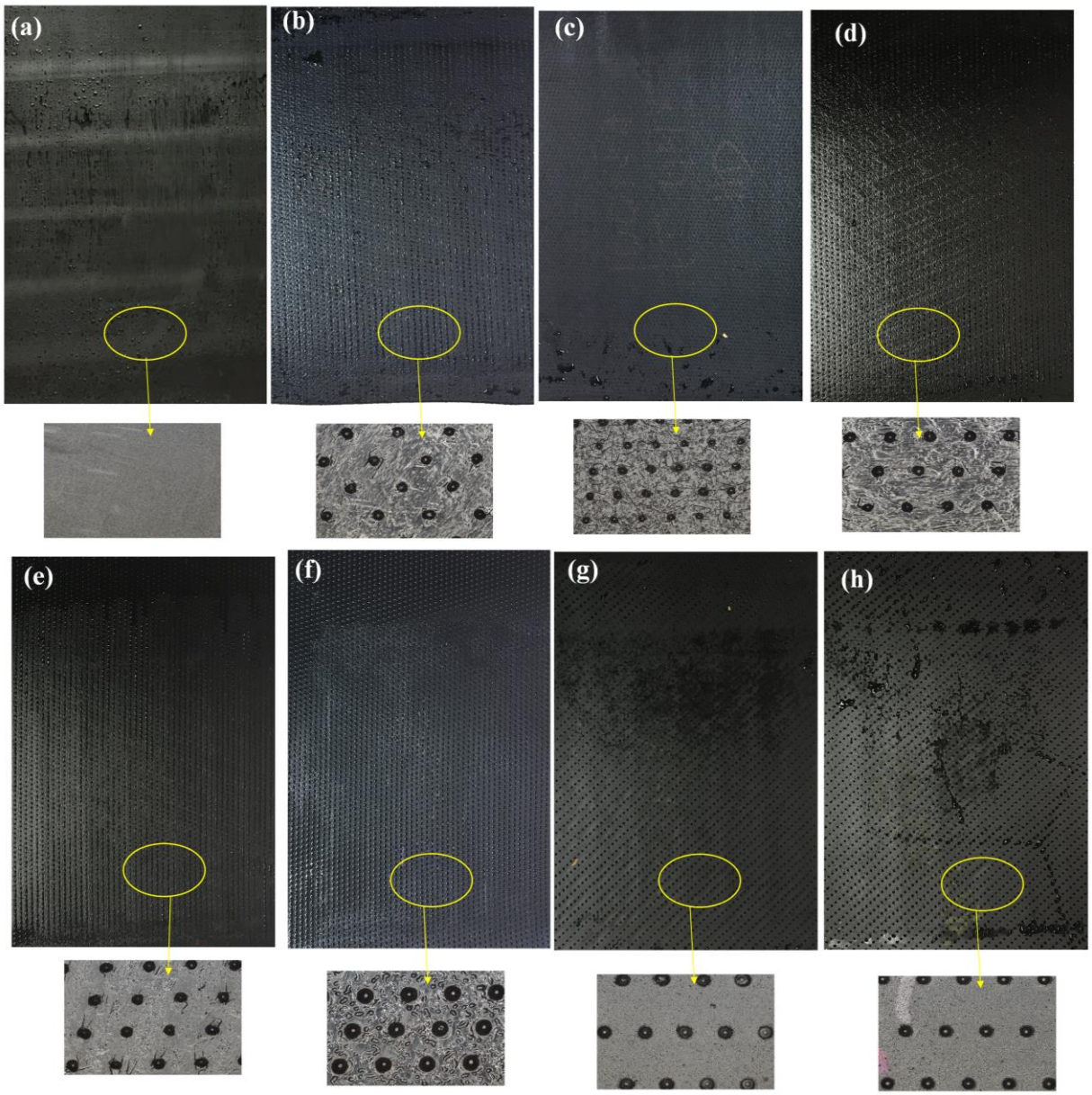

Figure 3-3: Plane and 50X magnification aerial view of geomembrane surfaces (a) GMB-S (b) GMB-T1 (c) GMB-T2 (d) GMB-T3 (e) GMB-T4 (f) GMB-T5 (g) GMB-T6 (h) GMB-T7

Table 3-3: The smooth and textured geomembrane asperity parameter

GMB	*Asp. height (mm)	Asp. density (knobs per 10000mm^2)	Asp. volume (mm^3/ mm^2)	Asp. Spacing (mm)		Asp. inclination θ°	GMB thickness (mm)	Asp. configuration	Asp. shape
				S_x	S_y				
GMB-S	0	0	0	0	0	0	2.0	-	-
GMB-T1**	0.70	332	242	4.34	4.78	56.5	2.0	Straight	Conical
GMB-T2	0.70	663	464	5.75	6.64	75.3	2.0	Straight	Conical
GMB-T3**	0.73	337	246	6.25	6.81	62.6	2.0	Inclined	hook-cone
GMB-T4	0.85	337	287	5.72	6.69	69.6	2.0	Straight	Conical
GMB-T5	1.20	306	367	6.50	6.50	69.6	2.0	Straight	Conical
GMB-T6	1.81	211	382	4.92	7.72	73.7	2.0	Inclined	Cylindrical
GMB-T7	2.02	217	439	6.17	9.76	71.1	2.0	Inclined	Cylindrical

*Asp represents asperity

**GMB-T1 &GMB – T3 were considered to establish the effect of asperity shape

3.3. Apparatus used

3.3.1. Large direct shear

The automated large direct shear device "Shear Trac-III" designed and built by Geocomp Corporation Company, USA was used in this investigation. According to the manufacturer and previous studies by Buthelezi (2017), and Sikwanda (2018), the Shear Trac-III had the capability of carrying out frictional interface tests on soil and geosynthetics, internal friction of geocomposite and direct shear on soil and aggregates. Also, the device could conduct tests under hydrated conditions to typify field conditions, using the water tank (Geocomp, 2018). As the critical interface shear characteristics determination was crucial to this study, the Shear Trac-III was used to determining the geomembrane/geotextile interface shear parameters.

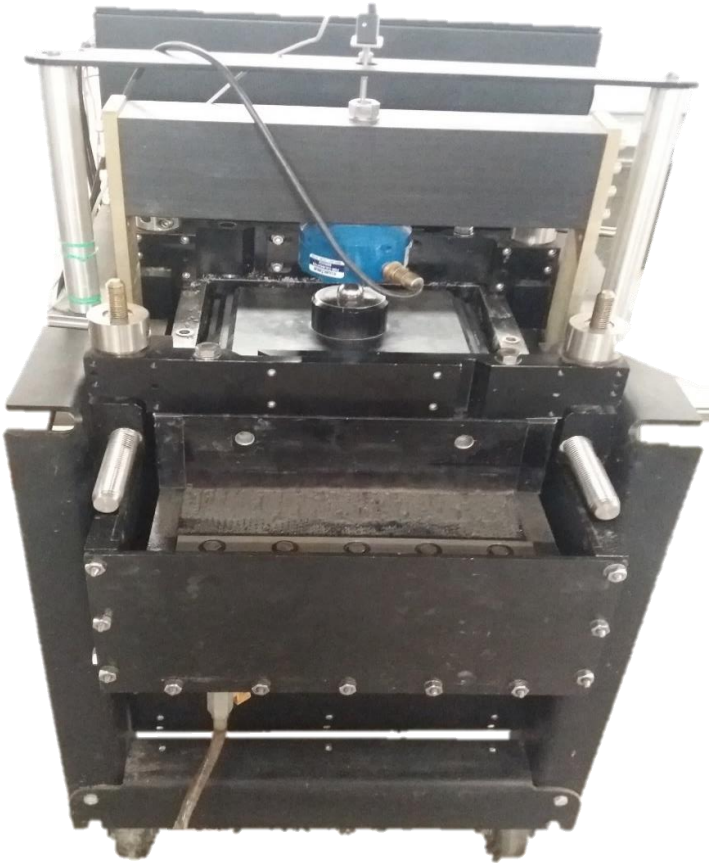

Figure 3-4: Large Shear Trac-III device

The shear device, as shown in Figure 3-4, consisted of a top-static and bottom-moving box. The top-static box had a dimension of 305 mm x 305 mm x 100 mm, while the bottom shear box had dimensions of 460 mm x 355 mm x 100 mm. Also, the lower substrate below the bottom box had a dimension of 400 mm x 300 mm x 100 mm. The device worked on the principle of applied

horizontal-movement of the bottom box against the fixed-top box. In this investigation, the geomembrane samples were screwed to the bottom box while the geotextiles were fastened to the top box. This was carried out to typify side-slope liner, where the geotextile is often placed above the geomembrane to act as its protective layer against the movement of sharp materials subjected to hydrodynamic and gravitational forces.

The device had two force and two displacement transducers sensors. Both transducers could capture horizontal and vertical measurement. Also, they ensure quality test control and prevent the Shear Trac-III from running beyond its physical limits. Geocomp (2018), indicated that the Shear Trac-III had a maximum load capacity of 44.5 kN (10,000 lbs) and maximum normal stress of 450 kPa. Also, shear displacement rate was approximately uniform throughout the width of each interface and duration of the test, the maximum and minimum shear displacement rate the apparatus can accommodate was 15 mm/min and 0.03 μm/min, respectively.

The device was suitable for this investigation as it fulfilled the minimum requirements stipulated by ASTM D5321 (2014) standards. Furthermore, studies by Alzahrani (2017), Buthelezi (2017), Sikwanda *et al.*, (2018a), and Aza-Gnandji *et al.*, (2019) related to geosynthetics had utilized this particular device for the determination of the interface shear parameters; thus, making its result comparable with other research outputs.

3.3.2. Tools required for test specimen preparation

Together with the large direct shear device, several other tools were required to prepare the test samples. Most of these tools were already part of the existing facilities within the laboratory. This section describes their function with a corresponding illustration presented in Figure 3-5.

- Mechanical saw machine: Due to the high tear resistance of geomembranes, the mechanical cutting machine was primarily used to cut it to the required dimension with an accuracy of +0.5 mm.
- Sewing scissor: This pair of 240 mm sewing scissor, was distributed by Fowkes Bros South Africa and was primarily used to cut geotextiles to the size required for the shear test.
- Hammer: The rubber hammer was utilized to punch the gripping holes on the geosynthetics. The holes are essential to secure the test samples to the top and bottom shear boxes.

- Puncher: An eclipse round-head centre punch with a 6.36 mm opening was used to pierce holes on the geosynthetics.
- Rachet: An adjustable rachet was utilised to drive bolts through the clamps and geosynthetics holes into the shear box compartment.

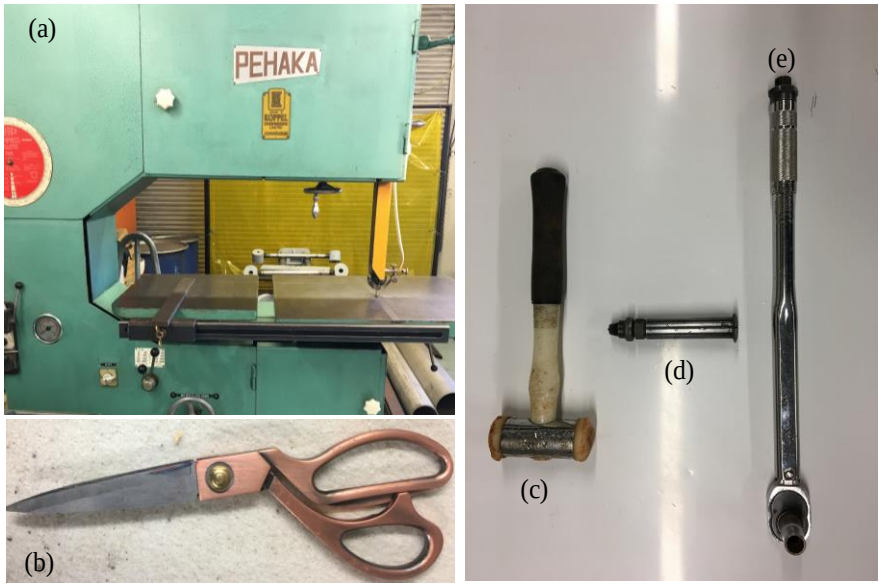

a - Mechanical sawing machine
b - Scissor
c- Rubber hammer
d - Puncher
e - Rachet

Figure 3-5: Accessories used in test sample preparation

3.3.3. Asperity properties and surface roughness measuring device

In this work, the "insize" digital depth gauge and M400 wild microscope were used to measure all textured geomembranes (GMB-Ts) asperity properties (height, spacing, and inclination). Specifically, the "insize" series 1145-25A digital depth gauge was used only for asperity height measurement, while the M400 wild microscope was used to measure all other parameters. Both measuring devices are illustrated in Figure 3-6 a-c. The depth gauge was made from stainless steel and calibrated in both millimetres and inches with a resolution of 0.01 mm and 0.0005", respectively. It had an average height, breadth and thickness of 60 mm, 20 mm, and 15 mm, respectively. Also, its accuracy is $\pm$ 0.03 mm, and it could measure asperity height up to 26.61 mm.

All geomembranes surface roughness measurement in this investigation was carried out with the Keyence VR 3100 3D scanner (Figure 3-6d). This scanner was selected because it was one of the latest and more sophisticated roughness measurement instruments as at the time of this study. It produced surface measurements such as geometry, form, contour, and flatness, along with

more detailed roughness analysis. Also, it could measure vertical relief of up to 10 mm with a maximum vertical resolution of 0.04 nm and optical resolution of 0.1 – 0.5 μm (Keyence, 2020).

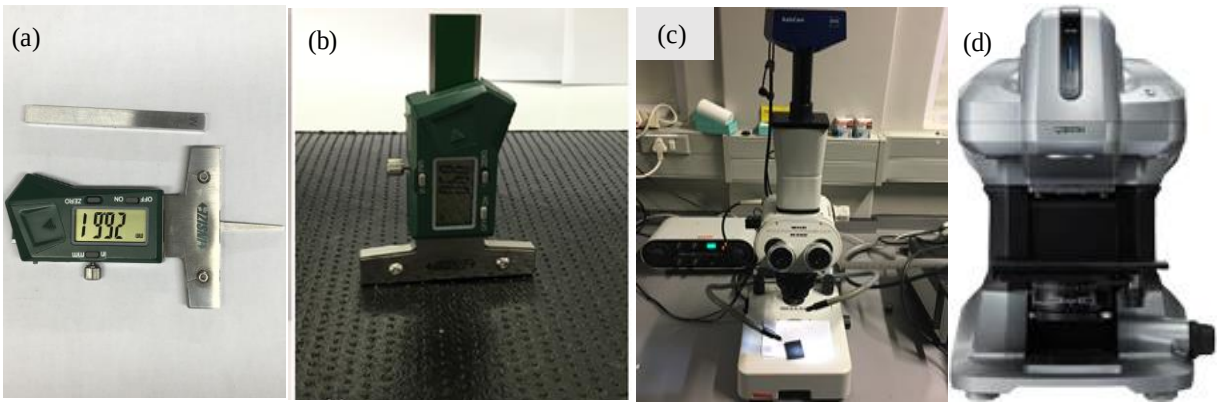

Figure 3-6: GMB surface property measuring device (a) & (b) Insize digital depth gauge; (c) M400 microscope (d) Keyence VR 3100 3D scanner

3.4. Characterization of geomembrane asperity and roughness

3.4.1. Asperity height

As shown in Figure 3-7, asperity height is the average rise of the protrusion from the datum-flat surface. According to Koerner & Koerner (1999) and ASTM D7466 (2015), digital depth gauge and M400 light microscope (6.3x magnification) were used to accurately and repeatably measure the asperity height of all the textured GMB samples investigated in this work. The asperity height measurement with the light microscope was carried out by firstly partitioning the supplied geomembrane roll into small sheets using a standard geomembrane template size of 300 mm x 450 mm (size was determined based on the lower shear box dimension). After which, an 18 mm x 18 mm specimen size was cut from the 300 mm x 450 GMB sheet. The 18 mm x 18 mm specimen size was afterwards carefully placed under the light microscope, and from this position, GMB samples asperity height measurements were taken and recorded.

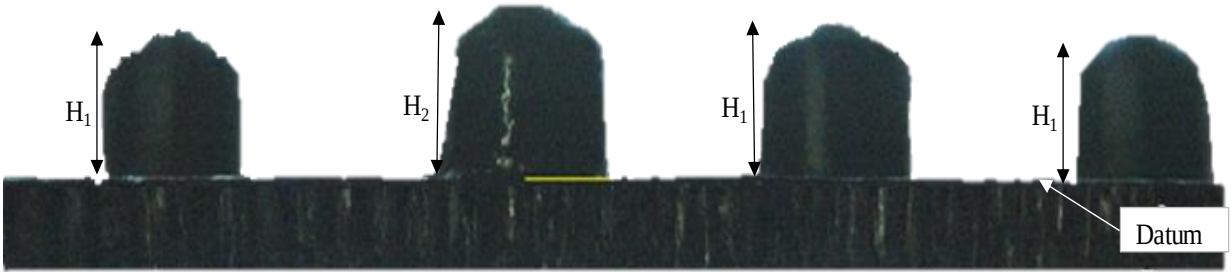

Figure 3-7: Magnified view (6.3x) of textured geomembrane asperity

Alternatively, to measure asperity height with the digital depth gauge, the small GMB sheets (300 mm x 450 mm) cut from the supplied roll were carefully moved and placed on a flat surface and clamped with a vice accordingly to minimise waviness. During the positioning of the GMB for clamping purposes, the surface whose asperity height was intended to be measured was directed upwardly. Subsequently, to initiate the measurement, the Insize digital depth gauge, was positioned perpendicularly on the GMB surface.

To measure the textured GMB asperity height, the 'I'-shaped" steel depth gauge with a measuring probe affixed at the centre, was placed on the HDPE surface. While being held in a vertical position, the measuring probe gauge was lowered slowly in the downwards direction between any two spikes/knobs until initial surface contact of the blunt 0.8 mm diameter micrometre point was made to contact the GMB surface without exerting excess pressure. The micrometre gauge was then read to give the height of the spike/knobs on the GMB surface.

After each measurement, the 50 x 13 cm rectangular steel bar was used to reset the gauge to default calibration. The zero calibration of the gauge was a requirement for accurate measurement, and it was carried out by establishing a surface contact between the gauge and the steel bar on a flat horizontal surface. For each textured GMB sample, the asperity height was obtained by averaging the height measurement at ten equally distributed locations on the sample.

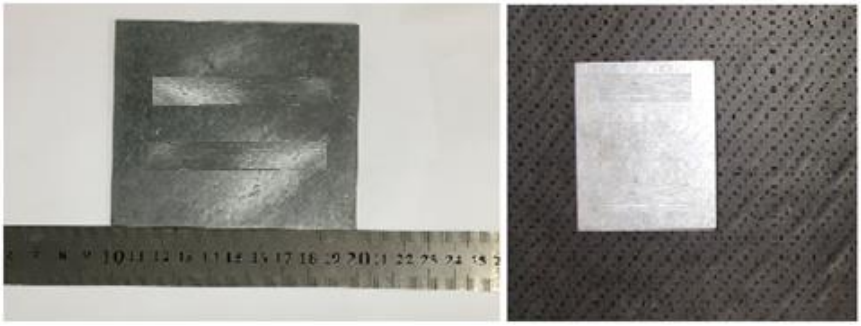

Figure 3-8: Asperity density measurement

3.4.2. Asperity density

According to Shamrock & Jabulile (2014), asperity density is the number of asperities/spikes on a geomembrane surface in a standard area (square millimetre). In this work, asperity density was quantified for all textured geomembranes by counting the spikes within the inscribed square (100 mm x 100 mm) perimeter on the geomembrane sample (see Figure 3-8). The inscribed squares on each GMB were marked out by using a 100 mm x 100 mm metal square plate and a steel pen.

Due to the manufacturing process and probability of asperity variability, asperity density quantification was carried out at three different locations on each textured GMB. Therefore, the average asperity density was obtained from the three measurements.

3.4.3. Asperity volume

Asperity volume (A_v) describes the space in three-dimensional coordinate (3D) directly influenced by asperities and available for material interaction. A_v was introduced as a unified index quantifying combined effects of asperity height and density on the geosynthetics interface behaviour. For this study, asperity volume was considered to be the product of asperity height and density (spacing) for a given geomembrane (see Figure 3-9).

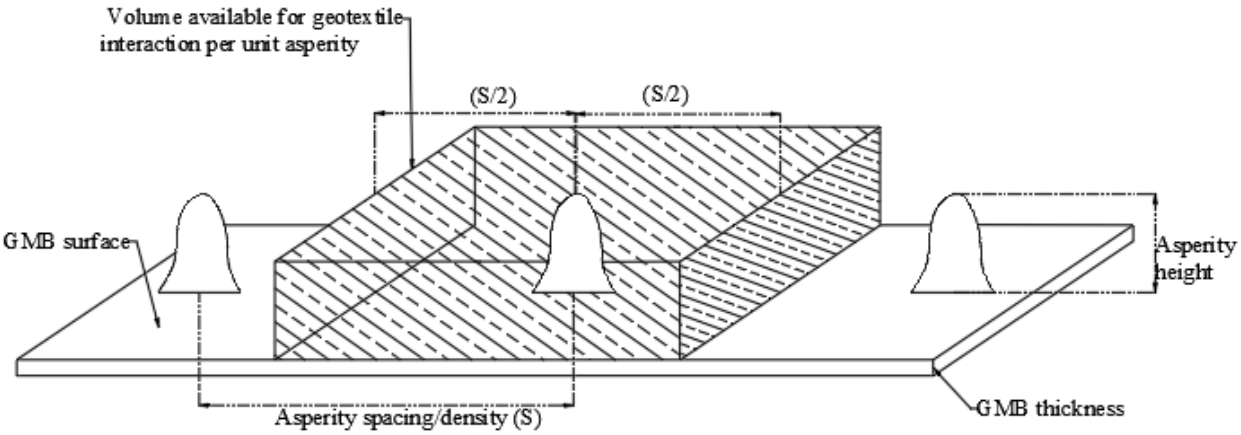

Figure 3-9: Illustration of asperity volume (after Zaharescu, 2018)

3.4.4. Asperity spacing, inclination, and configuration

Asperity spacing is the "centre to centre" linear measurement from two adjacent asperities in the minor (x-axis) or major (y-axis) coordinate. For each GMB-Ts, asperity spacing was measured in millimetres with the wild M400 light microscope and a metre-rule. While the asperity inclination measured in degrees is the angle between the major and minor coordinates. For all geomembranes, asperity inclination varied from 56.5° to 75.3°. Also, the asperity configuration is the angular orientation of the major coordinate about the horizontal axis.

3.4.5. Geomembrane surface roughness

Cut GMB specimens obtained from the supplied roll were trimmed to a recommended dimension of 18 mm x 18 mm to measure the surface roughness, where the sample dimension (18 mm x 18 mm) was very small compared to the overall dimensions of the geomembrane (300 mm x 450

mm). It should be noted that the recommended size was adopted because it perfectly fits into the roughness measurement device. The GMB surface whose roughness was to be measured was cleaned with a damp cloth to eradicate impurities. After which the specimen was coated with a thin metallic layer to ensure measurements accuracy since Keyence VR 3100 3D scanner works on the principle of light interference. The roughness measurement was then carried out on each geomembrane surface sample. The spatial variability of the geomembrane surface roughness was examined by testing five test specimens of the same geomembrane sample. It should be noted that "GRI GM13 specification" was followed to conduct the surface roughness measurement.

3.5. Specimen preparation

The geomembranes (GMBs) and geotextiles (GTXs) samples used in this study were cut to the required sizes from the supplied industrial geosynthetics roll in the machine direction. The machine direction is the direction of the manufacturing of the geosynthetics, and it was selected in order to match the laboratory test conditions to the anticipated site landfill slope direction (Kalumba, 1998; Karademir, 2011).

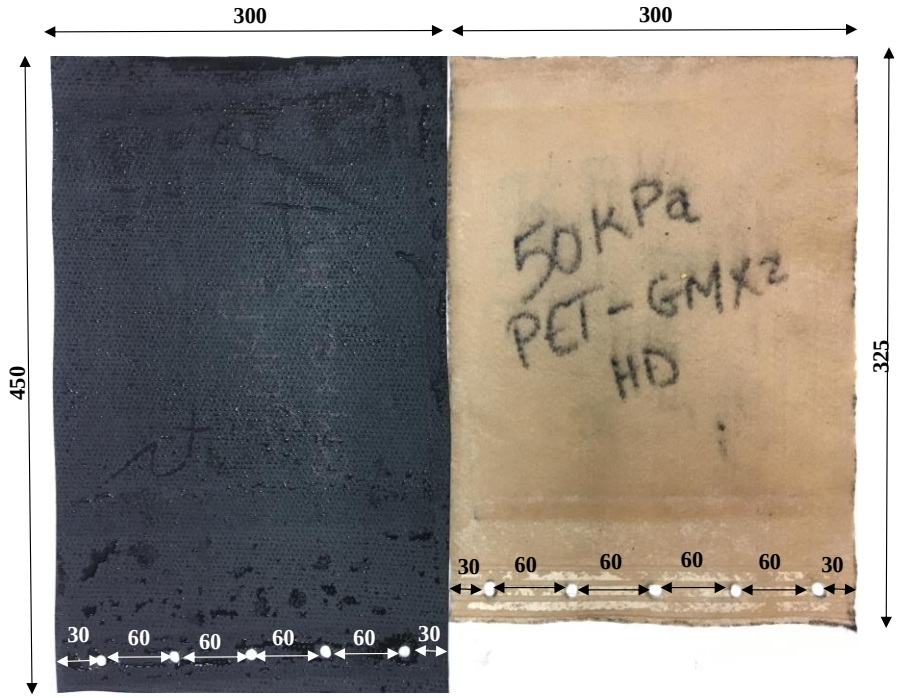

Figure 3-10: Plan view of the geomembrane and geotextile specimen (all dimension in mm)-

The supplied geosynthetics roll was unwrapped and carefully stretched out on a spacious flat surface. A flat surface was required to ensure that the partitioning of the geosynthetics roll into

the rectangular dimension was accurate. The partitioning of the geosynthetics was carried out using a standard geosynthetics-template and a marker. Subsequently, the geotextiles and geomembranes were cut into the required size using a pair of scissors and mechanical sawing machine, respectively. Geotextile and geomembrane specimen sizes (see Figure 3-10) were determined by the dimension of the top shear box (305 mm x 325 mm) and bottom shear box (305 mm x 450 mm), respectively.

In order to minimize surface irregularities, special care was taken in working with the GMBs and GTXs before, during, and after cutting. Also, geosynthetics specimen with excessive abrasions, wrinkles or any forms of damage were not used in the shear test preparation. More so, accurately cut specimens were labelled immediately with a specified code for easy and quick identification during each test set-up. The identification code was determined by the polymer-type, applied stress, and the direction of shear.

Once all test samples were cut into their respective sizes and labelled accordingly, five holes of 10 mm were punched at one edge of each test specimen with the aid of a geosynthetics-template with drilled holes. The geosynthetics-template was used to ensure accurate marking and punching of the holes on the cut geosynthetics. The holes were created using a 10 mm diameter mechanical-hole puncher and a hammer and were 30 mm from the edge and spaced at 60 mm apart (see Figure 3-10). These holes were necessary to secure the test specimen to the shear box together with the clamping system (washers and nuts) and to provide enough resistance which holds the specimen in position before and during shearing.

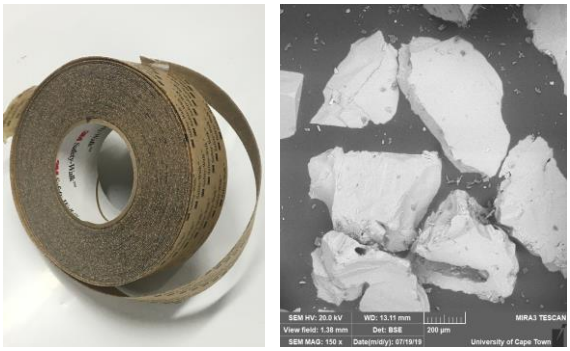

Figure 3-11: (a) 3M sandpaper roll (b) 150 x magnification of sandpaper SEM

Before affixing the geosynthetics to the shear boxes for the shear test, 3M sandpaper was used as a component of the gripping system, based on the recommendation by Sikwanda *et al.*, (2018b). A pair of scissor was used to cut the 50 mm width of sandpaper from the supplied roll

to the required length which was according to the shear box dimension (see Figure 3-11). The cut sandpaper pieces were glued closely to each other on the top and bottom boxes and allowed to cure (harden) for about 30 minutes. The top and bottom box surfaces covered with sandpaper were necessary to enhance the gripping system, to minimises the occurrence of slippage between the geosynthetics and the shear box, and to prevent the geotextile from stretching during testing (Kalumba, 1998).

After each set of completed interface test, it was imperative to replace the sandpaper for the subsequent tests. The procedure for removal and cleaning was; to first remove the used sandpaper with a sharp blade. After which, any impurities on the substrate surface were wiped off with paraffin oil. To further cleanse the metal surface, the lower box and top box gripping surfaces were washed with soap and water. After which the metal surfaces were cleaned with acetone. Acetone, being a suitable solvent for plastics and synthetics fibres was used to dissolve minute glue particles before installing the new sandpaper. The surface was left to dry for a minimum of 12 hours before the new sandpaper was placed.

3.6. Experimental procedures

The interface shear tests were divided into two groups: the smooth geomembrane (control) and the textured geomembrane (varied) test. For both control and varied tests, geomembranes were sheared against the polypropylene and polyester geotextiles at identified normal stresses. It should be noted that all the tests were prepared and carried out according to ASTM D5321 (2014) recommendations.

The cut geomembrane specimens (305 mm x 450 mm) were placed on the lower shear box directly above the sandpaper and fastened adequately to the lower shear box with a clamping system. Also, the trimmed geotextiles specimens (305 mm x 325 mm) were fastened with a similar clamping system to the upper box (see Figure 3-12). Each clamping system comprises a clamping plate and five bolts. The bolts were fastened into the metal strip holes of the clamping plate using a racket bolt-driver, this was necessary to prevent the movement of the sample during the direct shear test. Significantly, the operating torque of the racket bolt-driver was carefully selected based on the bolt tensile strength and thread size, because inaccurate torque could damage the bolts and ultimately affects the shear device.

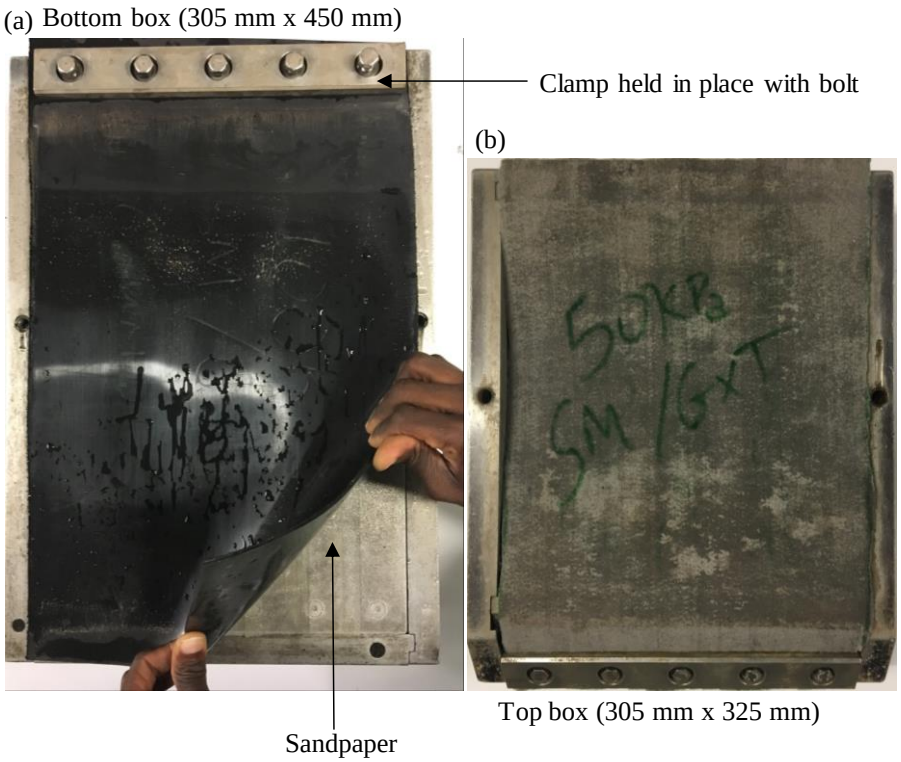

Figure 3-12: Fixation of geosynthetics to the bottom and top shear box

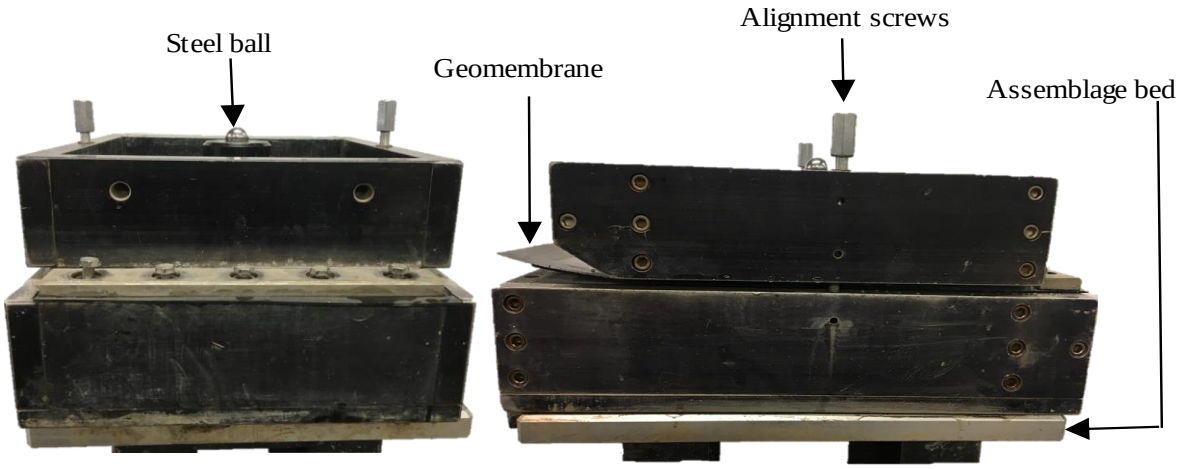

Figure 3-13: The front and side view of the top and bottom box

After the geomembranes and geotextiles were mounted unto their respective boxes, both surfaces were dampened with water. This was intended to simulate condensation/natural moist condition that can develop during a warm day and a cool night in the field. After this, the upper box, together with the geotextile, was carefully placed on the geomembrane and lower box which was sitting on the "assemblage bed", as shown in Figure 3-13. This positioning was required to ensure that the geotextile was in contact with the geomembrane and that both specimens were flat and,

free of folds, and wrinkles as well as facilitate proper interface shear interaction (ASTM D5321, 2014). Also, to assist the accurate positioning of the boxes, alignment screws were used to hold the boxes in place (see Figure 3-13).

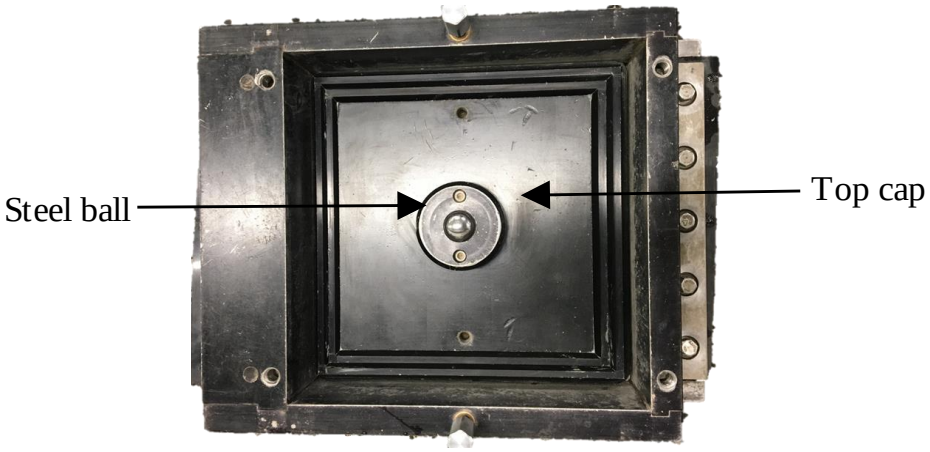

Figure 3-14: Plan view of the top and the bottom shear box together with cap and steel ball

With the shear boxes properly align, the upper gripping surface was then positioned in the top box. Afterwards, a top cap together with the stainless-steel ball was carefully placed inside the top shearing box, as illustrated in Figure 3-14. The aluminium top cap with mass and dimensions of 10 kg and 300 mm x 300 mm x 22 mm, respectively, was required to transfer the pressure from the vertical load-cell to the geosynthetics interface. Also, the stainless-steel ball with mass and diameter of 79.1 g and 26.6 mm, respectively, was placed on the top cap to make contact with the load-cell. This arrangement was required to ensure the applied load was uniformly distributed to the geosynthetics interface with little or no frictional loss. The complete shear test setup on the assemblage bed (see Figure 3-15) was then cautiously slid to the ShearTrac-III base container.

With the help of the connected computer desktop, the test assemblage was moved both horizontally and vertically to ensure that the loading plate was aligned properly with the vertical load cell of the device. Given that the top shearing box was designed not to move during each test, it was kept in position by the two steel reaction beams (front and rear reaction beams), which were screwed to the machine frame. Importantly, before a shear test could be initiated, the two aligning screws holding the top and the bottom shear box together was carefully removed without causing any form of distortion to the test assemblage.

After fulfilling the material and equipment setup requirements, the specialized ShearTrac-III software was launched via the laboratory desktop computer. The software was used to initiate the shear test after the essential parameters such as shear displacement rate (SDR), normal stress, consolidation duration (maximum and minimum), maximum displacement, and project specifications were correctly entered.

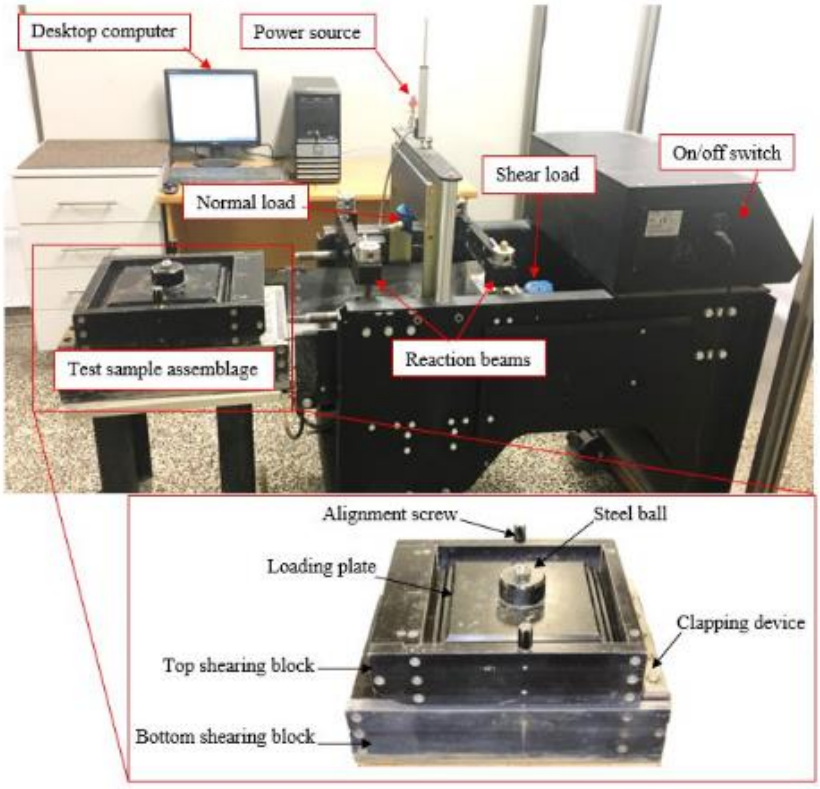

Figure 3-15: Complete setup of apparatus (after Sikwanda, 2018)

As recommended by ASTM D5321 (2014), the constant shearing rate of 1.0 mm/min was utilized for all tests as no excess pore pressures were observed at the interface. Also, the shear rate was selected to allow for comparison with other published literature (Orebowale, 2006; Buthelezi, 2017; Sikwanda, 2018). The shear tests were performed at normal stresses of 25, 50, 100, 200, 400 kPa to represent the varying load conditions experienced at a typical landfill liner system (Chrysovergis, 2012).

The tests were carried out in saturated conditions to represents moist field condition. As recommended by Stark *et al.*, (2015), a hydration time of one hour was used for the GMB/GTX interface; as there were no soils in the setup and the time was sufficient to consolidate the geosynthetics interface. After the tests had been initiated, an indication on the test monitor

prompted the introduction of the saturation solvent; which in this case was water. Clean water from the laboratory was used for the saturation conditioning during the consolidation stage.

At the end of the consolidation stage, a gap of approximately 1 mm to 5 mm between the upper box and the lower box was created. According to ASTM D5321 (2014), the created gap must be large enough to avoid friction between the boxes during shear. The shear test at the GMB/GTX interface was initiated after the gap was created. The horizontal force that produced the shearing was calculated by the direct shear program and was applied to the lower shear box through a lead screw of 37.5 mm and a hydraulic motor. During the shearing stage, the ShearTrac-III program recorded data from the displacement and load LVDTs, maintaining a constant shear rate, and captured recorded data in an output file.

Table 3-4: Test program summary for all interfaces

GTX	GMB	Consolidation time (min)	Shearing rate (mm/min)	Normal stress (kPa)	No of tests
GTX-PP	GMB - S	60	1.0	25, 50, 100, 200, 400	5
	GMB – T1	60	1.0	25, 50, 100, 200, 400	5
	GMB – T2	60	1.0	25, 50, 100, 200, 400	5
	GMB – T3	60	1.0	25, 50, 100, 200, 400	5
	GMB – T4	60	1.0	25, 50, 100, 200, 400	5
	GMB – T5	60	1.0	25, 50, 100, 200, 400	5
	GMB – T6	60	1.0	25, 50, 100, 200, 400	5
	GMB – T7	60	1.0	25, 50, 100, 200, 400	5
GTX-PET	GMB - S	60	1.0	25, 50, 100, 200, 400	5
	GMB – T1	60	1.0	25, 50, 100, 200, 400	5
	GMB – T2	60	1.0	25, 50, 100, 200, 400	5
	GMB – T3	60	1.0	25, 50, 100, 200, 400	5
	GMB – T4	60	1.0	25, 50, 100, 200, 400	5
	GMB – T5	60	1.0	25, 50, 100, 200, 400	5
	GMB – T6	60	1.0	25, 50, 100, 200, 400	5
	GMB – T7	60	1.0	25, 50, 100, 200, 400	5
					80

3.7. Test program

A total number of 80 direct shear testing were conducted at normal stresses of 25, 50, 100, 200 and, 400 kPa. The stresses were selected based on the recommendation by Chrysovergis (2012), where it was suggested that to accurately represent typical landfill liner conditions, the direct

shear test should be performed at stresses ranging from 25 to 400 kPa. Where 25 to 50 kPa and 100 to 400 kPa, represent cover liner and basal/side slope liner, respectively. Therefore, the complete test program and essential input parameter for the direct shear test are presented in Table 3-4.

3.8. Data processing

3.8.1. Shear output parameters

The automated ShearTrac-III, and the connected computer set up, which could record and store shear data from experiments, were used for the shear test. Data obtained from the test was used to derive shear parameters, tables and figures. Plots such as shear stress against horizontal displacement, peak displacement against normal stress, and shear stress versus applied normal stress which represents the failure envelope were obtained after each test.

The process of deriving the figures involves raw data exportation from the ShearTrac-III report to a similar template in Microsoft Excel software. From this template, multiple analyses were carried out on horizontal displacement, vertical displacement, and horizontal stress, with results plotted as graphs. For each complete interface test, a line or curve of best fit was drawn to connect the points on the graph of shear stress against normal stress; this line establishes the Mohr-Coulomb failure plane. The equation of the failure plane presents the interface friction angle and the apparent adhesion value; the former is obtained from the slope of the line or curve while the latter is the intercept on the shear stress axis.

3.8.2. Mohr-Coulomb criterion

The failure criterion by Mohr-Coulomb is the simplest and most widely used criterion as recommended by ASTM D5321 (2014). It assumes that the failure between soil or geosynthetics would occur along a plane due to the shear stress acting along that plane. Researchers such as Rouncivell (2007) and Bacas *et al.*, (2015a), have utilised the Mohr-Coulomb criterion to model geosynthetics interface frictional behaviour. According to ASTM D5321 (2014), a properly defined Mohr-Coulomb shear strength envelope, which is represented by Equation 3-1 describes the linear relationship between shear and normal stress. The interface shear strength (τ) is obtained by the summation of the frictional force ($\sigma\ tan\delta$) and apparent cohesion force of the

material (c_a). Depending on the type of geosynthetics materials tested, adhesion could be negligible (Bacas *et al*., 2015a).

$$\tau = c_a + \sigma_n \tan\delta$$

Equation 3-1

where:

$\tau =$ Peak or large displacement shear strength

$c_a =$ Apparent adhesion taken as the y-intercept value

$\sigma_n =$ Applied normal stress

$\delta =$ Interface friction angle

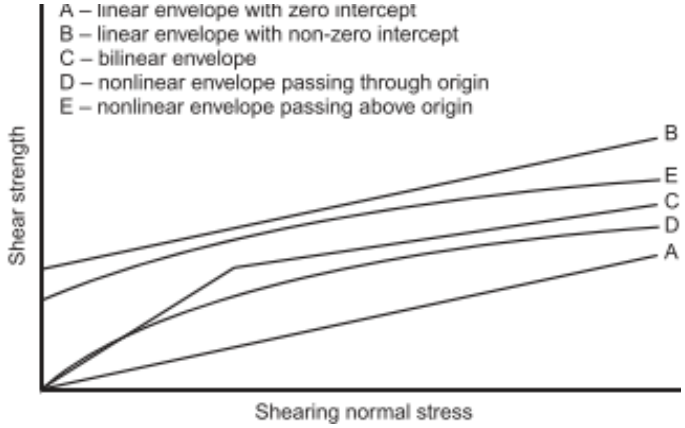

Figure 3-16: Standard shear strength envelopes for geosynthetics interfaces (Fox & Stark, 2009)

However, it is not unusual to obtain non-linear and multi-linear shear-normal stress relationships in geosynthetics interface (Bacas *et al.*, 2011; Karademir, 2011; and Chrysovergis, 2012). In such instances, other "best-fit" options besides linear envelope as shown in Figure 3-16 could be used. According to Bacas *et al*., (2015b), non-linear/curvilinear failure envelope shear parameter could be estimated by a mathematically generated hyperbolic function as given by Equation 3-2. Non-linear failure envelope parameters can also be obtained by using linear approximation, which entails drawing a tangent to the curve at each stress-level to obtain δ and c_a. The average of the obtained shear parameters for the stress-range is taken as the non-linear failure envelope shear parameter (Thiel, 2001; Fox & Stark, 2004; and Fox & Stark, 2015).

$$\tau = a{\sigma_n}^2 + b\sigma_n + c_a$$

Equation 3-2

where:

$\tau =$ Peak or large displacement shear strength

$c_a =$ Apparent adhesion taken as the y-intercept value

$\sigma_n =$ Applied normal stress

$a\ and\ b =$ Hyperbolic functions

3.9. Quality assurance

3.9.1. Controls adopted

In order to ensure repeatability of results from the interface tests carried out in this study, some measures were strictly followed to minimise the risk of errors. They are as follows;

- All interface tests incorporated geosynthetics specimens which were carefully cut from the supplied geosynthetics rolls with a standard rectangular geosynthetics-template.
- Cutting of each geosynthetic sample was carried out in the machine direction as indicated by the supplier.
- To ensure that the intended field conditions were correctly represented, all interface tests were conducted with the geosynthetics affixed to the appropriate boxes.
- To ensure that no geosynthetics samples were reused, a new and fresh set of test specimens were used for each interface shear experiment.
- All interface shear tests were conducted according to ASTM D5321.
- To ensure that the same quality of water was used during the saturation stage of all interface tests, only tap water from the geotechnical engineering laboratory was utilized.
- During the experimental procedure, standard calibration of the direct shear device was performed as recommended by Geocomp (2012) and ASTM D5321.
- As recommended by ASTM D5321, all interface shear tests were conducted at room temperature and relative humidity of 22 ^{0}C and 50 – 70 %, respectively.

3.9.2. Repeatability of test results

In order to demonstrate the repeatability of the test results from the experimental procedure, three repeats of selected GMB/GTX interface tests were performed at applied normal stresses of 25 kPa and 400 kPa. These stresses were selected as they represented the lowest and highest stresses acting on a typical landfill (cover, side slope, and basal) liner in this study. The repeated tests were carried out on both polypropylene (GTX – PP) and polyester (GTX – PET) geotextiles at

the same conditions with other tests. Each set of the three curves presented in Figure 3-17 a & b signifies the behaviours of the first, second, and third interfaces shear test for identical specimens. The close match of measured responses from these tests confirms the repeatability of the test results. Likewise, the GMB/GTX interface similar peak displacement (displacement required to attain peak shear stress) proved the procedure's reproducibility.

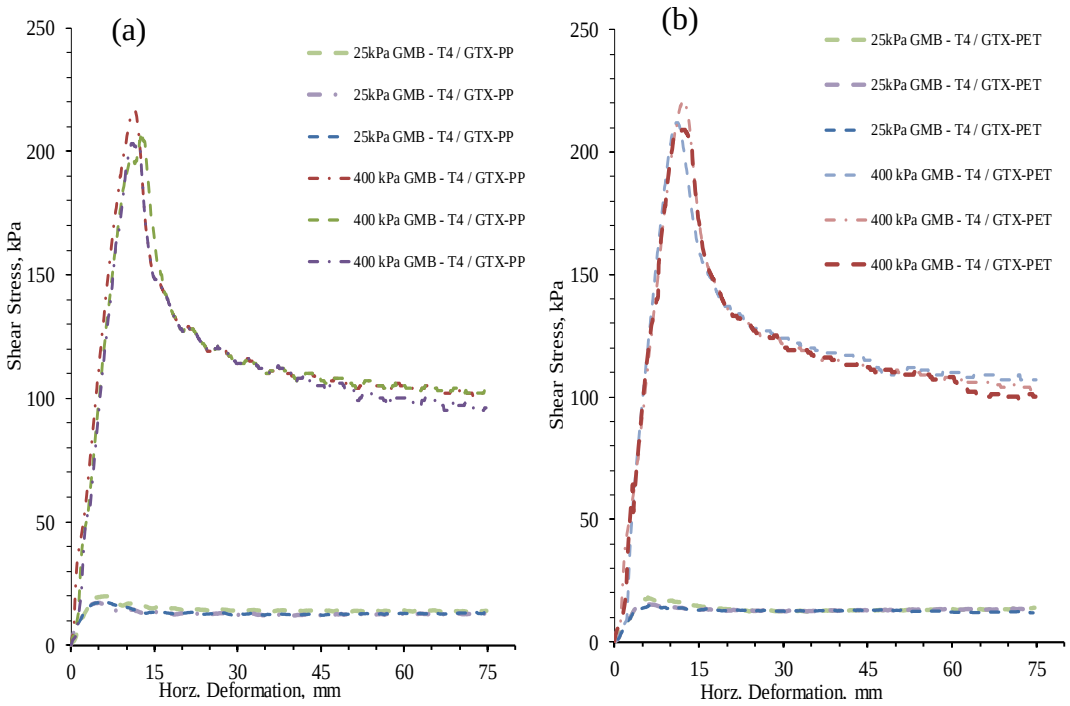

Figure 3-17. Shear stress versus horizontal displacement for GMB-T4 against (a) GTX-PP (b) GTX-PET

In examining the repeatability results presented in this study, the percentage difference (PD) of 10 % was considered to be the upper limit (Carlson, 2002). The PD between the different peak and large displacement (LD) stresses were computed using Equation 3-3 (Carlson, 2002).

$$PD = \frac{|E_1 - E_2|}{\left[\frac{E_1 + E_2}{2}\right]}$$

Equation 3-3

Where PD = Percentage difference

E_1 = Initial experimental value

E_2 = Final experimental value

The data presented in Table 3-5 indicated that the maximum deviation from the peak and large displacement (LD) stress average was 7.11 % and 8.65 %, respectively. The degree of accuracy

obtained from the interface shear test was within the maximum allowable deviation from the mean value, according to Carlson (2002). Hence, the experimental procedure followed was reproducible and repeatable, as seen from the results consistency. The repeatability tests thus verified that the testing procedures and sample preparation followed in conducting the tests were consistent, as the PD in peak stress and LD stress were all below the 10 % capping value.

Table 3-5: Repeatability result analysis for GMB – T4/ GTX interface

Interface Specimen	Peak stress (kPa)	Mean peak stress (kPa)	Deviation from mean		LD stress (kPa)	Mean LD stress (kPa)	Deviation from mean	
			kPa	%			kPa	%
GMB–T4/GTX-PP/25-1	19.7	18.3	1.4	7.1	13.9	13.5	0.4	3.1
GMB–T4/GTX-PP/25-2	17.3		-1.0	5.8	13.1		-0.4	2.8
GMB–T4/GTX-PP/25-3	17.9		-1.0	5.5	13.4		-0.1	0.5
GMB–T4/GTX-PP/400-1	216.0	209.0	7.0	3.2	103.0	100.0	3.0	2.9
GMB–T4/GTX-PP/400-2	208.0		-1.0	0.5	101.0		1.0	0.1
GMB–T4/GTX-PP/400-2	203.0		-6.0	3.0	96.0		-4.0	4.2
GMB–T4/GTX-PET/25-1	16.9	15.7	1.2	6.9	14.0	12.9	1.1	7.6
GMB–T4/GTX-PET/25-2	15.5		-0.2	1.5	12.9		-0.0	0.2
GMB–T4/GTX-PET/25-3	14.8		-0.9	6.3	11.9		-1.0	8.7
GMB–T4/GTX-PET/400-1	212.0	214.0	-2.0	0.9	107.0	103.7	3.3	3.1
GMB–T4/GTX-PET/400-2	221.0		7.0	3.2	104.0		0.3	0.3
GMB–T4/GTX-PET/400-3	209.0		-5.0	2.4	100.0		-3.7	3.7

4. RESULT, ANALYSIS, AND DISCUSSION

4.1. Introduction

This chapter initially presents geomembrane roughness profiles and measurements. After which the result of the tests performed to investigate the effects of asperity height, density, volume and shape on the geomembrane/geotextile interface shear characteristics are presented. Test responses, such as interface shear stress, horizontal displacement, peak displacement, friction angle, and apparent adhesion, are further analysed with varying applied stress, asperity properties, roughness, and geotextile polymer. Lastly, the influence of surface roughness and asperities on the interface shear mechanism and a summary of the research findings are presented and discussed in the concluding section.

4.2. Geomembrane roughness

The roughness measurement and profile of all investigated geomembrane are presented in this section.

4.2.1. Geomembrane roughness profile

Generally, geomembranes roughness profiles are described by terminologies such as waviness, valley, peak, asperity, and microtopography according to international measurement standards (Zaharescu, 2018). Also, measurement parameters such as average roughness, root-mean-square (RMS), and maximum surface roughness parameter are used to describe geomembranes geometrical variability between asperities and the resulting shear interaction patterns (Zaharescu, 2018). In this study, a 3D scanner (Keyence VR 3100) was deployed to obtain the surface roughness profiles of the geomembranes, where measurements of area and line roughness were obtained for each geomembrane. It should be noted that the difference in observed GMB roughness was attributed to the manufacturing processes and material characteristics.

4.2.1.1 Geomembrane area roughness profile

GMB area roughness, as illustrated in Figure 4-1, is the measurement of the change in vertical relief in an aerial perspective. It is characterised by amplitude parameters namely: average area roughness (S_a), maximum area roughness (S_z), and square root area roughness (S_q). The average area roughness (S_a) is the average change in vertical relief measured on the area, whereas the maximum area roughness (S_z) is the maximum peak-to-valley asperity height measured. In

addition, the square root area roughness (S_q) is the standard deviation of the asperity heights above and below the datum (Zaharescu, 2018). In this work, measurements were taken on five different specimens to obtain an accurate representation of the GMB sheet roughness parameters. The measurement reveals the nature of the regular or irregular topography of the GMB surface. It was evident from Figure 4-1 that all GMB had specific surface and asperity features, where GMB-T2 and GMB-T5 have largest surface roughness and taller asperities, respectively (see Figure 4-1 c&f).

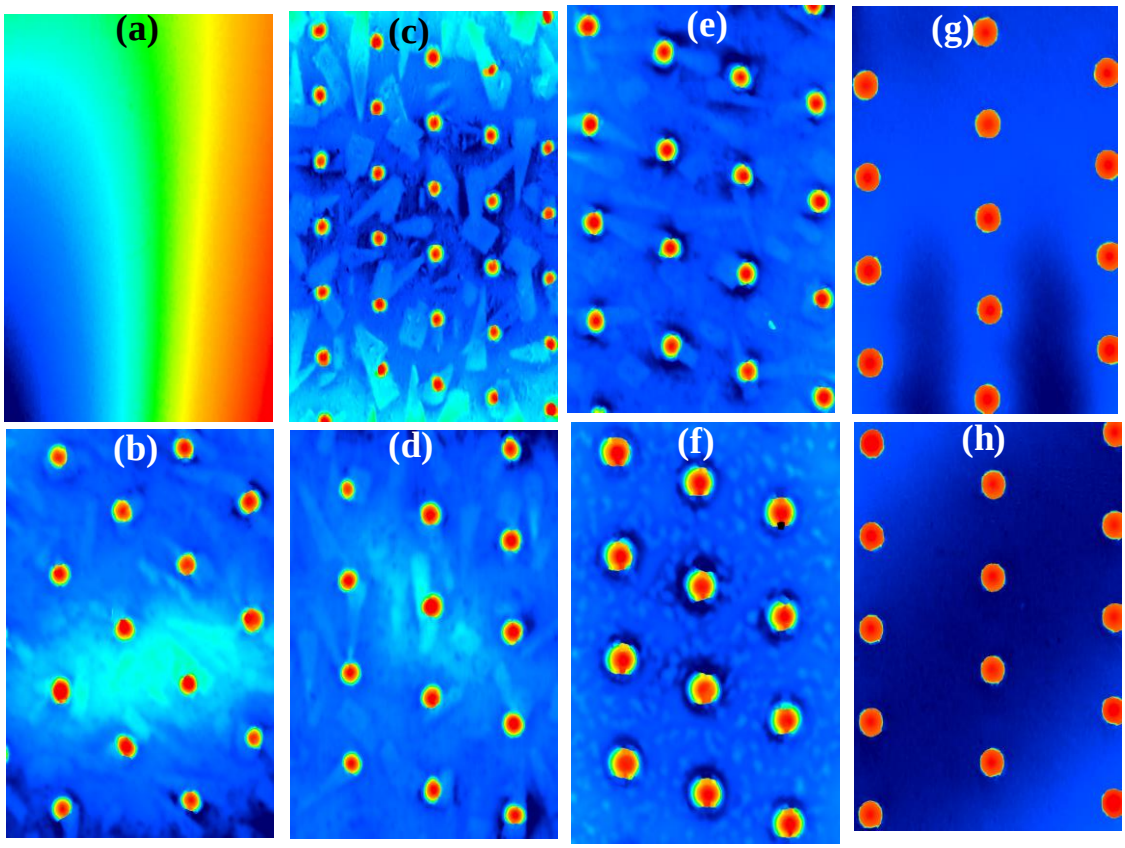

Figure 4-1: Geomembranes surface roughness; (a) GMB-S (b) GMB-T1 (c) GMB-T2 (d) GMB-T3 (e) GMB-T4 (f) GMB-T5 (g) GMB-T6 (h) GMB-T7 (note that height values represented by the warm and cool colours vary between the images)

4.2.1.2 Geomembrane line roughness profile

Similarly, geomembrane line roughness is the sectional roughness view taken across an imaginary line on the GMB surface. Again, the 3D scanner was used to generate GMB line roughness profiles, which were characterised by average line roughness (R_a) and maximum line roughness (R_z). In this work, each specimen was represented by six lines roughness profile/section (1-1, 2-2, 3-3, 4-4, 5-5, and 6-6). The first three sections (lines 1-1, 2-2, and 3-3)

represents roughness profile along asperities while the last three sections (lines 4-4, 5-5, and 6-6) denotes roughness profile between-asperities (see Figure 4-2). The roughness along-asperities profile quantifies the height of ridges along and around the asperities, while the roughness between-asperities is the measure of micro-ridges present on the GMB plane surface. Figure 4-3 illustrates the "along-asperities" line roughness profile, which indicates each geomembrane asperity heights and spacing on the y-axis and x-axis, respectively. While Figure 4-4 illustrates the "between-asperities" line roughness profile. The observed asperities heights, spacing and shape were in good agreement with geomembrane asperity properties presented in Table 3-3.

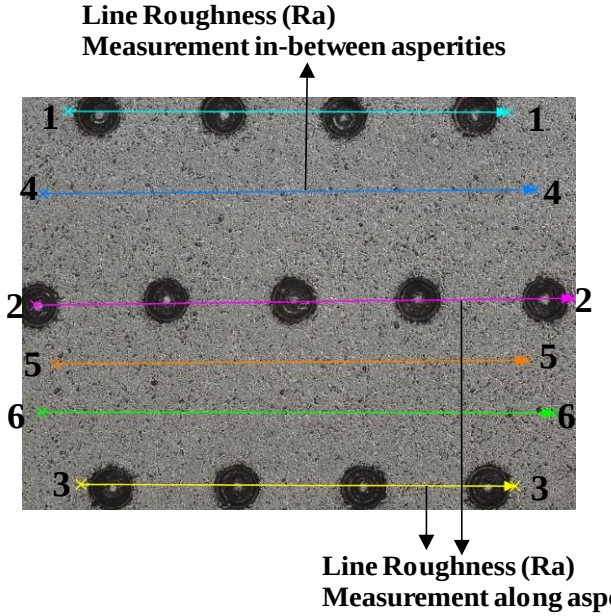

Figure 4-2: 50X magnification line roughness profile along and between-asperities

As will be discussed later in this chapter, the surface roughness of a GMB sheet can improve its interface shear resistance when sheared with other geomaterials such as geotextiles. The line profile for each geomembrane is presented to provide an illustrative viewpoint through which interface shear interaction can be evaluated. Figure 4-3 illustrates the macroscale (asperities) and microscale roughness, while Figure 4-4 mainly shows the microscale roughness. Also, the shape of the asperities and surface waviness was also noticed from the roughness profile. In particular, it was observed from Figure 4-4 that each GMB displayed a specific undulating trend, where each undulation profile exhibited a high and low altitude. Also, as shown in Figure 4-4, GMB-S, GMB-T1, GMB-T6, and GMB-T7 exhibited gentle undulating trends, whereas GMB-T2, GMB-T3, GMB-T4, and GMB-T5 exhibited sharp undulating trend. It is anticipated that sharp undulating trend would cause increased frictional resistance more than a gentle undulating trend

because of the propensity to contribute to the interface hook and loop interaction (Chrysovergis, 2012).

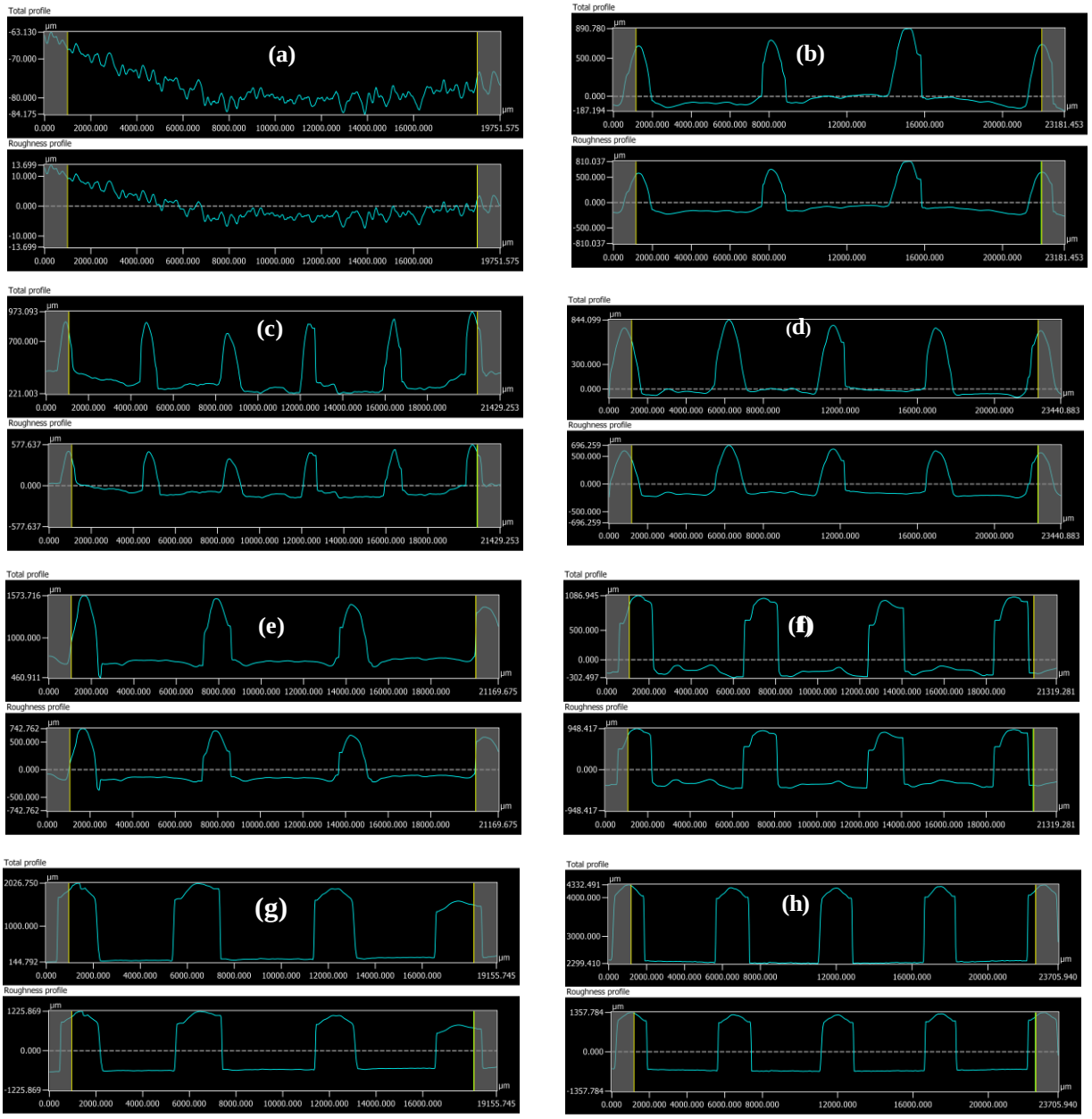

Figure 4-3: Along-asperities line roughness profile at reference scale of 0.1 µm for(a) GMB-S (b) GMB-T1 (c) GMB-T2 (d) GMB-T3 (e) GMB-T4 (f) GMB-T5 (g) GMB-T6 (h) GMB-T7

Alongside the graphical representation of the roughness profiles, each geomembrane-specimen area and line roughness measurements were recorded from the 3D scanner. The geomembrane average area-roughness value was obtained from five specimen roughness data. Similarly, for each geomembrane, the scanner recorded five specimens line roughness measurements (along-

asperities and between-asperities). Table 4-1 presents both surface (S_a, S_z, and S_q) and line roughness (R_a and R_z) parameters for all geomembranes.

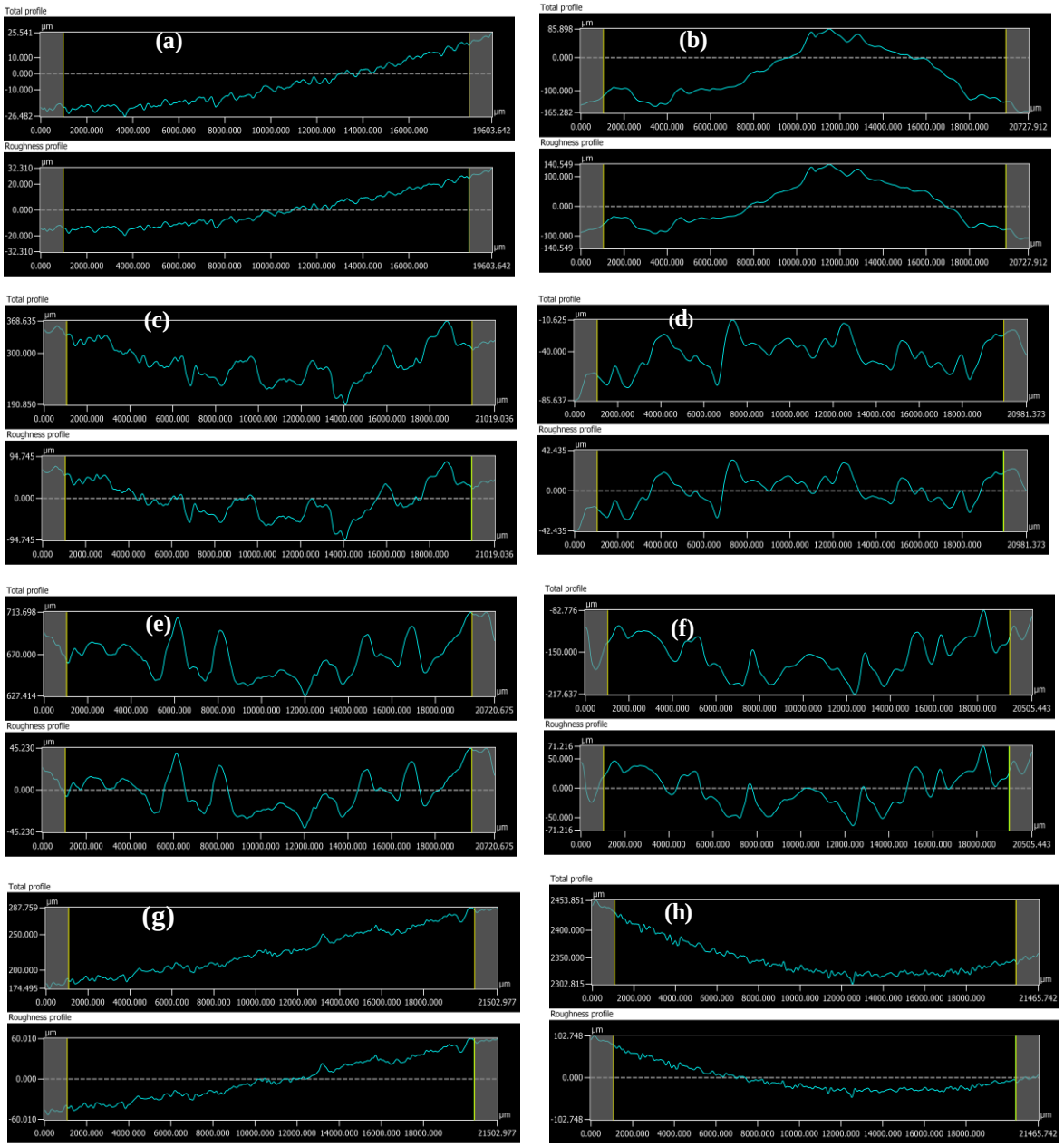

Figure 4-4: Between-asperities line roughness profile at reference scale of 0.1 µm for (a) GMB-S (b) GMB-T1 (c) GMB-T2 (d) GMB-T3 (e) GMB-T4 (f) GMB-T5 (g) GMB-T6 (h) GMB-T7

Each geomembrane roughness measurement was recorded in three categories; namely average (a), maximum (z), and RMS (q) measurements. Though the maximum roughness measurement is in good agreement with measured asperity height, the average roughness measurement exhibited special features that distinguish each geomembrane, therefore, it was used to further

characterise each geomembrane. From Table 4-1, the smallest roughness measurement was attributed to GMB-S with average surface roughness, along-asperities line roughness, and between-asperities roughness of 19.77, 9.09, and 6.61 μm, respectively. The introduction of texturing to smooth geomembrane surface resulted in a significant increase of the roughness parameters, where GMB-T6 exhibited the highest average area and line roughness value of 201.89 μm and 708.22 μm, respectively. For the geomembranes considered, the average area surface roughness, average along-asperities line roughness and average between-asperities line roughness measurements ranged from 19.77 μm to 198.68 μm, 9.09 μm to 708.22 μm, and 6.61 μm to 30.18 μm, respectively. Also, it was observed that area surface roughness (S_a) increased directly proportional to the increase in along-asperities line roughness. On the contrary, random changes in between-asperities line roughness caused an increased in S_a measurement. Therefore, since line roughness measurements provide more material details and influences area roughness measurements, they were prioritized over area roughness measurements for the shear strength comparative analysis discussed later in this chapter.

Table 4-1: Summary of geomembrane surface and line roughness measurement

GMB	Surface Roughness (μm)			Line Roughness along-asperities		Line Roughness between-asperities	
	S_a(μm)	S_z(μm)	S_q(μm)	R_a (μm)	R_z (μm)	R_a (μm)	R_z (μm)
GMB-S	19.77	167.15	24.55	9.09	41.30	6.61	29.62
GMB-T1	60.17	907.00	93.59	146.83	725.10	29.90	154.49
GMB-T2	63.99	912.86	105.86	172.43	759.51	30.18	164.73
GMB-T3	64.05	896.50	89.28	186.55	666.00	28.29	129.75
GMB-T4	63.92	1066.30	125.91	228.15	928.41	17.55	96.76
GMB-T5	140.77	1622.88	248.49	434.71	1375.59	24.50	139.43
GMB-T6	201.89	2081.63	401.69	708.22	1911.09	26.66	109.96
GMB-T7	198.68	2246.46	413.23	696.11	2064.32	21.64	101.26

4.3. Influence of asperity shape on interface shear characteristics

4.3.1. Introduction

One of the geomembrane feature identified in the along-asperities profile as shown in Figure 4-4 is the asperity shape and this section present and discusses the result of shear tests conducted on

GMB/GTX interface as asperity shape was varied while other asperity parameters and test conditions remained unchanged.

4.3.2. Influence of asperity shape on the GMB/GTX interface shear stress – horizontal displacement relationship

In this study, in order to evaluate the effects of asperity shape, two textured geomembranes with slightly different asperity shape were selected. The first geomembrane (GMB-T1), had a conical shape asperity while the second geomembrane (GMB-T3) had asperities with "hook-cone" shape. It should be noted that, although both asperities were conically shaped with approximately the same base-dimension, one was without hook while the other was with a hook when viewed at 63X magnification scale (see Figure 4-5). The geomembranes had constant asperity height and density of 0.70 mm and 337 spikes per 10000 mm^2, respectively, and were interfaced against GTX-PP and GTX-PET during the shear test.

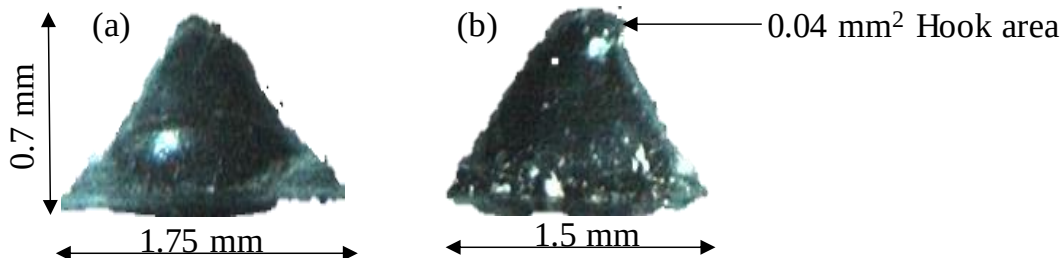

Figure 4-5: Geomembrane with similar properties except for asperity shape (a) conical asperity (b) "hook-cone" asperity

Figure 4-6 presents the relationships of shear stress against horizontal displacement for GMB-T1/GTX-PP, GMB-T3/GTX-PP, GMB-T1/GTX-PET, and GMB-T3/GTX-PET, where Figure 4-6a and Figure 4-6b represents interfaces with polypropylene and polyester geotextile, respectively. Also, interface with conical shape asperity were illustrated as "dashed lines" while "solid lines" characterised geosynthetics interface with "hook-cone" shape.

From Figure 4-6, it was apparent that the "hook-cone" asperity shape, depending on the counter faced geotextile, gave a slightly significant change in peak shear strength in relation to conical shape asperity. Considering GTX-PP interfaces, "hook-cone" asperity shape produced a 2.1, 5.5, and 9.4 kPa increase in peak stress at 50, 100, and 200 kPa confining stress, respectively. However, at 400 kPa, hooked asperities gave a slightly lower peak strength. On the contrary, considering GTX-PET interface, "hook-cone" asperity shape produced 6.4, 5.8, and 8.1 kPa decrease in peak stress at 50, 100, and 200 kPa confining stress, respectively. However, at 400

kPa, hooked asperities gave a slightly higher peak strength. Therefore, the inclusion of hooks could either increase or decrease the interface shear strength depending on the interfaced geotextile. It should be noted that GTX-PP interfaces exhibited an increase in peak shear than GTX-PET fibres because GTX-PP fibres which were made from virgin polypropylene interacted significantly with the GMB asperities. The observed trend is in good agreement with the findings of Fowmes *et al.*, (2017). In addition, although asperity shape also influenced large displacement (LD) shear strength, the changes were very minimal, especially at lower stresses.

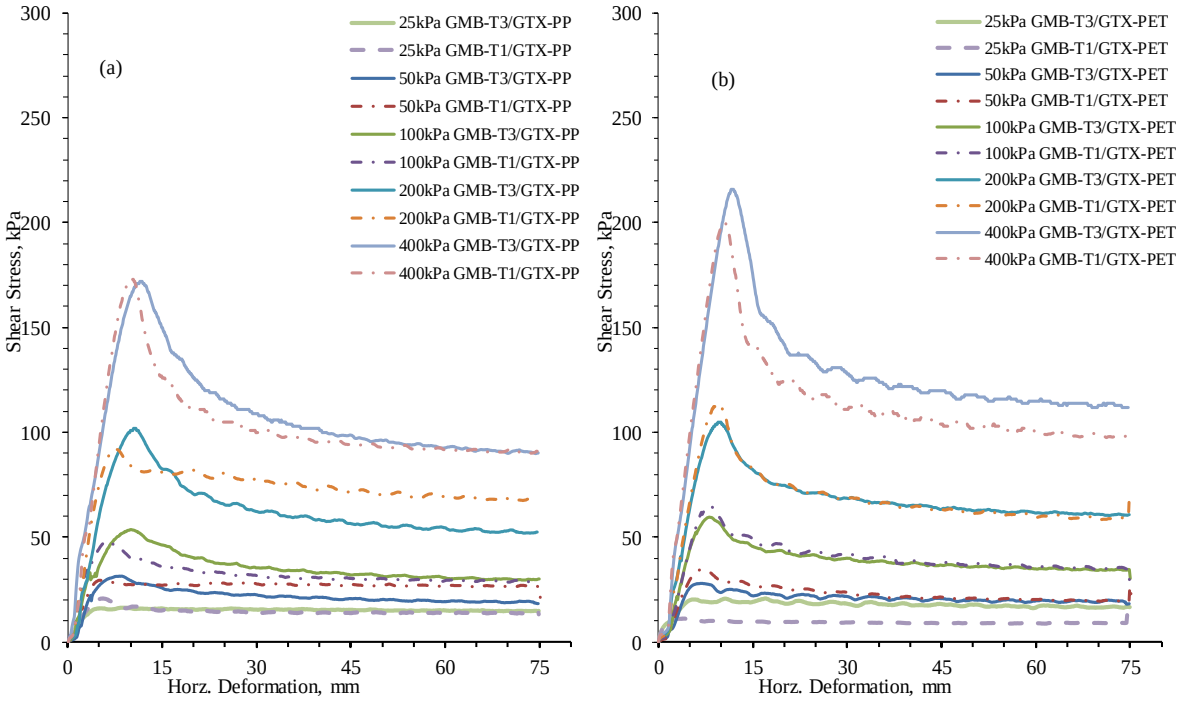

Figure 4-6: Shear stress versus horizontal displacement relationships for interface with different asperity shape (GMB-T1 and GMB-T3) (a) GMB/GTX-PP (b) GMB/GTX-PET

As related to applied stress, it was observed that at lower stresses, both asperity shapes did not produce a significant difference in the recorded peak and LD shear strength. However, at higher stresses, differences in the peak and LD shear strength was observed. The difference in shear strength at higher stresses was attributed to the distinct matrix-level hook and loop interaction between asperities and geotextile fibre. More so, "waviness" which was directly proportional to the normal stress, was observed during the post-peak phase of Figure 4-6, where "hook-cone" asperity shape produced more waviness than interfaces without hook shape. It was also evident that at all applied stresses, the difference in asperity shape produced changes in the displacement required to mobilize peak stress. The "hook-cone" asperities mobilised peak shear at greater displacement than conical-shaped asperities.

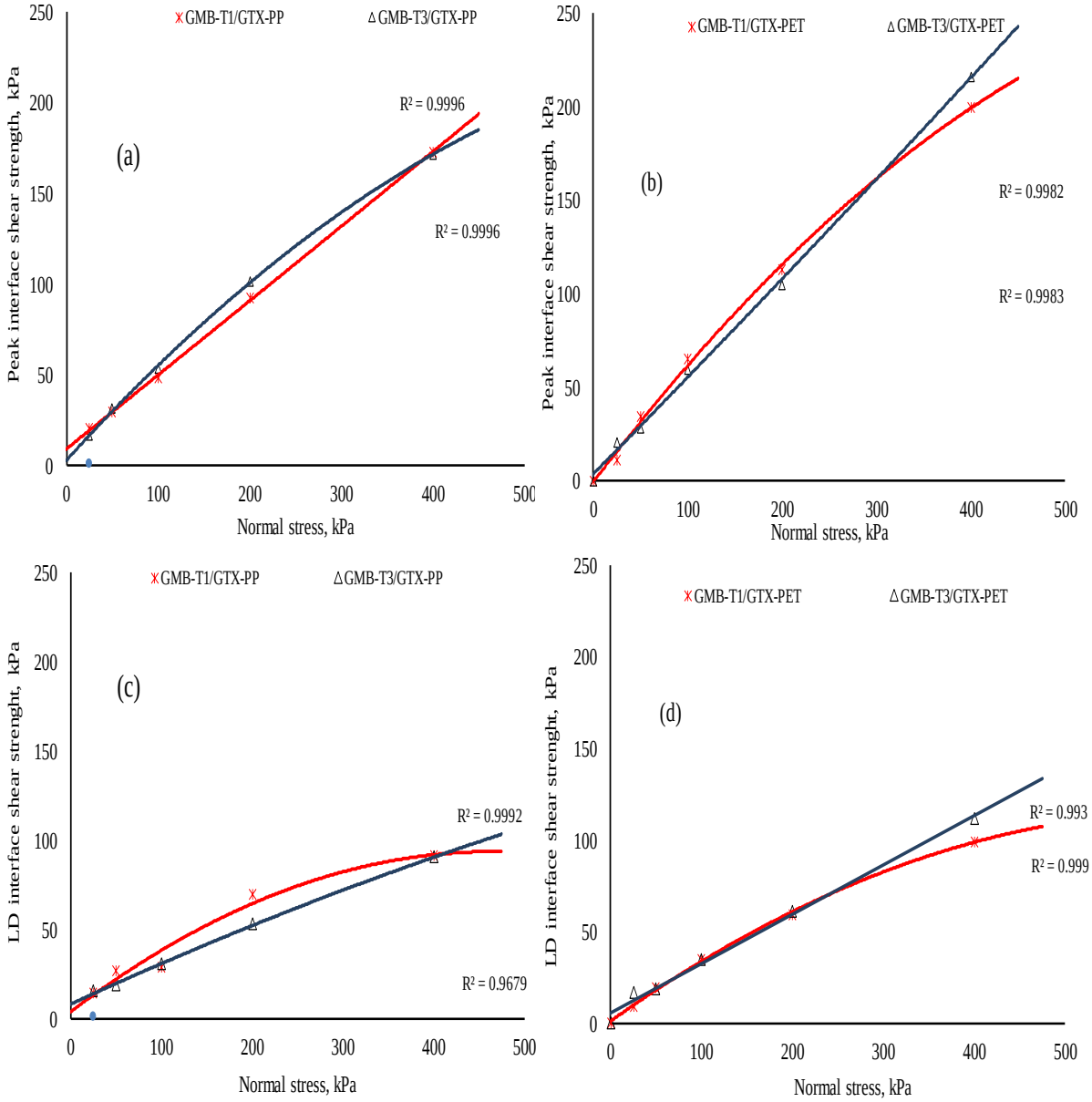

Figure 4-7: Shear stress versus applied normal stress for interfaces with varying asperity shape (a) GMB/GTX-PP "Peak" (b) GMB/GTX-PET "Peak" (c) GMB/GTX-PP "LD" (d) GMB/GTX-PET "LD"

4.3.3. Influence of asperity shape on GMB/GTX interface failure envelope

This section discusses the relationship between peak and LD shear stress and the applied normal stress for the GMB/GTX interface as asperity shape was varied. Figure 4-7 showed the typical Mohr-Coulomb envelopes obtained from the data read-off from the relationships in Figure 4-6. The best-fit lines or curves were fitted through the respective test points. For a line, the inclination to the horizontal axis and the intercept on the vertical axis corresponds to the friction angle (δ) and apparent cohesion (c_a), respectively. Whereas, for curve failure envelope, the slope of

tangents drawn to the curve at applied stresses was used to determine δ and c_a. Each interface peak and LD shear parameters were quantitatively summarized and presented in Table 4-2.

In this analysis, only the friction angle was considered as it followed an observable trend unlike the apparent cohesion (see Table 4-2). Based on the material configuration of the geosynthetics considered, it was evident that the asperity shape did not produce significant changes to the peak and LD friction angle. Since previous studies by Bacas *et al.*, (2015a) and Fowmes *et al*., (2017) identified that asperity shape influences the geosynthetics shear parameter and the reverse was observed in this scenario, it was considered that the distinguishing hook area of 0.04 mm^2 was relatively small compared to the asperity shape cone size. Thus, the hook-feature was insufficient to cause significant changes to the peak and LD friction angle, though minimal effects were observed on the measured peak and LD interface shear strength. Therefore, based on these observations, differences in asperity shape were not considered in subsequent result presentation and discussion.

Table 4-2: Effects of asperity shape on GMB/GTX interface shear parameter

GMB	GTX	Asp. shape	Interface friction angle δ (°)		Apparent cohesion c_a (kPa)	
			Peak	LD	Peak	LD
GMB-T1	PP	Conical	27.5	13.2	9.2	13.8
	PET		26.5	13.7	6.2	5.5
GMB-T3	PP	"hook-cone"	27.5	13.0	11.4	9.8
	PET		26.5	15.1	6.2	5.6

* Asp = Asperity

4.4. Interface shear stress against horizontal displacement

4.4.1. Introduction

In this section, the shear stress against horizontal displacement plot for both smooth and textured geomembrane/geotextile interface tests are presented. All shear tests were conducted at 25, 50, 100, 200, and 400 kPa applied normal stresses according to the test program detailed in Table 3-4. Also, the tests were performed at constant shear displacement rate (SDR) of 1 mm/min after been fully submerged in water for one hour. The resulting interfaces were labelled based on the applied stress and geosynthetics used.

4.4.2. Smooth geomembrane/ geotextile (GMB-S/ GTX) interface test

The smooth geomembrane (GMB-S) utilized in this investigation was a 2 mm thick high-density polyethylene (HDPE), manufactured from virgin polymeric resin. The geotextiles used in the tests were a staple-fibre nonwoven needle-punched geotextile, manufactured from virgin polypropylene (GTX–PP) fibres and 100% recycled polyester (GTX–PET) fibres. From the conducted shear test of GMB-S against GTX–PP and GTX–PET at different stresses, plots of interface shear stress against horizontal displacement relationships are presented in Figure 4-8, where solid lines represented the GMB-S /GTX–PP interfaces and dashed lines characterised the GMB-S /GTX–PET interfaces.

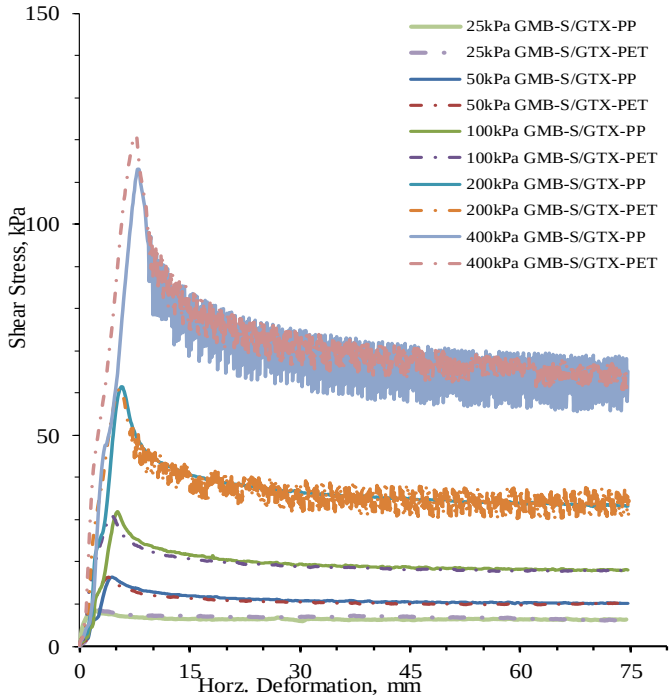

Figure 4-8: Relationship of shear stress against horizontal displacement for GMB-S / GTX-PP & GMB-S /GTX-PET

It was observed from Figure 4-8 that the stress-displacement plot followed the theoretical pattern peculiar to geosynthetics interface according to ASTM D7702 - 14 (2014). The first identified stage after the initiation of the shear test was the “pre-peak” stage, and it was characterised by the steady increase in shear stress as the horizontal displacement increased. As the shear test continued, the “peak” stage was reached, and this stage represented the maximum (peak) shear strength the interface can attain. However, as the test proceeded beyond the peak stage, a noticeable soft strength reduction (softening) was identified; this was the “post-peak” stage. This

observed behaviour which was attributed to plastic deformation of the geosynthetics at the interface is in good agreement with the findings by Dove & Frost (1999); Triplett & Fox (2001); and Bacas *et al*., (2015a).

As illustrated in Figure 4-8, GMB-S/ GTX-PP and GMB-S/ GTX-PET interfaces showed a similar "pre-peak and post-peak" stress path, particularly at applied stresses lower than 200 kPa. An apparent reason for the stress path similarity of the GMB-S/GTX interfaces was that the smooth GMB did not develop distinct shearing interaction with the geotextiles; hence the GTX fibres slide easily at the contact surface. Therefore, as regards GMB-S/GTX interfaces sheared at stresses lower than 200 kPa, it was suggested that the type of geotextile does not significantly affect the stress-horizontal displacement curve.

As regards the post-peak stage behaviour of Figure 4-8, it was noticed that 60 % of the total stress-displacement plot exhibited smooth behaviour, whereas the remainder exhibited "undulating" behaviour. The plots with smooth post-peak behaviours were conducted at normal stress range of 25 to 100 kPa. While, as the applied stress increased, undulating behaviours at the post-peak stage were evident, particularly at the 400 kPa normal stress. The "undulating" behaviour was caused by the forced sliding/polishing and frictional resistance at the interface, particularly at higher stresses (> 200 kPa). Additionally, the geotextiles responded differently to the undulations, where GMB-S/GTX-PP interfaces exhibited higher "undulations" than GMB-S/GTX-PET interfaces. Increased resistance to sliding was observed at GTX-PP interface than GTX-PET interface because GTX-PP was manufactured from virgin polypropylene while GTX-PET was made from recycled polyester. Also, increased resistance at GTX-PP was attributed to the greater fibre surface area which allowed for greater interaction.

4.4.3. Textured geomembrane/geotextile interface test

Textured HDPE geomembranes of 2 mm thickness were used in this shear investigation together with staple-fibre nonwoven needle-punched virgin GTX–PP and recycled GTX–PET geotextiles at the GMB-T/GTX interface. The resulting plots of GMB-T/GTX interfaces shear stress against horizontal displacement relationships are presented in this section. On each plot, GMB-T/GTX–PP interfaces were represented as solid lines while GMB-T /GTX–PET interfaces were labelled as dashed lines. Also, the textured geomembranes were alphanumerically differentiated as GMB-T1, GMB-T2, GMB-T3, GMB-T4, GMB-T5, GMB-T6, and GMB-T7, where "T", and "1-7"

signified textured GMB, and asperities order, respectively. It should be noted that all GMB-T/GTX interfaces stress-displacement relationships were further discussed by examining the corresponding sheared geotextile under a scan electron microscope (SEM). In this study, it was estimated that the maximum shear effects of the asperities on geotextile fibres would occur at the highest applied stress (i.e. 400 kPa) since according to ASTM D5321 (2014), shear stress increases proportionally with an increase in applied normal stress. Therefore, the sheared geotextiles SEM images after the "400 kPa interface test" were taken and examined.

4.4.3.1 GMB-T1/GTX interface test

This section presents the shear-displacement plot of GMB-T1/ GTX-PP and GMB-T1/ GTX-PET interfaces. Where the textured geomembrane (GMB-T1) had average asperity height and density of 0.7 mm and 332 spikes per 10000mm^2, respectively.

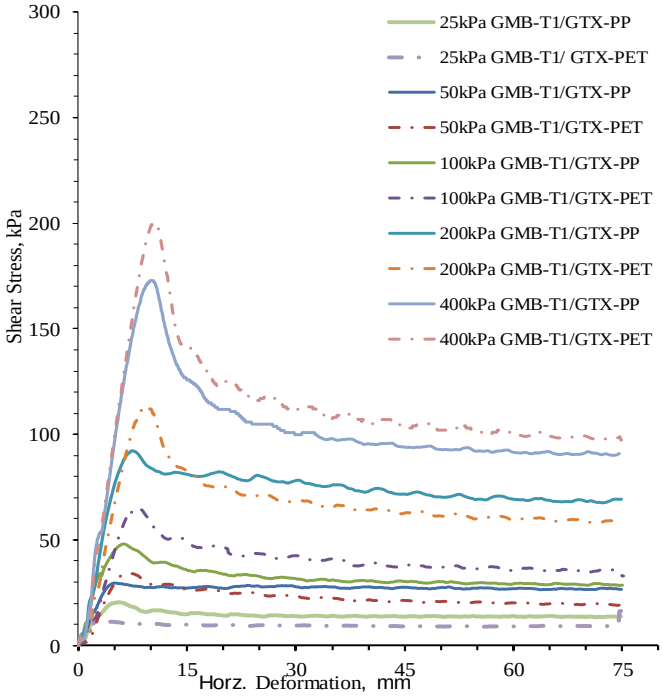

Figure 4-9: Relationship of shear stress against horizontal displacement for GMB-T1 / GTX-PP & GMB-T1 /GTX-PET

From Figure 4-9, it was observed that the shear stress-horizontal displacement plots followed the general geosynthetics interface pattern. Also, all interface stress-displacement plot exhibited a smooth initial increase in shear stress at the "pre-peak" stage, irrespective of the geotextile-type, asperities properties and applied normal stress. At the "peak" stage, it was observed that the higher the normal stress, the higher the recorded peak shear stress and the displacement required

to mobilise peak shear. While as regards the post-peak stage, the interfaces stress-displacement plots were affected by both applied stress and asperities. For instance, post-peak interface plots at lower stresses of 25, 50, and 100 kPa were smooth. While the plots at higher stresses of 200 & 400 kPa exhibited some waviness, which was attributed to the matrix-level ploughing at the GMB/GTX interface.

Furthermore, at lower applied stresses of 25 & 50 kPa, it was observed that GTX-PP interfaces exhibited higher peak and large displacement (LD) shear strength than GTX-PET interfaces. Conversely, at higher applied stresses of 100, 200, & 400 kPa, GTX-PET interfaces exhibited higher peak and LD shear strength than the GTX-PP interfaces. The differences in interface shear strength at varying stress level were caused by the hook and loop interaction and the respective geotextile fibre properties; where GTX-PP consist of thick and loosely clustered virgin fibres (see Figure 4-10a), and GTX-PET comprises of thin and tightly clustered recycled fibres (Figure 4-10c). For instance, at 400 kPa applied stress, the GMB/GTX-PET interface exhibited higher strength than GMB/GTX-PP interface because the thin and tightly clustered GTX-PET fibres developed strong interlocking mechanism with the GMB asperities and roughness, which was not possible with the thick and loosely clustered GTX-PP fibres. As a result, the fibre/asperities interlock interaction caused the GTX-PET fabric to experience minimal structural-deformations, as shown in Figure 4-10d. Whereas at the same 400 kPa stress, the GTX-PP fibres, due to its thicker filaments and greater gaps could not develop sufficient interlock with the GMB asperities and roughness, and this resulted in compression, deformation and breakage of GTX-PP fabric (see Figure 4-10b).

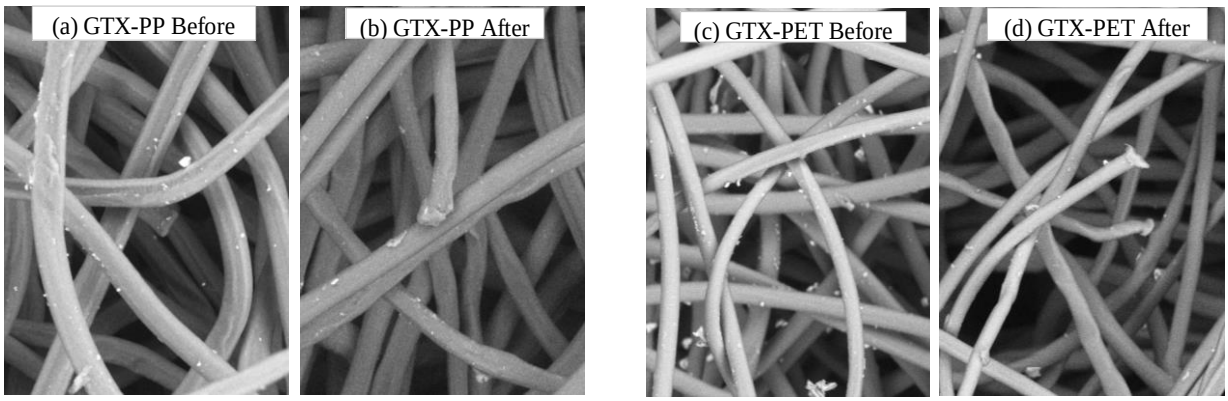

Figure 4-10: 500x SEM image of geotextiles before and after shearing against GMB-T1 at 400 kPa stress; (a) GTX-PP before (b) GTX-PP after (c) GTX-PET before (d) GTX-PET after

With the addition of asperities to the GMB/GTX interface, the GMB-T1/GTX interfaces exhibited better characteristics as regards the stress-displacement plot when compared with the GMB-S/GTX interfaces. First, GMB-T1/GTX interfaces displayed greater peak displacement as well as peak and LD shear strengths than GMB-S/GTX interfaces. Also, at lower stresses of 25 & 50 kPa, the "post-peak" stage of the stress-displacement plots was relatively smooth for both interfaces. While at higher stresses of 100, 200, & 400 kPa, the plot "post-peak" stage of GMB-S and GMB-T1 interfaces displayed undulations and waviness, respectively.

4.4.3.2 GMB-T2/GTX interface test

This section presents and discusses the shear stress-horizontal displacement behaviour of GMB-T2/GTX-PP and GMB-T2/GTX-PET interfaces. The GMB-T2 had average surface asperity height and density of 0.7 mm and 667 spikes per 10000 mm^2, respectively.

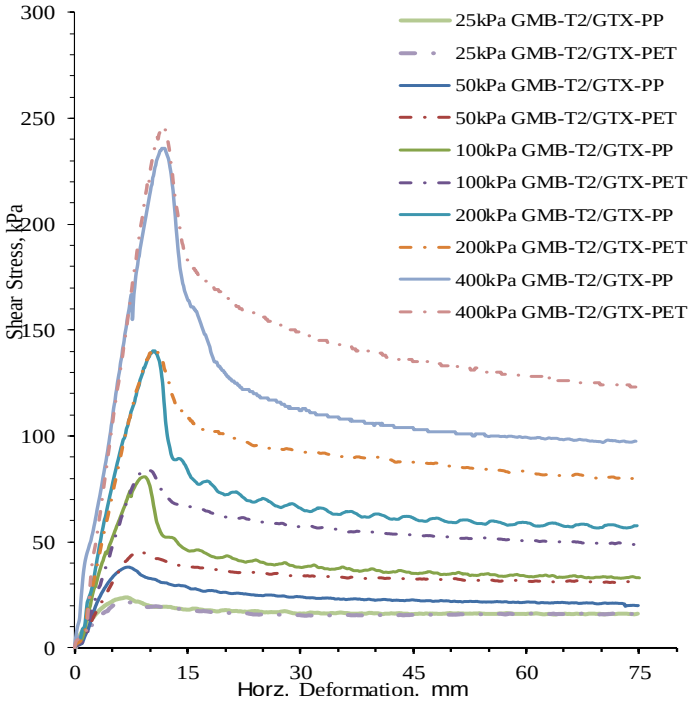

Figure 4-11: Relationship of shear stress against horizontal displacement for GMB-T2 / GTX-PP & GMB-T2 /GTX-PET

Figure 4-11 illustrates the graphs of shear stress against horizontal displacement derived from the GMB-T2/GTX interface shear tests. At the "pre-peak" stage of the plot, the GMB-T2/GTX-PP and GMB-T2/GTX-PET interfaces exhibited 'smooth' responses and transition at all applied stresses. While at the "post-peak" stage, the stress-displacement plot exhibited waviness, where

the scale of waviness was directly proportional to the applied normal stress, geotextile-type, and matrix-level hook and loop interactions.

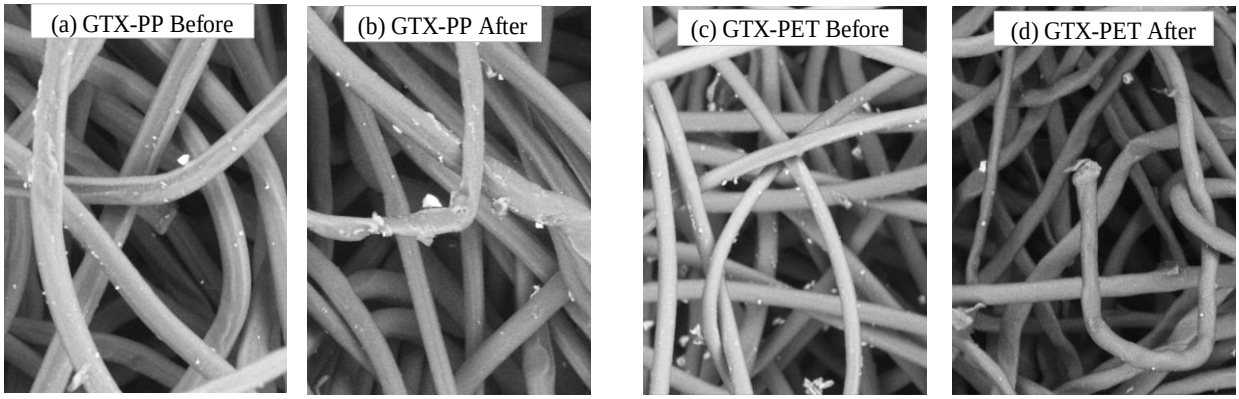

Figure 4-12: 500x SEM image of geotextiles before and after shearing against GMB-T2 at 400 kPa stress; (a) GTX-PP before (b) GTX-PP after (c) GTX-PET before (d) GTX-PET after

Furthermore, it was examined from Figure 4-11 that the GTX-PP interfaces exhibited similar peak and large displacement (LD) shear strength with the GTX-PET interfaces at 25 kPa applied stress. On the contrary, at 50, 100, 200, & 400 kPa applied stresses, GTX-PET interfaces exhibited higher peak and LD shear strength than the GTX-PP interfaces. It should be noted that GTX-PP lower LD strength was attributed to the rapid-stress reduction at the "post-peak" stage. It was considered that the similarity between GTX-PET and GTX-PP interfaces stress-displacement plot at 25 kPa was because GMB-T2 could not develop distinct matrix-level interlocking interaction for both geotextiles. Comparatively, interfaces with applied stresses of 50 kPa to 400 kPa displayed a different stress-displacement behaviour for both geotextiles, where GTX-PET interface produced larger shear value than GTX-PP interfaces. The differences in interface shear strength at higher stresses were anticipated to be caused by the distinct asperities interaction with the geotextile fibre matrix. For instance, at 400 kPa, the high stress-reduction sustained at the GMB-T2/GTX-PP interface was considered to be caused by the dense GMB-T2 asperities and roughness interacting with the thick and loosely clustered virgin GTX-PP fibres. Due to the asperities concentration, roughness and fibre structure, GTX-PP fabrics experienced compression, deformation and acute-breakage (see Figure 4-12b), as compared to the initial SEM image (see Figure 4-12a). Contrarily, thin and tightly clustered GTX-PET fibres (see Figure 4-12c), due to their quantity and size were able to interlock appropriately with the concentrated asperities density; hence, there was limited fibre deformation (see Figure 4-12d) and little strength reductions for GMB-T2/GTX-PET interface.

With the variation of asperity density at the GMB/GTX interface, where GMB-T2/GTX interface (663 spikes) had higher asperity density than GMB-T1/GTX interface (332 spikes), the following characteristics as related to the shear stress-horizontal displacement plot were noticed. First, GMB-T2/GTX interfaces displayed more peak displacement than GMB-T1/GTX interfaces. Also, GMB-T2/GTX interfaces displayed increased peak shear strengths than GMB-T1/GTX interfaces, while GMB-T1/GTX interfaces exhibited higher LD shear strengths than GMB-T2/GTX interfaces.

4.4.3.3 GMB-T4/GTX interface test

This section presents the shear-displacement plot of GMB-T4/ GTX-PP and GMB-T4/ GTX-PET interfaces; where the textured geomembrane (GMB-T4) had average asperity height and density of 0.85 mm and 337 spikes per 10000mm^2, respectively.

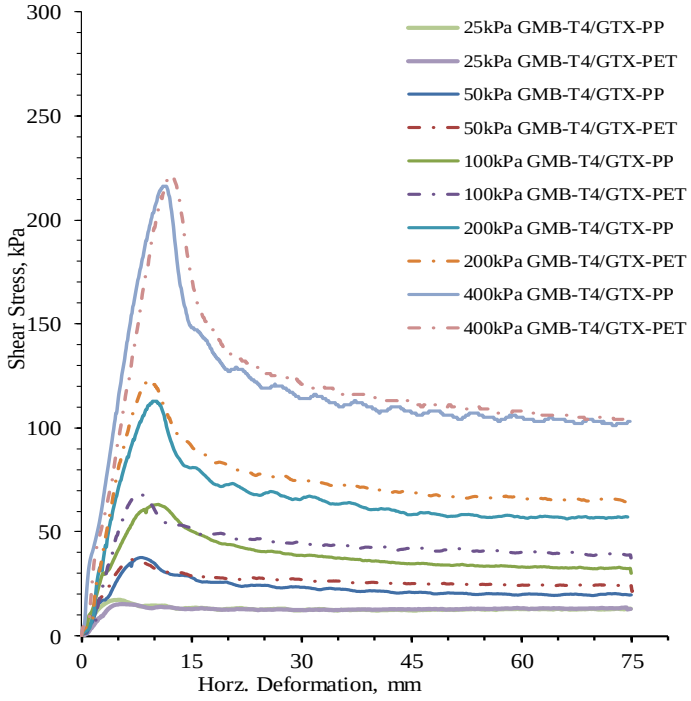

Figure 4-13: Relationship of shear stress against horizontal displacement for GMB-T4 / GTX-PP & GMB-T4 /GTX-PET

From the "pre-peak" and "post-peak" stage of Figure 4-13, it was observed that GMB-T4/GTX-PET interfaces exhibited greater gradient than GMB-T4/GTX-PP interfaces. Also, at the "post-peak" stage, both interfaces stress-displacement plot exhibited waviness, though dependent on the applied stress. The GMB-T4/GTX-PP interfaces had more waviness than GMB-T4/GTX-PET interfaces because of the matrix-level ploughing of GTX-PP fibres by GMB-T4 asperities.

Furthermore, it was examined from Figure 4-13 that the GTX-PP interfaces exhibited similar peak and large displacement (LD) shear strength as GTX-PET interfaces at 25 & 50 kPa applied stresses. Conversely, at 100, 200, & 400 kPa applied stresses, GTX-PP and GTX-PET interfaces exhibited different peak and LD shear strength, where GTX-PET interfaces were higher than GTX-PP interfaces. An apparent reason for the similarity of GTX-PET and GTX-PP interfaces stress-displacement plot at 25 & 50 kPa was the relatively low-activity of the hook and loop interaction at the interface. Comparatively, interfaces with applied stresses of 100 kPa to 400 kPa displayed similar stress-displacement behaviour for both geotextile interface. For instance, at 400 kPa, the GMB-T4/GTX-PET and GMB-T4/GTX-PP interfaces exhibited similar LD shear strength which was caused by the GTX fibre compression and superficial-level interaction between GMB-T4 asperities and the geotextile fibres. Also, it was observed from the SEM image for both geotextiles that the degree of distortions on GTX-PP surface (compare Figure 4-14a & b) was similar to that on GTX-PET surface (compare Figure 4-14 c & d). An apparent reason for this similar behaviour was that besides GMB-T4 asperity height and density, the between-asperities roughness has gentle undulating trends; hence GMB-T4 could not develop distinct matrix-level hook and loop interactions with the interfaced geotextiles fibre.

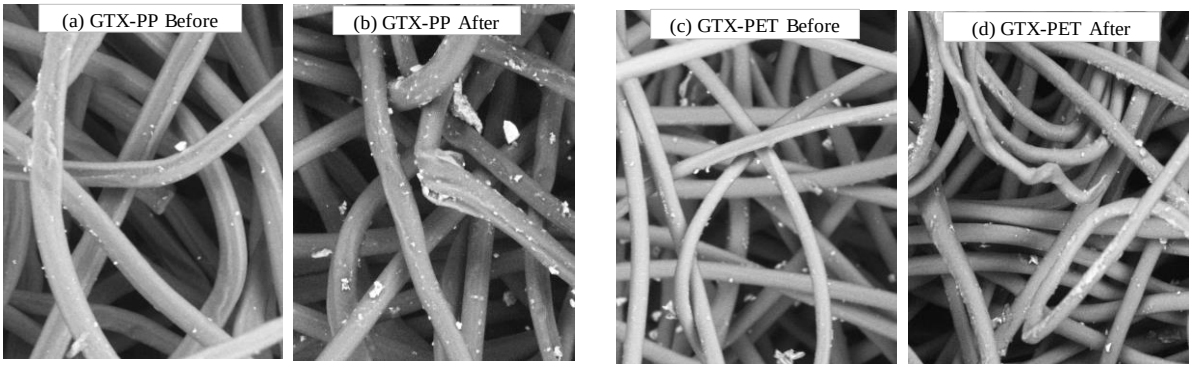

Figure 4-14: 500x SEM image of geotextiles before and after shearing against GMB-T4 at 400 kPa stress; (a) GTX-PP before (b) GTX-PP after (c) GTX-PET before (d) GTX-PET after

The following characteristics as related to the shear stress-horizontal displacement plot were observed for GMB-T4/GTX & GMB-T1/GTX interfaces, where both have similar asperity density but slightly different asperity height (GMB-T4/GTX; 0.85 mm > GMB-T1/GTX; 0.70 mm). Primarily, GMB-T4/GTX interfaces displayed greater peak displacement than GMB-T1/GTX interfaces. Also, both interfaces exhibited similar peak and LD shear strength.

4.4.3.4 GMB-T5/GTX interface test

This section presents and discusses the shear stress-horizontal displacement behaviour of GMB-T5/GTX-PP and GMB-T5/GTX-PET interfaces. The GMB-T5 had average surface asperity height and density of 1.2 mm and 302 spikes per 10000 mm^2, respectively.

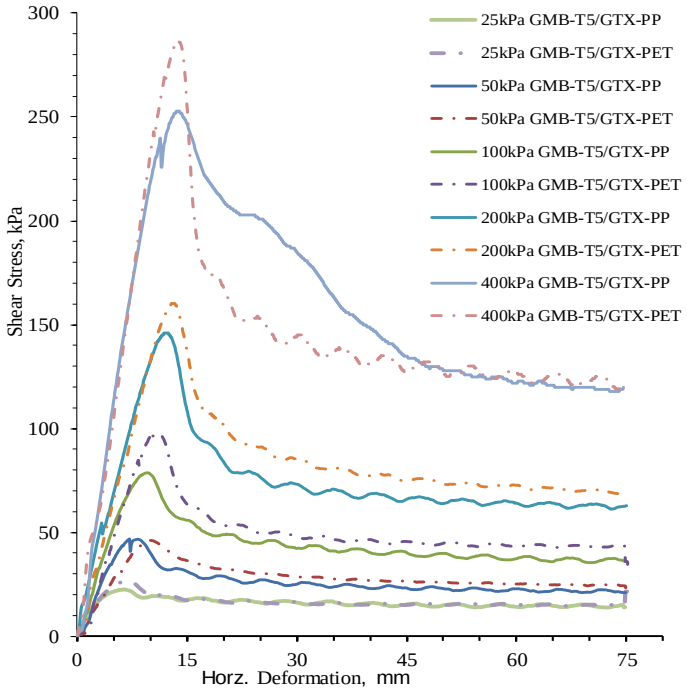

Figure 4-15: Relationship of shear stress against horizontal displacement for GMB-T5 / GTX-PP & GMB-T5 /GTX-PET

It was examined from Figure 4-15 that the "pre-peak" stage of GMB-T5/GTX-PP and GMB-T5/GTX-PET interfaces exhibited 'smooth' stress development. While at the peak stage, GTX-PET interfaces displayed higher stress than GTX-PP interfaces. Also, at the "post-peak" stage, the stress-displacement plot exhibited waviness and rapid strength reduction, where GTX-PP interfaces displayed more waviness and strength reduction than GTX-PET interfaces. It was also revealed from Figure 4-15 that at 25 & 50 kPa applied stress, GTX-PP interfaces exhibited similar peak and large displacement (LD) shear strength with GTX-PET interfaces. Conversely, at 100, 200, & 400 kPa applied stresses, GTX-PET interfaces exhibited higher peak and LD shear strength than the GTX-PP interfaces. An apparent reason for the similarity of GTX-PET and GTX-PP interfaces stress-displacement plot at 25 & 50 kPa stresses was the absence of distinct fibre/asperities interaction. Comparatively, at 100, 200, & 400 kPa stresses, GTX-PP interfaces displayed lower shear strength than GTX-PET interfaces because of the different degree of hook and loop interaction at the GMB-T5 asperities/geotextile fibre interface, where GTX-PP consist

of thick and loosely clustered virgin fibres, and GTX-PET comprises of thin and tightly clustered recycled fibres. For instance, at 400 kPa, the non-conventional strain-softening exhibited at the GMB-T5/GTX-PP interface was considered to be caused by the matrix-level hook and loop interaction of GMB-T5 asperities with GTX-PP thick and loosely clustered fibre. Therefore, as seen on the SEM images, the scale of fibre compression and bending in GTX-PP fabric (compare Figure 4-16a & b) was more than that on GTX-PET fabric (compare Figure 4-16c & d).

As the asperity height was varied and asperity density fixed, where GMB-T5/GTX (1.20 mm) interface had greater asperity height than GMB-T1/GTX interface (0.7 mm), the interfaces shear stress-horizontal displacement plot revealed that GMB-T5/GTX interfaces exhibited greater peak displacement, peak shear strength, and LD shear strength than the GMB-T1/GTX interfaces.

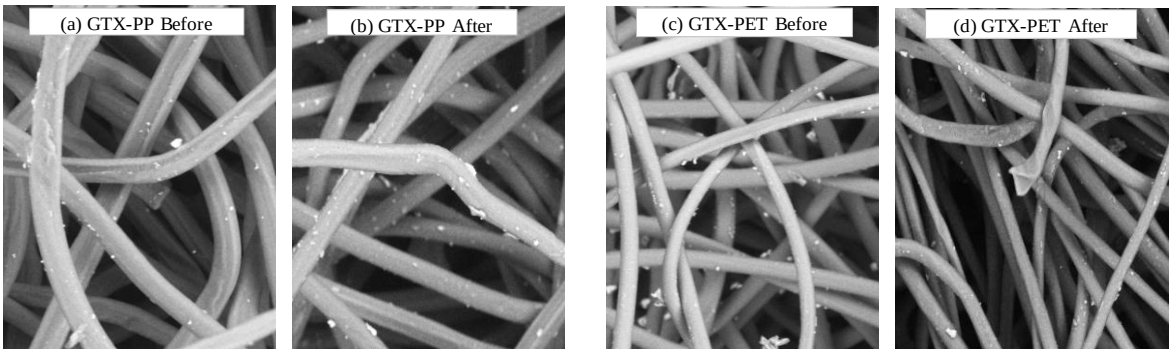

Figure 4-16: 500x SEM image of geotextiles before and after shearing against GMB-T5 at 400 kPa stress; (a) GTX-PP before (b) GTX-PP after (c) GTX-PET before (d) GTX-PET after

4.4.3.5 GMB-T6/GTX interface test

This section presents the shear-displacement plot of GMB-T6/ GTX-PP and GMB-T6/ GTX-PET interfaces; where the mega-textured geomembrane (GMB-T6) had average asperity height and density of 1.81 mm and 211 spikes per 10000mm^2, respectively.

From Figure 4-17, both GTX-PP and GTX-PET interfaces displayed similar and smooth gradient in the "pre-peak" stage. While from the "post-peak" stage, it was observed that GMB-T6/GTX-PP interfaces exhibited more waviness than GMB-T6/GTX-PET. Also, it was examined that GTX-PP interfaces exhibited approximately similar peak and large displacement (LD) shear strength with GTX-PET interfaces at all applied stress except at 400 kPa.

An apparent reason for the similarity of GTX-PET and GTX-PP interfaces stress-displacement plot at 25, 50, 100, & 200 kPa applied stresses was the lack of distinct matrix-level fibre/asperities interaction at the interface. Comparatively, at 400 kPa stress, both interfaces displayed different

stress-displacement behaviour because of the presence of matrix-level hook and loop interaction at the interface. From this behaviour, it was observed that greater asperity height requires higher stress to develop matrix-level interaction in addition to superficial-level fibre/asperities interaction.

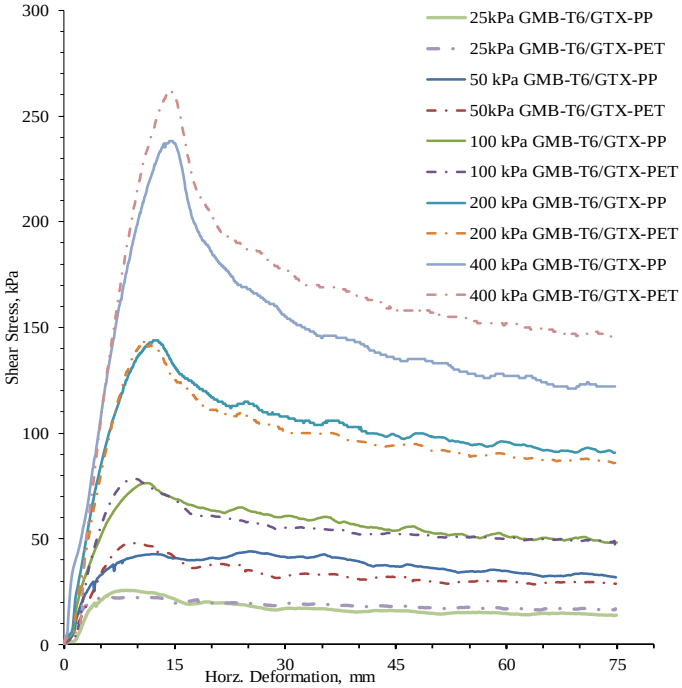

Figure 4-17: Relationship of shear stress against horizontal displacement for GMB-T6 / GTX-PP & GMB-T6 /GTX-PET

For instance, it was only 400 kPa applied normal stress that could distinguish GMB-T6/GTX-PP interfaces from GMB-T6/GTX-PET interfaces, where the former recorded lower peak and LD strength than the latter. The lower shear strength behaviour was observed for GMB-T6/GTX-PET interfaces because of the engagement between GMB-T6 (1.81 mm) asperities height and less-ductile, thick and loosely clustered virgin GTX-PP fibres. As a result, GTX-PP fibres could not adequately absorb the interlocking pressure from the GMB-T6 asperities. Whereas GTX-PET ductile, thin and tightly clustered recycled fibres were adequately engaged by the GMB-T6 asperities, hence the higher shear strength. Therefore, more fibre compression, deformations and breakage were observed on GTX-PP surface (compare Figure 4-18a & b) than GTX-PET surface (compare Figure 4-18c & d).

As GMB/GTX interface asperity height and density were varied simultaneously, where GMB-T6/GTX interface (211 spikes of 1.81 mm high) had higher asperity parameters than GMB-T1/GTX interface (332 spikes of 0.7 mm high). It was observed from the shear stress-horizontal

displacement plot that the GMB-T6/GTX interfaces exhibited improved peak displacement, peak shear strengths and LD shear strengths than GMB-T1/GTX interfaces.

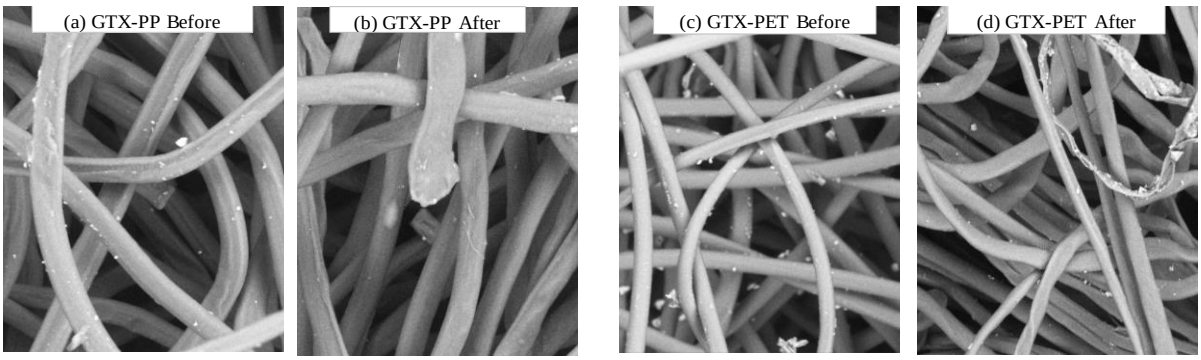

Figure 4-18: 500x SEM image of geotextiles before and after shearing against GMB-T6 at 400 kPa stress; (a) GTX-PP before (b) GTX-PP after (c) GTX-PET before (d) GTX-PET after

4.4.3.6 GMB-T7/GTX interface test

This section presents and discusses the shear stress-horizontal displacement behaviour of GMB-T7/GTX-PP and GMB-T7/GTX-PET interfaces. GMB-T7 had average surface asperity height and density of 2.02 mm and 217 spikes per 10000 mm^2, respectively.

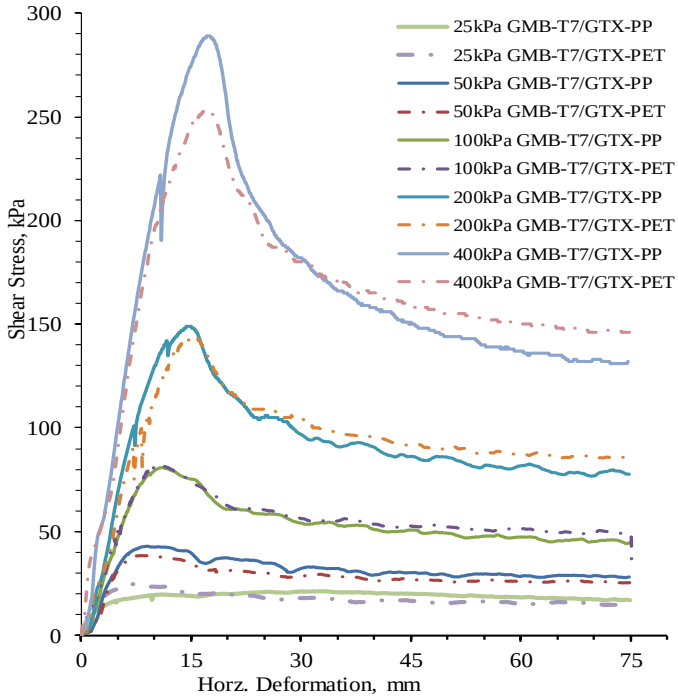

Figure 4-19: Relationship of shear stress against horizontal displacement for GMB-T7 / GTX-PP & GMB-T7 /GTX-PET

It was examined from Figure 4-19 that the "pre-peak" stage of both GMB-T7/GTX-PP and GMB-T7/GTX-PET interfaces exhibited 'smooth' stress development. While, at the "post-peak"

stage, the GTX-PP interfaces displayed more waviness than GTX-PET interfaces, particularly at higher stresses. Also, it was examined that the GTX-PP interfaces exhibited similar peak and large displacement (LD) shear strength with GTX-PET interfaces at all applied stress except at 200 & 400 kPa. Thus, at 200 & 400 kPa stresses, GMB-T7/GTX-PP peak shear strength was higher than GMB-T7/GTX-PET values while GMB-T7/GTX-PP LD shear strength was lower than GMB-T7/GTX-PET LD strength. This behaviour was related to the interaction between the GTX fibre and the GMB asperities at large displacement. For instance, at 400 kPa, the GMB-T7/GTX-PP interfaces recorded lower LD shear strength than GMB-T7/GTX-PET interfaces because of GTX-PP less-ductile, thick and loosely clustered virgin fibres engagement with the GMB-T7 (2.02 mm) asperities. As a result, GTX-PP fibres could not sufficiently interlock with the GMB-T7 asperities. While GTX-PET ductile, thin and tightly clustered recycled fibres were adequately interlocked with GMB-T7 asperities, hence the higher shear strength. Therefore, more fibre compression and deformations were observed on GTX-PP surface (compare Figure 4-20a & b) than GTX-PET surface (compare Figure 4-20c & d).

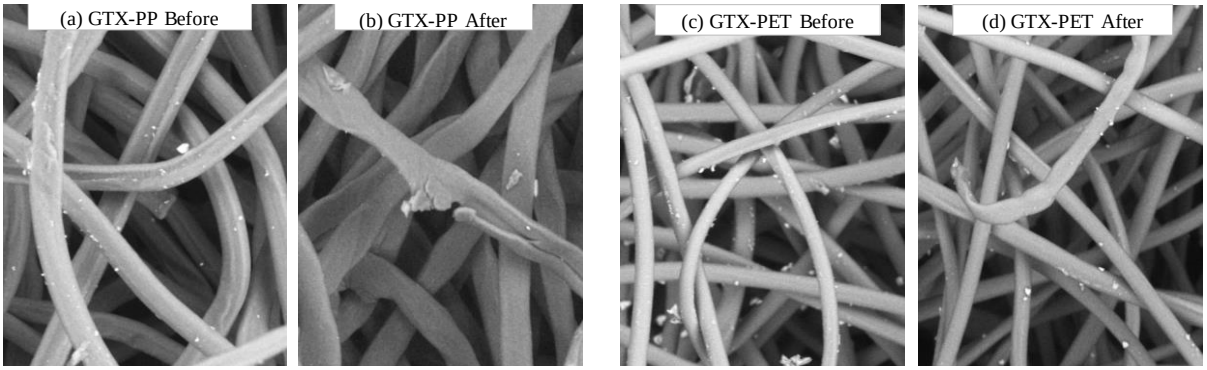

Figure 4-20: 500x SEM image of geotextiles before and after shearing against GMB-T7 at 400 kPa stress; (a) GTX-PP before (b) GTX-PP after (c) GTX-PET before (d) GTX-PET after

As GMB asperity height was varied at fixed asperity density, where GMB-T7 (2.02 mm) had greater asperity height than GMB-T6 (1.81 mm), it was revealed from the shear stress-horizontal displacement plots that GMB-T7/GTX interfaces exhibited greater peak displacement, peak shear strength, and LD shear strengths than GMB-T6/GTX interfaces.

4.4.4. Summary of GMB/GTX shear stress - horizontal displacement relationship

For all GMB/GTX interfaces in this study, the shear stress – horizontal displacement relationship was considered as linear up to the peak stress, after which, a gradual strength-reduction (softening) was observed. The slope of the linear relationship and the rate of strength reduction

was dependent on the applied stress, asperity height, asperity density, and geotextile polymer. With regard to applied stress, geotextile filaments superficial engagement with GMB asperities was the primary interaction at lower normal stresses. While at higher normal stresses, matrix-level interactions including GTX fibres compression and GTX fibres interlock with GMB asperities were observed. Also, peak and LD shear strength increased with the introduction and variation of asperities. Where the LD shear strength was accompanied with the deformation and rearrangement of the GTX fibres by GMB asperities (as seen on the SEM images). Additionally, considering the effects of geotextile-type, GTX-PET interfaces, due to its fibre structure, exhibited higher shear strength value than GTX-PP interfaces.

4.5. Peak displacement against normal stress

4.5.1. Introduction

This section presents the relationship between peak displacement and normal stress for all geomembrane/geotextile (GMB/GTX) interfaces. For each tested interface, the peak displacement is the distance (in mm) in the shearing direction required to mobilise the maximum interface shear stress. According to ASTM D7702 - 14 (2014), peak shear strength is the maximum shear resistance attained at an interface during a shear test. The plot of peak displacement against normal stress presented in this section demonstrates that the displacement needed to develop peak stress increases non-linearly with confining stress.

4.5.2. Influence of asperity height alteration at constant asperity density on GMB/GTX interface peak displacement

The plots of peak displacement against normal stress relationships for all tested GMB-Ts/GTX and GMB-S/GTX interfaces are presented in this section, where GMB-S/GTX interface acted as the control interface because it exhibited the least frictional resistance. GMB-Ts/GTX interfaces were varied in asperity height at fixed asperity density. The variation in asperities height, discussed in the subsequent sub-sections, was grouped into two categories according to the dimension of the GMB asperity height; namely interfaces with asperity height of approximately 1 mm and 2 mm.

4.5.2.1 GMB/GTX interface peak displacement characteristics at varying asperity height (approximately 1 mm) and constant asperity density

This section presents and discusses the peak displacement-normal stress behaviour for GMB-S/GTX, GMB-T1/GTX, GMB-T4/GTX, and GMB-T5/GTX interfaces. The textured geomembrane interfaces had an average constant asperity density of 335 spikes per 10000 mm^2 and varied asperity height (approximately 1 mm). It should be noted that both GTX-PP and GTX-PET were utilised at the geosynthetics interface.

Figure 4-21 presents the peak displacement against normal stress plot for the GMB/GTX interfaces in this category. It was observed from the plot that all interface exhibited a non-linear increase in the displacement required to mobilise peak stress as the applied stress increased. The increase in peak displacement was caused by increased normal-stress that was exerted on the interface and the corresponding interactions (increased hook and loop interaction) at the GTX fibre-GMB asperity interface. Displacements required to mobilise peak stress values were read-off from Figure 4-21 and tabularized in Table 4-3 with the corresponding GMB asperities properties.

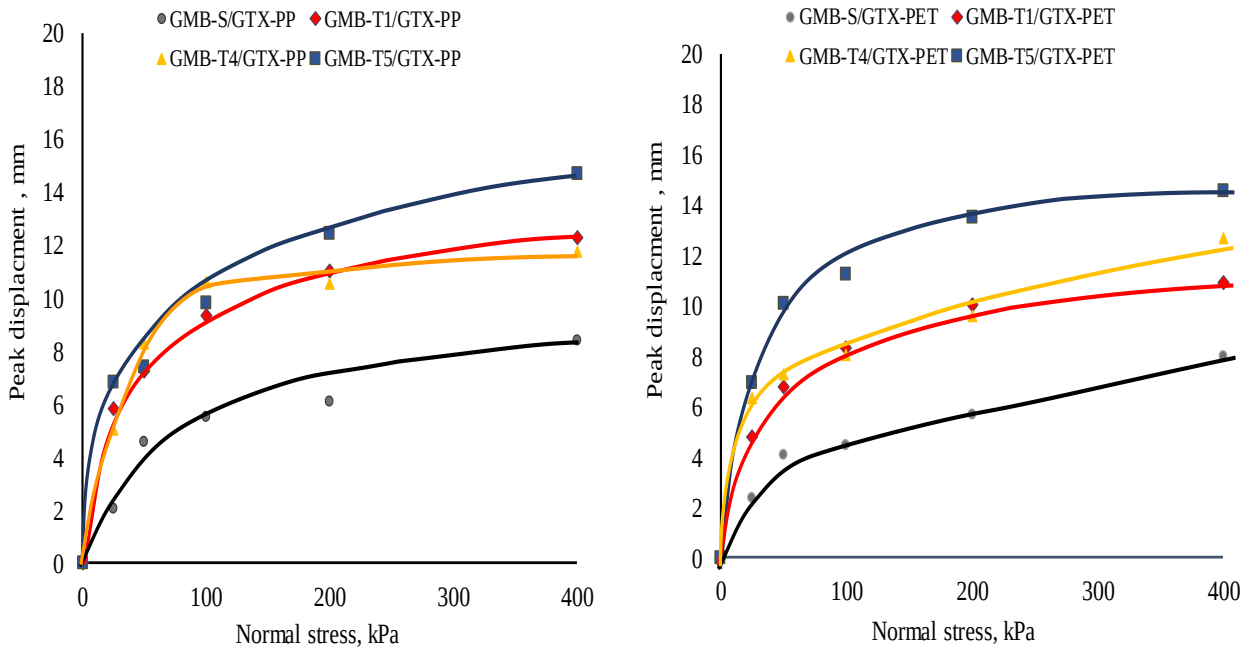

Figure 4-21: Peak displacement versus normal stress relationships for interfaces with varied asperity height (approximately 1mm)

Generally, with the incorporation and variation of asperity height to GMB/GTX interface, there was a relative increase in the displacement required to mobilize peak stress conditions when

compared with smooth geomembrane interfaces. It was apparent that with the inclusion of 0.70 mm asperity height, peak displacement increased by 80 % relative to a smooth geomembrane. Subsequently, a further increment of 21 % to the asperity height (now 0.85 mm) and 70% to the asperity height (now 1.20 mm), produced a corresponding average increase of 20 % and 26%, respectively, to the peak displacement. The difference in horizontal displacements required to develop peak stresses were considered to be due to different degree of geotextile compression and raking by the geomembrane asperities. Where the propensity to raking is related to the tensile strength and the fibre needling of the geotextile.

Table 4-3: Summary of the effects of varying asperity height (approximately 1 mm) on the GMB/GTX interface peak displacement

GMB	GTX	*Asp height (mm)	*Asp density	Interface peak displacement (mm) at various stress (kPa)				
				25	50	100	200	400
GMB-S	PP PET	0	0	2.02 2.34	4.54 4.06	5.52 4.47	6.06 5.66	8.36 8.00
GMB-T1	PP PET	0.70	332	5.82 4.79	7.21 6.77	9.30 8.29	11.01 10.00	12.26 10.93
GMB-T4	PP PET	0.85	337	5.01 6.32	8.29 7.28	10.60 8.06	10.54 9.61	11.73 12.69
GMB-T5	PP PET	1.20	306	6.81 6.94	7.37 10.09	9.78 11.25	12.41 13.49	14.65 14.53

*Asp = Asperity

Notably, the geotextile-type also influenced the horizontal displacement required to mobilized peak stress. With regard to the GMB-S/GTX interface, GTX-PP interfaces needed larger displacement than GMB-S/GTX-PET interfaces to develop peak shear at all applied stresses except at 25 kPa (see the first row of Table 4-3). Also, GTX-PP interfaces required greater horizontal displacements than GTX-PET interfaces to attain peak stress as they were sheared against geomembranes with asperity heights below 1 mm (GMB-T1 & GMB-T4). However, as asperity height increased above 1 mm (GMB-T5), the horizontal displacement required to develop peak shear stress was greater for GTX-PET interfaces than GTX-PP interfaces. The difference in the recorded peak displacement for the GMB/GTX interfaces was due to the interaction between GTX fibre geometry and arrangement, and GMB asperities. This conclusion was reached because the displacement required to mobilize peak shear varied for the same GTX as asperity height was altered, where the magnitude of the variation is dependent on GMB asperity height measurement. For instance, in considering asperity height below 1 mm, GTX-PP,

because of its higher tensile strength exhibited larger peak displacement than GTX-PET. Contrarily, as asperity height rises above 1 mm, the peak displacement was mainly determined by the matrix-level hook and loop interaction between GMB-T5 asperity height (1.2 mm) and the GTX-fibres characteristics. Thus, GTX-PET thin and tightly clustered fibres interlocked sufficiently with GMB-T5 asperities than GTX-PP thick and loosely clustered fibres. It should be noted that the significance of a higher peak displacement for geosynthetics interface is that with such displacement characteristics they are more appropriate for use in landfills designed according to serviceability limit state (Adeleke *et al.*, 2019). Therefore, geotextile should be selected based on the anticipated counteracting GMB asperity properties and design criteria.

4.5.2.2 GMB/GTX interface peak displacement characteristics at varying asperity height (approximately 2 mm) and constant asperity density

This section presents and discusses the peak displacement-normal stress behaviour of GMB-S/GTX, GMB-T6/GTX, and GMB-T7/GTX interfaces. The textured geomembrane interfaces had an average constant asperity density of 214 spikes per 10000 mm^2 and varied asperity height (approximately 2 mm). Again, both GTX-PP and GTX-PET were utilised at the GMB/GTX interface.

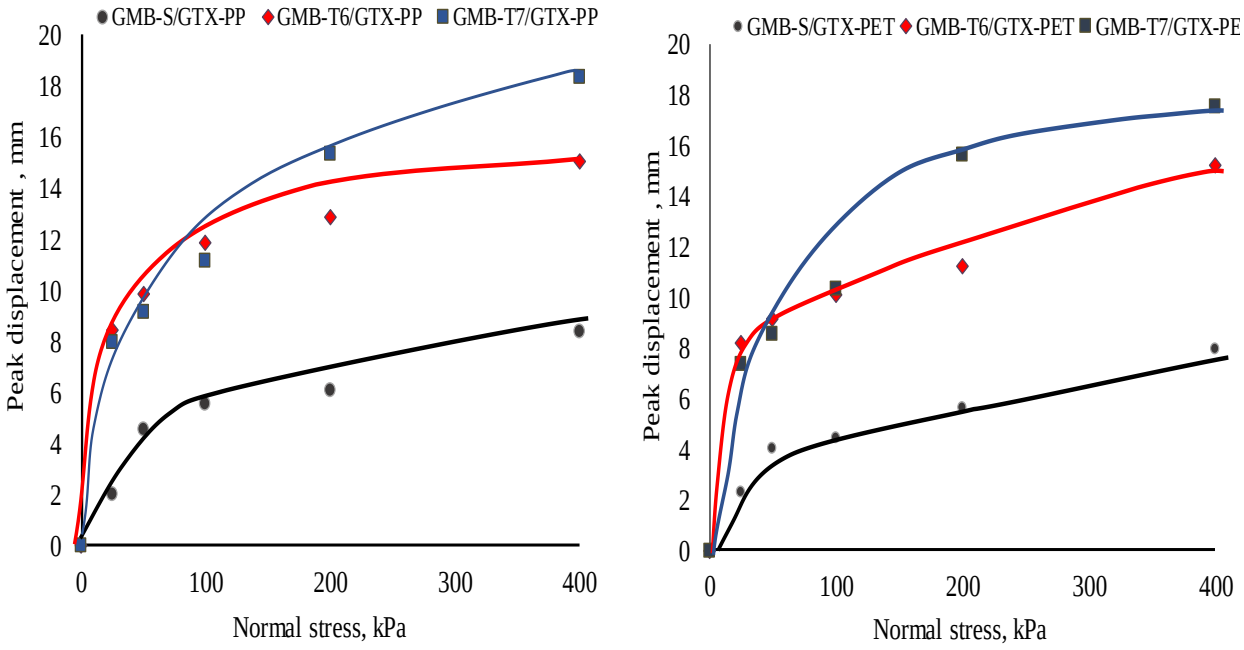

Figure 4-22: Peak displacement versus normal stress relationships for interfaces with varied asperity height (approximately 2 mm)

The graphical relationship of peak displacement against applied stress for GMB/GTX interfaces with approximately 2 mm asperity height is illustrated in Figure 4-22. Relatively to a smooth geomembrane, it was evident from Figure 4-22 that the inclusion of 1.81 mm asperity height caused an average increase of 150 % to displacement required to attain the peak shear stress at all stresses. Subsequently, an increase in asperity height above 1.81 mm at applied stresses of 25, 50, and 100 kPa, resulted in peak displacement reduction. While at 200 kPa and 400 kPa applied stresses, a further increment of 12 % to the asperity height (now 2.02 mm) at the same constant asperity density, produced a corresponding average increase of 21 % to the displacement required to mobilize peak stress. The interactions between GTX fibre geometry and GMB asperities was considered to produce the differences in the recorded peak displacement. A scientific explanation for the peak displacement reductions (at lower stresses) as asperity height increased above 1.81 mm was the optimum superficial-level interlock between the GMB asperities and the geotextile fibre. Whereas a minimal increase in peak displacement was recorded (at higher stresses) because the asperity height (> 1.81 mm) and the geotextile exhibited matrix-level hook and loop interaction. Therefore, though it was expected that greater asperity height would cause the peak stress to be mobilized at a larger displacement, this is not always the case. As an increase in asperity height beyond a "critical value" could result in geotextile-fibre damage and reduction in the displacement required to mobilise peak stress. Hence, for landfill liners designed according to serviceability limit and subjected to lower applied stresses; higher asperities might result in little or no improvement in peak displacement when compared with relatively lower asperities, provided asperity density remains constant.

Table 4-4: Summary of the effects of varying asperity height (approximately 2 mm) on the GMB/GTX interface peak displacement

GMB	GTX	*Asp height (mm)	*Asp density	Interface peak displacement (mm) at various stress (kPa)				
				25	50	100	200	400
GMB-S	PP	0	0	2.02	4.54	5.52	6.06	8.36
	PET			2.34	4.06	4.47	5.66	8.00
GMB-T6	PP	1.81	211	8.42	9.87	11.83	12.88	15.02
	PET			8.19	9.18	10.14	11.23	15.27
GMB-T7	PP	2.02	217	7.94	9.16	11.16	15.31	18.37
	PET			7.40	8.55	10.33	15.65	17.59

* Asp = Asperity

Peak displacement and normal stresses were read-off from Figure 4-22 and tabularized with the respective GMB asperity properties (see Table 4-4). The result presented in Table 4-4 revealed that peak displacement generally increased with applied stress increases. Furthermore, the horizontal displacement required to attain peak shear stress was influenced by the geotextile-polymer, where the GTX-PP interfaces needed more displacement than GTX-PET interfaces to develop peak shear in all interfaces. For instance, in considering an interface with asperity height of 1.81 mm and beyond, GTX-PP, due to its higher tensile strength required more displacement than GTX-PET to achieve peak shear stress. This behaviour was possible because according to Fibertex (2017b), GTX-PET fabric possesses strains less than 40 % while GTX-PP has more strains of about 50 %. The polymer behaviour is in good agreement with finding by Karademir (2011).

4.5.3. Influence of asperity density alteration at constant asperity height on GMB/GTX interface peak displacement

This section considered GMB/GTX interfaces with varied GMBs asperity density at constant asperity height. Precisely, the textured geomembranes had asperity height of 0.7 mm and densities of 332 & 663 spikes per 10000 mm^2. The investigated GMB/GTX interfaces besides the smooth geomembrane interfaces were; GMB-T1/GTX-PP, GMB-T2/GTX-PP, GMB-T1/GTX-PET, and GMB-T2/GTX-PET.

Peak displacement-normal stress graphical relationship for the identified interfaces are illustrated in Figure 4-23. From the plot, it was evident that with the inclusion of (332 spikes per 10000 mm^2) asperity density, the displacement required to develop peak stress was increased by an average of 60 % in relation to the smooth geomembrane. Subsequently, the doubling of asperity density to "663 spikes per 10000 mm^2" as asperity height was fixed, caused the displacement needed to mobilize peak stress to increase by an additional 25 %. The changes to horizontal displacements required to achieve peak stresses were considered to be caused by the resulting fibre-asperities interaction as asperity density was varied. A possible explanation for the minimal increase of 25 % in peak displacement as asperity density was increased by 100 %, was the concentrated gripping of the asperities into the geotextile's fibres. Similarly, increment in peak displacement varied with applied stress, with the maximum increment recorded at mid stress (100 kPa). A scientific explanation for this behaviour at 100 kPa was the sufficient "hook and loop" interaction obtained at 100 kPa, as it was anticipated that relatively lower and higher

applied normal stresses results in inadequate and excessive fibre/asperities interaction, respectively.

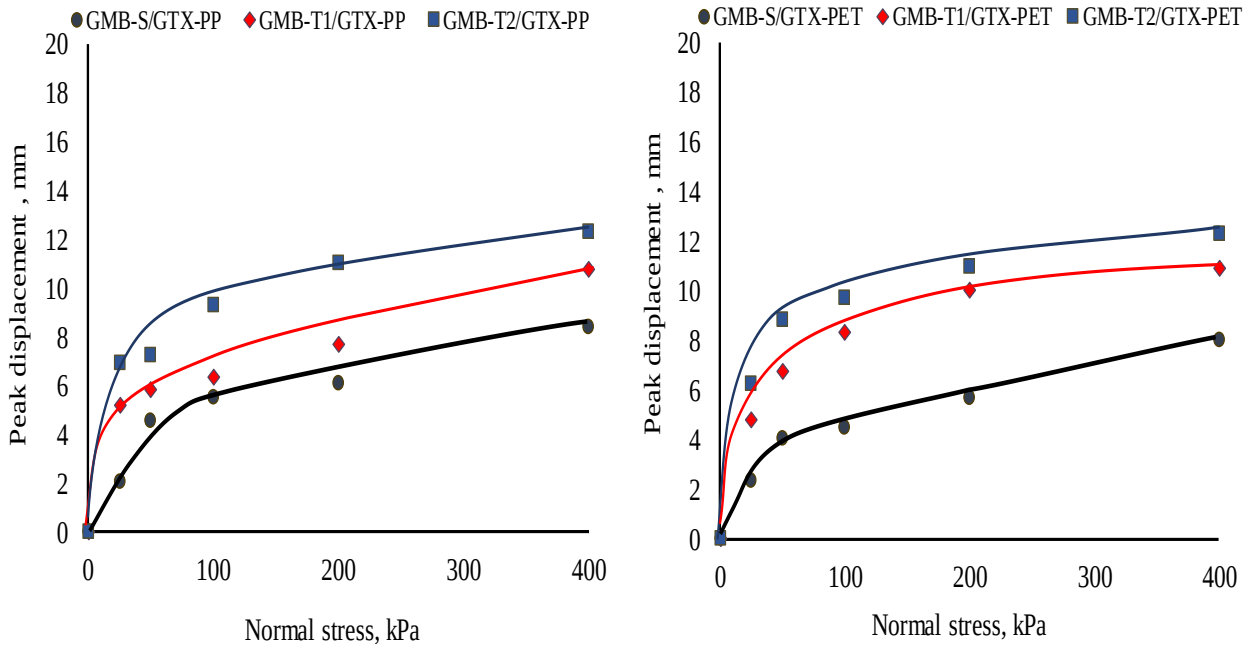

Figure 4-23: Peak displacement versus normal stress relationships for interfaces with varied asperity density

Table 4-5: Summary of the effects of varying asperity density on the GMB/GTX interface peak displacement

GMB	GTX	*Asp height (mm)	*Asp density	Interface peak displacement (mm) at various stress (kPa)				
				25	50	100	200	400
GMB-S	PP	0	0	2.02	4.54	5.52	6.06	8.36
	PET			2.34	4.06	4.47	5.66	8.00
GMB-T1	PP	0.70	332	5.16	5.82	6.30	7.70	10.77
	PET			4.79	6.77	8.29	10.00	10.93
GMB-T2	PP	0.70	663	6.90	7.21	9.30	11.01	12.26
	PET			6.26	8.80	9.71	10.95	12.27

* Asp = Asperity

Notably, the geotextile-type also influenced the horizontal displacement required to mobilized peak stress. With regard to the GMB-T/GTX interfaces, GMB-T/GTX-PET interfaces needed large displacement than GMB-T/GTX-PP interfaces to mobilize peak shear at all applied stresses except at 25 kPa (see Table 4-5). From Table 4-5, considering the 100% increase in asperity density at constant asperity height, it was observed that GMB/GTX-PP and GMB/GTX-PET interfaces increased by 30 % and 20 %, respectively, in the displacements required to develop

peak shear stress. The peak displacements increment demonstrated that GTX-PP due to its higher tensile strength undergoes more strains than GTX-PET. Therefore, the difference in the recorded peak displacement for the GMB-T/GTX interfaces was anticipated to be caused by the interaction between GTX fibre mechanical properties, and GMB asperities.

It was observed from the above analysis that a 100 % increase in asperity density at constant asperity height resulted in a minimal increase to the GMB/GTX interface peak displacement at all applied stresses except at 50 kPa and 100 kPa. From this investigation, it was considered that doubling of GMB asperity density under certain conditions might result in little or no peak displacement increment.

4.5.4. Summary of GMB/GTX peak displacement -normal stress relationship

In this study, all GMB/GTX interfaces peak shear strength were mobilized at 2 – 18.5 mm displacement range. It should be noted that the peak displacement magnitude was dependent on normal stress, geotextile type, and GMB asperities. From the presented graphs and tables, displacement required to attain peak stress increased with increases in normal stresses. As normal stress increases, "superficial-level" hook and loop interaction progress to "matrix-level" interlocking, hence resulted in greater peak displacement. Also, due to GTX-PP fibre tensile strength, GTX-PP interfaces developed peak stress at a greater displacement than GTX-PET interfaces. Hence, GTX-PP should be used instead of GTX-PET in long-term GMB/GTX applications where peak displacement criterion is the design criterion. More so, GMB/GTX interface peak displacement changes as asperity parameters vary. In particular, the variation in asperity height causes significant changes to the displacement needed to mobilise peak stress than asperity density.

4.6. Shear stress - normal stress relationship

4.6.1. Introduction

According to ASTM D5321 (2014), the Mohr-Coulomb failure envelope of a geosynthetics interface comprises of at least three conducted test-point. In this study, GMB/GTX shear test was conducted at five stresses, and the respective interface peak and large displacement (LD) shear stress were obtained and presented in Table A-1 of the appendix. From the obtained shear strength value, best-fit line or curves were produced and presented in this section.

4.6.2. Failure envelope determination

In this work, in order to determine the type of strength envelopes (linear or non-linear) that most described a given geosynthetics interface shear characteristics, the coefficient of regressions (R^2) was determined and examined. The closer R^2 values were to 1.0, the better the fit of the regression line (i.e. line or curves passed through most points). All interfaces shear stress - normal stress relationships were initially fitted using a linear representation. However, in order to ensure consistency of the R^2-values and the accurate representation of the shear stress-normal stress curve, all best-fit lines with R^2-values less than 0.98 were replaced with non-linear/curvilinear failure envelope (see Figure 4-24 to Figure 4-26), as a result, 80 % of the tests revealed non-linear failure envelopes (Fleming *et al.*, 2006; Sikwanda, 2018).

For each GMB/GTX interface failure envelope, the peak and LD shear strength values at all applied normal stresses were obtained from the shear stress-horizontal displacement plot presented in Figure 4-8, 9, 11, 13, 15, 17, and 19 and recorded in Table A-1. The obtained shear strength was plotted against the corresponding applied stress and an appropriate best-fit line/curve was used to connect the test point (see Figure 4-24 to Figure 4-26).

For linear envelopes, the interface friction angle was assumed to be constant at different applied normal stress. Whereas for a multi-linear and curvilinear envelope, the interface friction angle varies proportionally according to the confining stress. Thus, in the latter condition, the shear characteristics (friction angle and cohesion) at each stress level was obtained by drawing a tangent to the best-fit curve. The inclination of this line/slope corresponds to the tested geosynthetics interface friction angle, whereas, the vertical intercept represents the apparent adhesion. The general shear parameters of the curve were then derived by computing the mean of the shear characteristics at different applied stresses (Fox & Stark, 2009). This method of determining shear parameters for curvilinear failure envelope was recommended by Thiel (2001) and Fox & Stark (2004).

4.6.3. Asperity height alteration effects on GMB/GTX interface shear stress – normal stress relationship

This section evaluates the influence of asperity height variation at constant asperity density on the GMB/GTX interface failure envelope.

4.6.3.1 GMB/GTX failure envelope behaviour at varied asperity height (approximately 1 mm)

In Figure 4-24, the values of peak and LD shear stress were plotted against the normal stress, and the appropriate best-fit lines or curves were fitted through the test points. Generally, it was evident that the GTX-PET interfaces produced greater envelope than GTX-PP interfaces when sheared against different types of geomembranes such as GMB-S, GMB-T1, GMB-T4, and GMB-T5. This behaviour was caused by the higher interlock between the asperities and the GTX-PET thin and tightly clustered fibres. As a result, the GMB/GTX-PET interfaces corresponded to higher frictional resistance. On the contrary, GMB/GTX-PP interfaces recorded lower frictional resistance as the thick, and loosely clustered GTX-PP fibres were anticipated to be more stretched and brushed by the GMB asperities.

Considering GMB/GTX-PP interfaces, it was apparent that increasing the asperity height from 0.7 mm to 0.85 mm resulted in a minimal change in peak shear strength at all applied stress, compared to an increase of 9 %, 22 %, 3 %, 4 %, and 7 % in peak shear strength at 25, 50, 100, 200, and 400 kPa stress, respectively, as asperity height was subsequently increased to 1.2 mm. On the contrary, GMB/GTX-PET interfaces resulted in a 130 %, 34 %, 50 %, 42 %, and 44 % increase in peak shear strength at 25, 50, 100, 200, and 400 kPa stress, respectively, as asperity height increased to 1.2 mm. With regard to the effect of 70 % increase in asperity height on GMB/GTX-PET LD shear strength, 62 %, 25 %, 25 %, 17 % and 22 % increase in LD shear strength at 25, 50, 100, 200, and 400 kPa stress respectively were recorded. Conversely, GMB/GTX-PP interface LD shear strength recorded 15 %, 7 %, 9 %, 10 % and 23 % increase in LD shear strength at 25, 50, 100, 200, and 400 kPa stress, respectively, as asperity height increased to 1.2 mm. This analysis revealed that an increase in shear strength is dependent on asperity height increase as higher asperities provide greater interlocking depth into the geotextile-fibre. Also, the geotextile-fibre affects the interface shear characteristics, where GTX-PET produced greater shear values than GTX-PP.

With regard to asperity effects, textured geomembranes with asperity height below and slightly above 1 mm at constant average asperity density of 325 spikes per 10000 mm^2 were examined at the GMB/GTX interface. Although both asperities had similar shape and arrangement, the GMB-T5/GTX interfaces yielded a larger peak and LD failure envelopes because of the better hook and loop interaction developed by GMB-T5 asperity height. Also, GMB-T4/GTX

interfaces presented slightly greater failure envelope than GMB-T1/GTX interfaces because the asperity height of GMB-T4 was 10 % more than GMB-T1 asperity height. While GMB-S/GTX interface (smooth geomembrane) had the least failure envelopes, therefore, acted as the control interface.

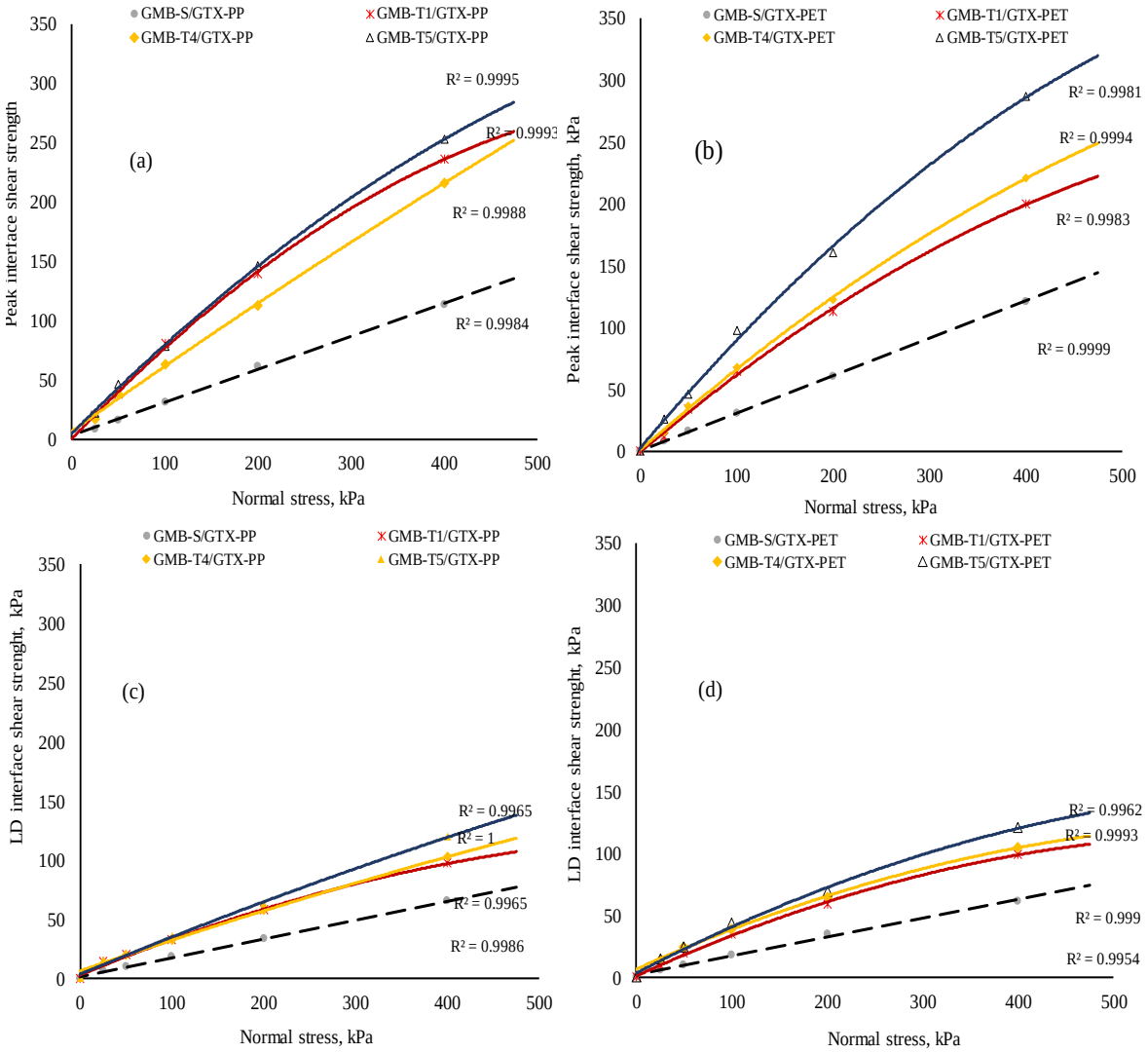

Figure 4-24: Shear stress versus normal stress for interfaces with varied asperity heights (approximately 1 mm) (a) GMB/GTX-PP "Peak" (b) GMB/GTX-PET "Peak" (c) GMB/GTX-PP "LD" (d) GMB/GTX-PET "LD"

From Table 4-6, it was noticed that dissimilarity in friction angle exists for different surface asperity heights, with the lowest friction angles being recorded for the smooth geomembrane interface. With the inclusion of asperities to smooth geomembrane, GMB-T1 (0.7 mm) interface produced an increase of 67 % and 54 % in peak and LD friction angle, respectively. Subsequently, a 20 % increase in asperity height (from 0.7 mm to 0.85 mm) at constant asperity

density led to an increase of 8 % in peak friction angle and no increase in LD friction angle. While a larger increase of 70 % in asperity height (from 0.7 mm to 1.20 mm) produced an increase of 25 % and 20 % in peak and LD friction angle, respectively. It should be noted that observations from apparent adhesion (c_a) did not reveal specific trends concerning asperity height, and geotextile type; hence, it was not examined. Also, regarding geotextile type, results obtained showed that the GMB/GTX-PET interfaces exhibited friction angle of about two degrees higher than the GMB/GTX-PP interfaces. GMB/GTX-PET exhibited higher friction angle because of its thin and tightly clustered fibre which allowed for stronger interlock with GMB asperities. Therefore, based on these results, it can be stated that GMB/GTX interfaces shear characteristic is dependent on changes to asperity height (even minor) and the type of geotextile used.

Table 4-6: GMB/GTX interface shear characteristics at varied asperity height (approximately 1 mm)

GMB	GTX	*Asp height (mm)	*Asp density	Peak shear strength parameter s			LD shear strength parameters		
				δ_p (°)	c_{a-p} (kPa)	**CoR	δ_{ld} (°)	c_{a-ld} (kPa)	**CoR
GMB-S	PP	0	0	15.6	3.3	0.998	8.9	2.4	0.999
	PET			16.8	0.8	1.000	8.6	2.1	0.995
GMB-T1	PP	0.70	332	26.5	9.2	0.999	13.2	8.8	0.997
	PET			27.5	9.1	0.998	13.7	8.1	0.999
GMB-T4	PP	0.85	337	29.7	6.2	0.999	13.4	5.6	1.000
	PET			28.3	6.5	0.999	13.3	8.7	0.999
GMB-T5	PP	1.20	306	31.2	10.6	1.000	16.1	5.3	0.997
	PET			35.2	11.7	0.998	16.2	7.8	0.996

* Asp = Asperity; **CoR = Coefficient of regression, δ_p = Peak interface friction angle, c_{a-p} = Peak apparent adhesion, δ_{ld} = LD interface friction angle, c_{a-ld} = LD apparent adhesion.

4.6.3.2 GMB/GTX interface failure envelope at varied asperity height (approximately 2 mm)

Given the details of the asperity height variation effect (approximately 1 mm) on GMB/GTX interface failure envelopes at constant asperity density, it is vital to investigate the effect of greater asperity height. Therefore, this section presents and discusses the failure envelope behaviour of GMB/GTX interface as asperity height (approximately 2 mm) was varied at constant asperity density. The investigated interfaces besides the GMB-S interfaces were; GMB-T6/GTX-PP, GMB-T7/GTX-PP, GMB-T6/GTX-PET, and GMB-T7/GTX-PET.

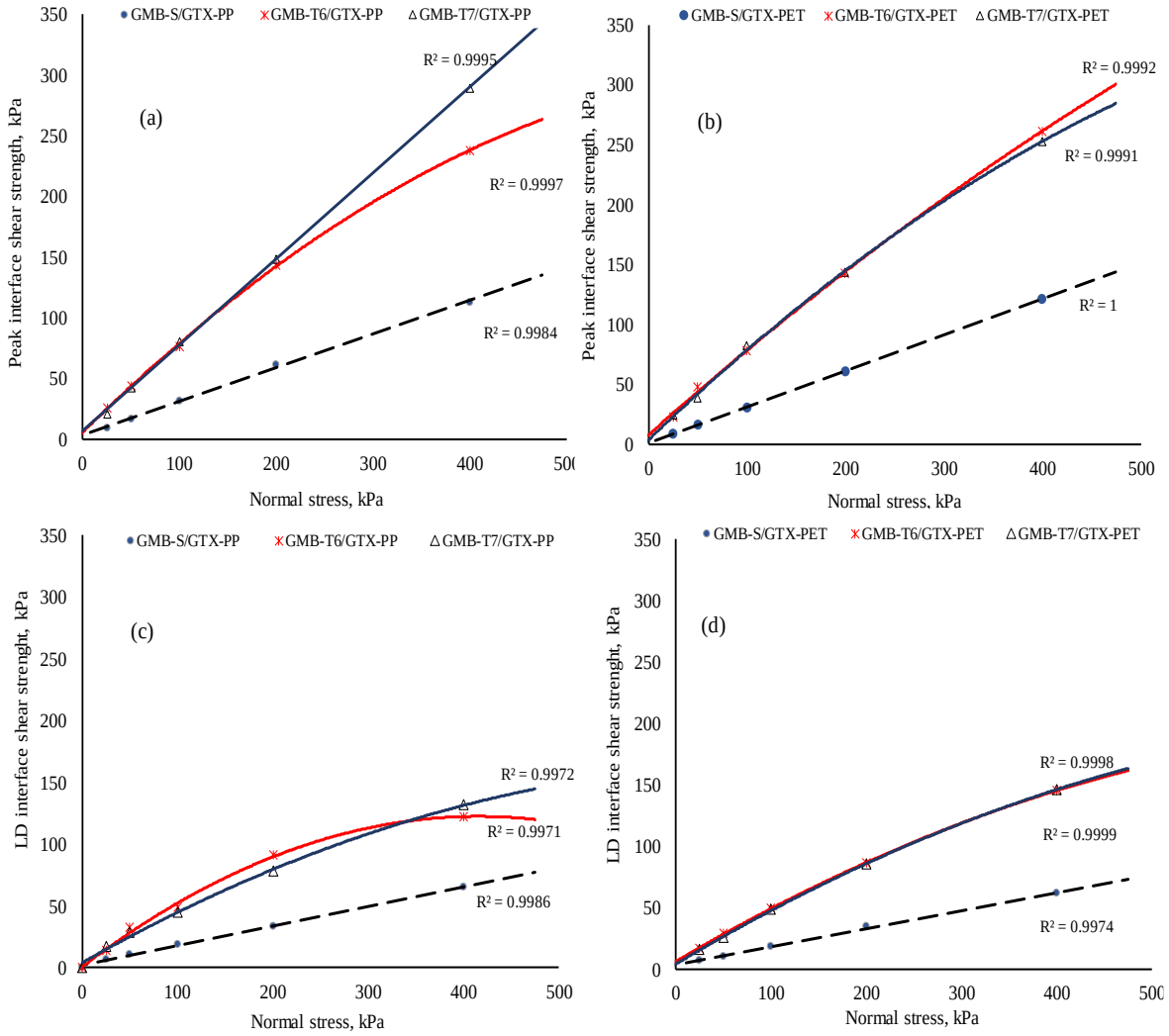

Figure 4-25: Shear stress versus normal stress for interfaces with varied asperity heights (approximately 2 mm) (a) GMB/GTX-PP "Peak" (b) GMB/GTX-PET "Peak" (c) GMB/GTX-PP "LD" (d) GMB/GTX-PET "LD"

It was apparent from Figure 4-25 that a 12 % increase in asperity height beyond 1.81 mm resulted in a -20 %, -3 %, 6 %, 3 %, and 20 % change in peak shear strength at 25, 50, 100, 200, and 400 kPa stress, respectively, for GMB/GTX-PP interfaces. On the contrary, GMB/GTX-PET interfaces resulted in an 8 %, -20 %, 5 %, 0.4 %, and -3 % change in peak shear strength at 25, 50, 100, 200, and 400 kPa stress, respectively. With regard to the effect of 12 % increase in asperity height beyond 1.81 mm on GMB/GTX-PET LD shear strength, 8 %, 11 %, 10 %, 15 % and 0.6 % decrease in LD shear strength at 25, 50, 100, 200, and 400 kPa stress, respectively, were recorded. Conversely, GMB/GTX-PP interface LD shear strength recorded 22 %, -13 %, -8 %, -15 % and 8 % change in LD shear strength at 25, 50, 100, 200, and 400 kPa stress respectively, as asperity height increased beyond 1.81 mm. This analysis revealed that asperity

height increase results in improved shear characteristics, although only minor changes or reductions in shear strength were identified beyond 1.81 mm asperity height. It was suggested that the minor changes in shear strength were caused by matrix-level raking of the geotextile-fibre by the asperities.

Although it was considered from Figure 4-25 that no significant alteration to the failure envelope occurred beyond 1.81 mm asperity height, GMB/GTX-PP interfaces still exhibited some minor changes in peak and LD failure envelope plot as asperity height increases. The GMB/GTX-PET failure envelope (Figure 4-25 b&d) displayed similar behaviour for both GMB-T6 and GMB-T7 interfaces because GTX-PET low-tensile fibre could not interlock further with higher asperities (2.02 mm) than it did at lower asperities (1.81 mm). Whereas, the GMB/GTX-PP interfaces failure envelope (Figure 4-25 a&c) exhibited minor differences as the asperity height was increased from 1.81 mm to 2.02 mm because GTX-PP high-tensile fibre could still interlock with asperities even at higher asperities.

Table 4-7: GMB/GTX interface shear characteristics at varied asperity height (approximately 2 mm)

GMB	GTX	*Asp height (mm)	*Asp density	Peak shear strength parameters			LD shear strength parameters		
				δ_p (°)	$c_{a\text{-}p}$ (kPa)	**CoR	δ_{ld} (°)	$c_{a\text{-}ld\delta}$ (kPa)	**CoR
GMB-S	PP	0	0	15.6	3.3	0.998	8.9	2.4	0.999
	PET			16.8	0.8	1.000	8.6	2.1	0.995
GMB-T6	PP	1.81	211	29.5	17.9	1.000	16.8	12.2	0.997
	PET			32.1	13.7	0.999	18.7	12.5	1.000
GMB-T7	PP	2.02	217	35.3	6.8	1.000	17.6	8.8	0.997
	PET			31.4	13.9	0.999	19.1	10.3	1.000

* Asp = Asperity; **CoR = Coefficient of regression, δ_p = Peak interface friction angle, $c_{a\text{-}p}$ = Peak apparent adhesion, δ_{ld} = LD interface friction angle, $c_{a\text{-}ld}$ = LD apparent adhesion.

From Table 4-7, the inclusion of asperities caused GMB-T6 (1.81 mm) interface to produce an increase of 90 % and 102 % in peak and LD friction angle, respectively, relative to GMB-S interface. Subsequently, a 12 % increase in asperity height (from 1.81 mm to 2.02 mm) together with a 3 % minimal increase in asperity density (from 211 spikes to 217 spikes) led to an increase of 10 % and 4 % in peak and LD friction angle, respectively. Furthermore, observation from apparent adhesion (c_a) did not reveal specific trends concerning asperity height, and geotextile type; therefore, it was not considered. The minimal increase in shear parameters beyond 1.81 mm asperities was considered to be caused by the increased asperity breakage and geotextile

fibre raking at increased asperity height. Therefore, it can be stated that considering the geotextile mass-density and provided the asperity density changes minimally, increases in asperity height beyond a specific value make asperity breakage easier and eventually produce a decrease or minor increment in the interface shear characteristics.

4.6.4. Asperity density alteration effects on GMB/GTX interface shear stress – normal stress relationship

This section presents and discusses the failure envelope behaviour of GMB/GTX interface as asperity density was varied at constant asperity height. The investigated interfaces besides the GMB-S interfaces were; GMB-T1/GTX-PP, GMB-T2/GTX-PP, GMB-T1/GTX-PET, and GMB-T2/GTX-PET.

From Figure 4-26, for GMB/GTX-PP interfaces, it was apparent that doubling asperity density (from 332 to 663 spikes) resulted in a 16 %, 30 %, 67 %, 51 %, and 37 % increase in peak shear strength at 25, 50, 100, 200, and 400 kPa stress, respectively. On the contrary, GMB/GTX-PET interfaces resulted in a 94 %, 33 %, 30 %, 25 %, and 23 % increase in peak shear strength at 25, 50, 100, 200, and 400 kPa stress, respectively. With regard to the effect of 100 % increase in asperity density on GMB/GTX-PET LD shear strength, 77 %, 61 %, 40 %, 35 % and 24 % increase in LD shear strength at 25, 50, 100, 200, and 400 kPa stress, respectively, were recorded. Conversely, GMB/GTX-PP interface LD shear strength recorded 17 %, 25 %, 15 %, 17 % and 6 % increase in LD shear strength at 25, 50, 100, 200, and 400 kPa stress, respectively, as asperity density was doubled.

This analysis revealed that doubling asperity density resulted in improved shear characteristics, where GTX-PET interfaces produced higher shear increase than GTX-PP interfaces because its fibres which were thin and tightly clustered accommodated matrix-level interaction with GMB asperities. Also, the effects of doubling asperity density were observed to reduce as applied stresses increased. It was suggested that increased asperity density at higher applied stresses caused excess interlocking and raking of geotextile fibres by asperities. Therefore, due to the relatively low percentage increase in shear strength as asperity density was increased by 100 %, asperity density effects on shear value and failure envelopes are relatively minimal.

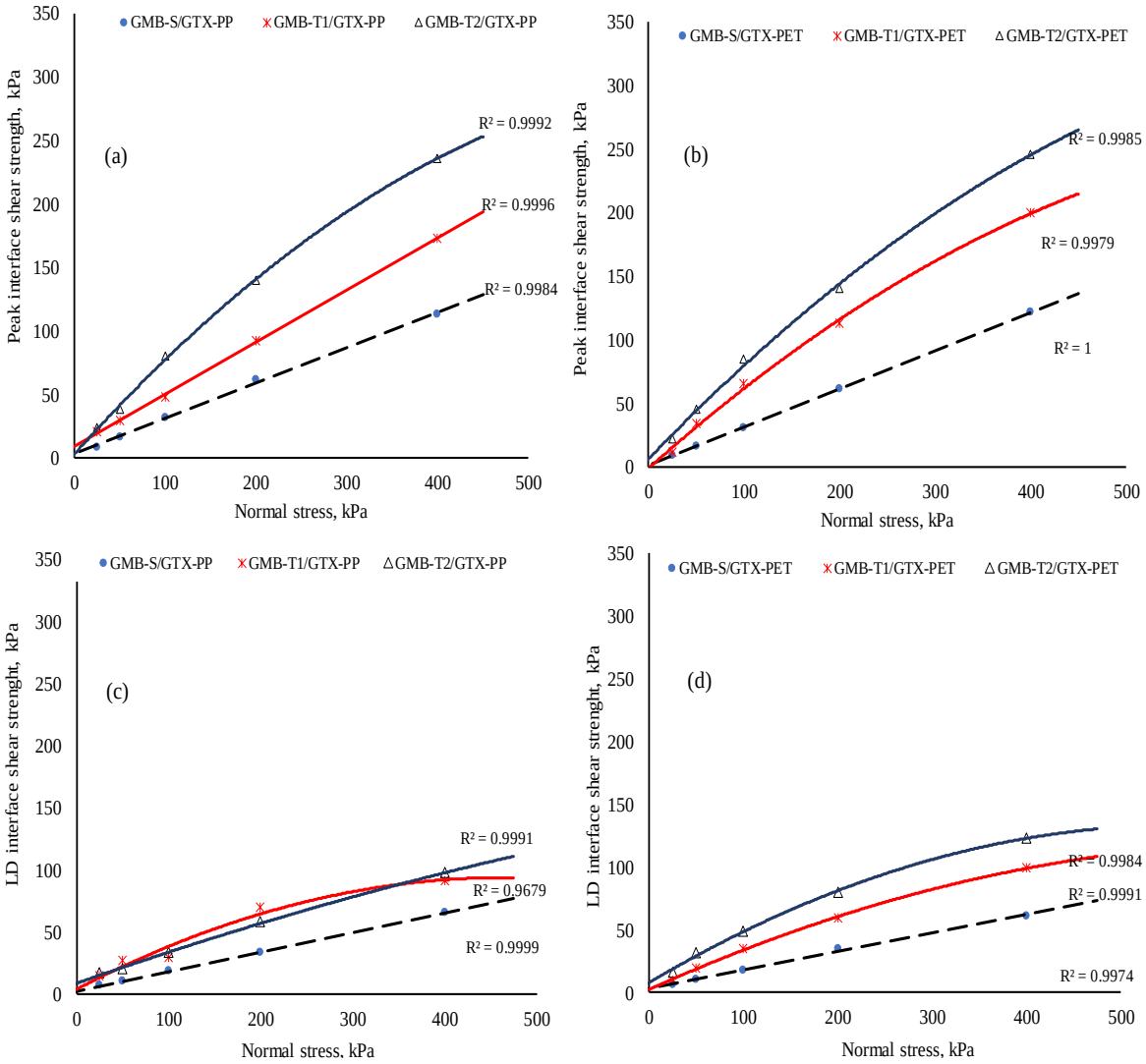

Figure 4-26: Shear stress versus normal stress for interfaces with varied asperity density (a) GMB/GTX-PP "Peak" (b) GMB/GTX-PET "Peak" (c) GMB/GTX-PP "LD" (d) GMB/GTX-PET "LD"

It was identified from Table 4-8 that with the inclusion of asperities, GMB-T1 (332 spikes) interface relative to GMB-S interface produced an increase of 67 % and 54 % in peak and LD friction angle, respectively. Subsequently, a 100 % increase in asperity density (from 332 to 663 spikes) at constant asperity height led to an increase of 11 % and 12 % in peak and LD friction angle, respectively. Again, observations from apparent adhesion (c_a) were not considered as it did not reveal specific trends concerning asperity density. The minimal increase in friction angle even at a 100 % increase in asperity density was considered to be caused by the weakening of the geotextile-fibre strength as the asperities tip mobilized concerted matrix-level interaction. Therefore, it can be stated that provided the GMB asperity height remains fixed, an increase in

asperity density produced a correspondingly less effect on the shear characteristic, particularly at large displacement.

Table 4-8: GMB/GTX interface shear characteristics at varied asperity density

GMB	GTX	*Asp height (mm)	*Asp density	Peak shear strength			LD shear strength		
				δ_p (°)	$c_{a\text{-}p}$ (kPa)	**CoR	δ_{ld} (°)	$c_{a\text{-}ld}$ (kPa)	**CoR
GMB-S	PP	0	0	15.6	3.3	0.998	8.9	2.4	0.999
	PET			16.8	0.8	1.000	8.6	2.1	0.995
GMB-T1	PP	0.70	332	26.5	9.2	0.999	13.2	15.8	0.997
	PET			27.5	9.1	0.998	13.7	8.1	0.999
GMB-T2	PP	0.70	663	29.5	16.2	0.999	12.4	10.8	0.999
	PET			30.3	17.2	0.999	15.4	17.2	0.999

* Asp = Asperity; **CoR = Coefficient of regression, δ_p = Peak interface friction angle, $c_{a\text{-}p}$ = Peak apparent adhesion, δ_{ld} = LD interface friction angle, $c_{a\text{-}ld}$ = LD apparent adhesion.

The significance of the above findings demonstrates the importance of maintaining sufficient spacing between asperities (density) to obtain better interface shear results rather than assuming greater asperity density would produce higher interface shear strength.

4.6.5. Asperity volume effect on GMB/GTX interface shear stress – normal stress relationship

Asperity volume represents the 3-dimensional volumetric space available for geosynthetics (GMB/GTX) interaction. The concept of asperity volume (A_v), which is the product of geomembranes asperity height and density, was developed to provide a further understanding of the geosynthetics interaction that occur during shear tests. The degree of interaction accommodated within the asperity volume corresponds to the shear characteristics derived from the failure envelope. The effects of GMB asperity volume were only observed on the friction angle, as adhesion was considered negligible.

In previous analyses, one of the asperity parameters was fixed while the other was varied. However, in this section, asperity volume, which involves the simultaneous variation of asperity height and density was considered. As a result, a comprehensive analysis of the relationships between asperity height, density, spacing, and friction angle (δ) was evaluated simultaneously. The outcome of the analysis was represented by the plot of δ against asperity volume (see Figure 4-27), where the asperity volume and the friction angle value were obtained from Table A-2 presented in the appendix.

As observed from Figure 4-27, friction angle gradually increased as A_v increased, this behaviour continued until the maximum friction angle was reached. After which any subsequent increase in asperity volume beyond the maximum value led to a reduction in friction angle. The A_v at which the maximum friction angle occurs was called "optimal volume". Also, an increase in asperity volume (caused by progressive changes to asperity density) caused a reduction in the large displacement (LD) interface friction angle. It was anticipated that the reduction at large displacement was caused by the deformation of GMB asperities and GTX fibre pull-out due to the weakening of the geomaterial at the interface. Similarly, A_v influences both the GMB/GTX-PP and GMB/GTX-PET interface friction angle, where the GMB/GTX-PET interfaces exhibited higher friction angle than GMB/GTX-PP interfaces, (see Figure 4-27). This behaviour implies that GTX-PET would develop improved frictional resistance against sliding failure at the weakest landfill-liner interface than GTX-PP, provided test or field conditions remained constant.

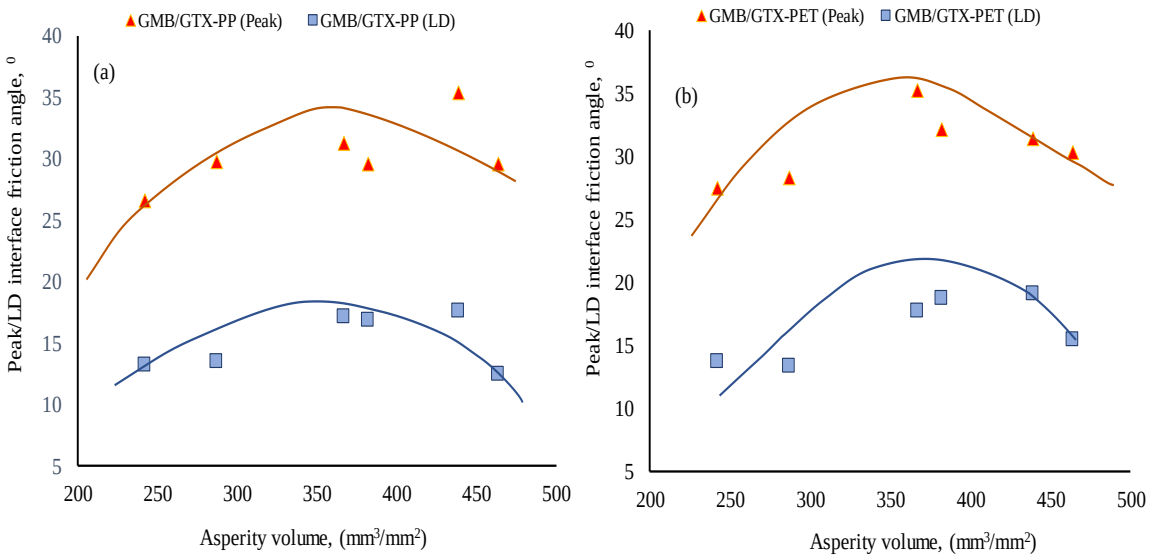

Figure 4-27: Relationship between asperity volume and peak and LD interface friction angle for (a) GMB/GTX-PP (b) GMB/GTX-PP, interface

In summary, the exhibited relationship between the GMB/GTX interfaces friction angles and asperity volume (A_v) was parabolic. Importantly, asperity density, which is dependent on asperity spacing and inclination, is a determinative factor of this parabolic relationship. The results in Figure 4-27 suggest that there is an optimal asperity volume of 370 mm^3/mm^2, beyond which the friction angle decreases. The corresponding average peak and LD interface friction angles at the optimum A_v are 35° and 20°, respectively. Again, this demonstrates the importance of achieving

sufficient fibre-asperity interaction rather than merely assuming greater asperity distribution is proportional to shear strength.

4.6.6. Influence of geomembrane roughness parameter on GMB/GTX interface shear strength

The geomembrane roughness parameters and the corresponding interface friction angles are presented in Table 4-9. From the data, it was evident that the GMB/GTX interfaces exhibited a corresponding change in the peak and LD friction angle as line and area roughness parameters were varied. The smaller friction angle belonged to interface with lower roughness parameters while the larger friction angle corresponded to higher roughness measurement. Also, at the lower roughened interface, the shear strength was supplied by the friction mechanism only, while friction and interlocking mechanism produced the shear strength at higher roughened interface. Also, it should be noted that the applied normal stress affects the anticipated interface shear mechanism.

Table 4-9: Summary of the roughness parameter and the corresponding interface friction angle

GMB label	GTX	R_a along-asperities (µm)	R_a between-asperities (µm)	S_a(µm)	Interface friction angle(°)	
					Peak	LD
GMB-S	PP PET	9.09	6.61	19.77	15.6 16.8	8.9 8.6
GMB-T1	PP PET	146.83	29.90	60.17	27.5 26.5	13.2 13.7
GMB-T2	PP PET	172.43	30.18	63.99	29.5 30.3	12.4 15.4
GMB-T3	PP PET	186.55	28.29	64.05	27.5 26.5	13.0 15.1
GMB-T4	PP PET	228.14	17.55	63.92	29.7 28.3	13.4 13.3
GMB-T5	PP PET	434.71	24.50	140.77	31.2 35.2	17.1 17.7
GMB-T6	PP PET	708.13	26.66	201.89	29.5 32.1	16.8 18.7
GMB-T7	PP PET	696.11	21.64	198.68	35.3 31.4	17.6 19.1

It was observed that both roughness measurements R_a (along-asperities and between-asperities) and S_a (average area roughness) are crucial to evaluate the geomembrane roughness effect on the interface friction angle, where S_a represents an average of the along- asperities and between-

asperities. This was necessary because roughness (R_a) variation determines the type of interaction obtainable between geomembrane texturing and interfaced geotextile fibres. For instance, GMB-T1 with along-asperities and between-asperities R_a values of 146.83 μm and 29.90 μm, respectively, exhibited peak and LD friction angles of 27° and 13.5°, respectively. While GMB-T7 with along-asperities and between-asperities R_a values of 696.11 μm and 21.64 μm, respectively, exhibited peak and LD friction angles of 33.5° and 18.5°, respectively. It was anticipated that GMB-T1 produced lower friction angle as a result of the superficial-level hook and loop interaction between its roughness and geotextile fibre, whereas GMB-T7 roughness aptly interacted with the fibre at the matrix-level and produced an increase of 25 % and 37 % in peak and LD friction angle, respectively. Also, it was observed that the degree of shear interaction at the matrix-level is largely dependent on the between-asperities roughness as along-asperities roughness was expected to undergo deformation earlier during shearing motion. For instance, both GMB-T6 and GMB-T7 have similar along asperities roughness of 700 μm; however, they exhibited different friction angles at the GMB/GTX interface because they differ in between-asperities roughness. Where GMB-T6 exhibited average peak and LD friction angle of 30.8° and 17.8°, respectively, and GMB-T7 exhibited average peak and LD friction angle of 33.5° and 18.5°, respectively. It was observed that although GMB-T6 had greater between-asperities roughness than GMB-T7, it developed the lower frictional angle. Therefore, it was anticipated that for a given interface geotextile, there exists a GMB roughness parameter above which there would be little or no improvement in friction angle.

Regarding the geomembrane roughness effects on GTX-PP and GTX-PET interfaces friction angle, it was observed that for both geotextiles, increase in geomembrane roughness (R_a) caused a corresponding rise in GMB/GTX friction angle. In particular, due to GTX-PET fibre structure and arrangement, its interfaces exhibited higher friction angles than GTX-PP interfaces. Also, GTX-PET and GTX-PP interfaces exhibited the highest peak friction angle when interfaced against GMB-T5 and GMB-T7 interfaces, respectively. This pattern was considered to be caused by fibre characteristics, where GTX-PP was made of virgin polypropylene and GTX-PET manufactured from recycled polyester. Therefore, GTX-PP fibre can interlock with higher asperities, whereas GTX-PET cannot.

Another critical factor that determines which roughness parameter (along-asperities or between-asperities) is of more significant impact on the GMB/GTX shear strength is the applied normal

stress. For instance, at lower normal stresses of 25 and 50 kPa, along-asperities roughness influences interface shear characteristics more than between-asperities roughness. This behaviour at lower stresses occurred because the between-asperities roughness was not actively interacting with the geotextile fibres. While, at higher normal stresses of 100, 200 and 400 kPa, both roughness parameter (along-asperities and between-asperities) was able to interact with the geotextile fibres in a series of matrix-level hook and loop interactions. The outcome of geosynthetics interaction at higher and lower stresses was visually observed and illustrated in Figure 4-28, where limited and excessive indentations were observed on the GTX surface at lower stresses and higher stresses, respectively. These observations are in good agreement with the finding of Hebeler *et al*., (2005).

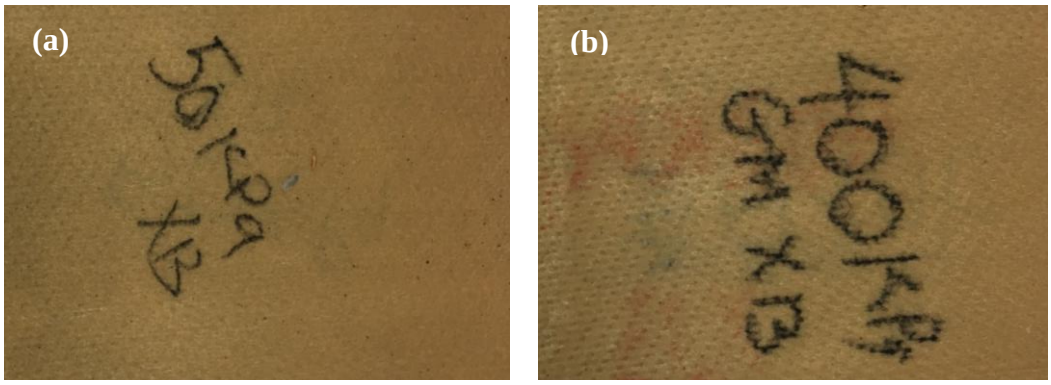

Figure 4-28: Sheared geotextile with observed indentation at (a) low stress (b) high stress

From Figure 4-29, a bilinear trend between peak interface friction angle and surface roughness (along-asperities, between-asperities, and average area) was evident, with the interface friction angle increasing with R_a roughness value to a critical value and then stabilizes or reduces. Also, a similar trend was observed for the LD friction angles as it increases gradually with changes in roughness up to a limiting value, beyond which, the rate of friction angle increase reduces or stays fixed. Although both peak and LD friction angle exhibited similar trends, the behaviour at the LD exhibited gentle gradients than those identified at the peak behaviour. It should be noted that, except for the friction angle/between-asperities relationship, the bilinear trend agrees with graphs presented by Uesugi & Kishida (1986); Frost & Lee (1990); and Martinez & Frost (2017). All friction angle/roughness relationship except friction angle/between-asperities relationship exhibited no change in friction angle as the surface roughness increased past the critical value. It was anticipated that at lower surface roughness (the first section of the bilinear) the shear mechanism was mainly sliding, however as surface roughness increased higher particle

interactions occurred between the geomaterials. The continuation of this interaction, particularly at higher stresses, was considered to result in geotextile fibre pull out and GMB roughness

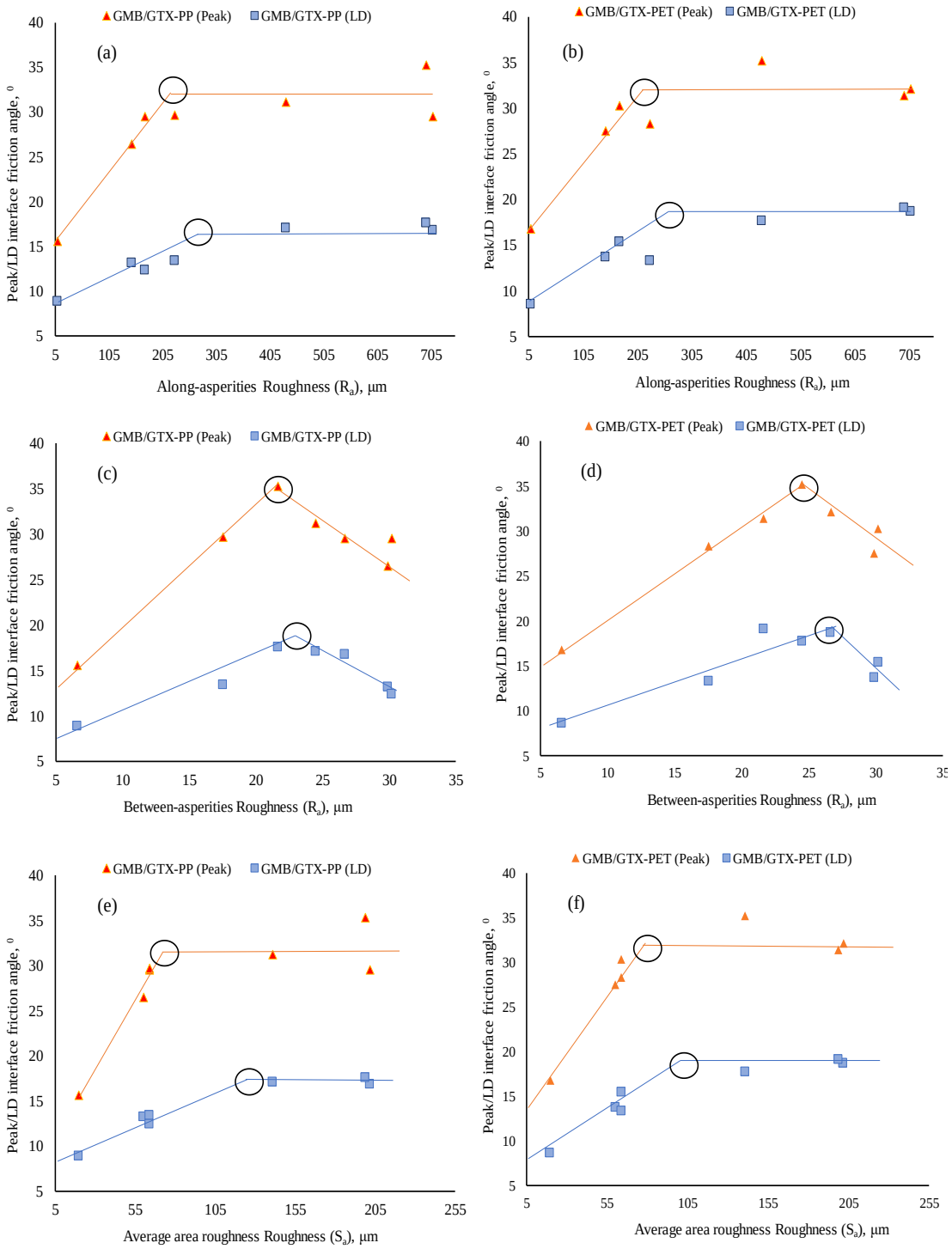

Figure 4-29: Relationship between GMB/GTX-PP & GMB/GTX-PET interface friction angle and average roughness (a) & (b) along-asperities line roughness (c) & (d) between-asperities line roughness (e) & (f) area roughness

scraping, which eventually caused the observed friction angle reduction or stabilization (the second section of the bilinear). The surface roughness at which the friction angle either reduces or stabilizes is termed the "critical" roughness (see the inflexion points in Figure 4-29). The summary of critical roughness required to mobilise the highest peak and LD friction angle are presented in Table 4-10, where GTX-PET interfaces due to its fibre structure, were observed to require more roughness than GTX-PP interfaces. The maximum peak and LD friction angle for along-asperities roughness, between-asperities roughness, and average area roughness comparison is 35° and 19°, respectively.

Table 4-10: Summary of GMB/GTX interface critical surface roughness parameters

Interface	Along-asperities Roughness (R_a), µm		Between-asperities Roughness (R_a), µm		S_a(µm)	
	Peak	LD	Peak	LD	Peak	LD
GMB/GTX-PP	225	210	22	23	72	125
GMB/GTX-PET	270	265	25	27	78	100

4.6.7. Summary of asperity properties variation and roughness on GMB/GTX interface failure envelope

In summary, the geotextile fibre influences both the peak and LD interface shear strength. Also, some trends were evident in the obtained shear characteristics (frictional angles and apparent adhesion) from Table 4-6 through Table 4-10. These patterns were attributed to GMB asperity parameters variation, roughness properties, and geotextile-type. Regarding asperities, significant differences in the shear parameters were observed as GMB asperity height was varied, thus, signifying that GMB/GTX interface shear parameters are more susceptible to changes from asperity height than asperity density, particularly at heights close to 1 mm. Also, it was observed that the influence of along-asperities and between-asperities roughness on the interface friction angle is dependent on applied stresses and geotextile properties.

4.7. Roughness and asperities effects on GMB/GTX interface wear mechanism

According to Dove & Frost (1996), the primary shear mechanism that occurs at geomembrane/geotextile (GMB/GTX) interface includes sliding (friction between geomaterials) and ploughing (hook and loop interlocking) shear mechanism, where ploughing mechanism requires more roughness and higher applied stresses than sliding mechanism. Usually, both shear

mechanisms are accompanied by a measure of wear during interface relative movement, where wear is the process of physical and mechanical characteristics alterations and is often influenced by the surface roughness profile (Thomas, 1999).

Due to the different asperities and roughness properties of the geomembranes used in this study, specific wear mechanisms were considered to have occurred at the GMB/GTX interface at the end of the shear tests. The observed load-induced wear mechanisms at the interface are explained and illustrated below. Notably, the observed mechanisms were in good agreement with experimental findings by Frost & Lee (1990) and Zaharescu (2018).

- Geosynthetics polishing –This is the simplest wear mechanism, and it was considered to be activated during consolidation or immediately after initiating the direct shear test (pre-peak stage). Among other wear mechanisms considered in this study, geosynthetics polishing might be difficult to notice at the end of the shear test and during the post-shear surface evaluation because it is often superimposed by peak and post-peak stage shear characteristics. It was anticipated to be characterised by the clean abrasion of geotextile-fibre and along-asperities roughness without scraping or raking (Thomas, 1999).

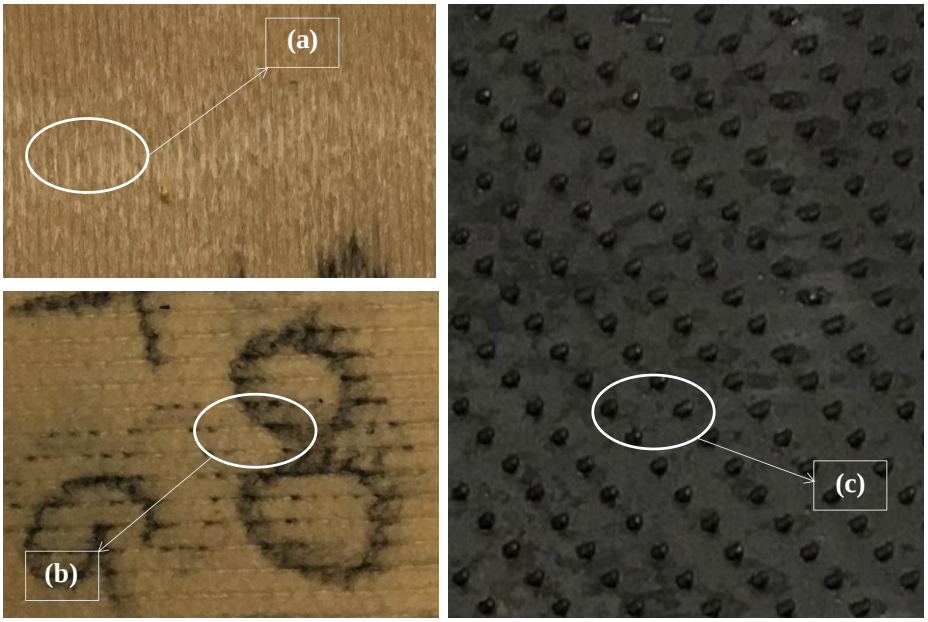

Figure 4-30: Illustration of GMB/GTX interface wear mechanism; (a) geotextile filament pulling (b) geotextile fibre breaking (c) geomembrane asperities damage

- Geotextile filament pull-out – During this mechanism that occurred at both higher and lower applied stress, it was considered that the GMB along-asperities roughness rearranged the geotextile fibres to the shearing direction and subsequently caused the

pulling out of geotextile fibres (see Figure 4-30a). It should be noted that as sufficient fibres were removed, superficial-level hook and loop interaction began to diminish.

- Geotextile filament breakage – In this case, matrix-level hook and loop interaction were considered to begin as the shear test continues (see Figure 4-30b). At this stage, it was anticipated that the geotextile filaments were exposed to further deformation by the geomembrane along-asperities and between-asperities roughness. This deformation is termed "filament breakage" and is more likely to occur at higher applied stress.
- Geomembrane asperities damage – It was anticipated that at a later stage of the matrix-level hook and loop interaction, GMB asperities were prone to deformation such as bending, breakage, and removal especially when sheared against a high-tensile geotextile at higher normal stresses (see Figure 4-30c). It should be noted that asperities deformations are easier when the asperity height is increased beyond a certain value. Although the damage mechanism eventually resulted in interface shear strength reduction, the between-asperities roughness still interacts with the geotextile fibre and contribute to the shear strength.

4.8. Summary of research findings

This chapter has presented the results of an extensive laboratory investigation that was designed to assess the potential of increasing geomembrane/geotextile interface shear strength across different surface textures. The research has further improved the understanding of the primary mechanism governing GMB/GTX interfaces. The study also provides the opportunity to optimize interfaces in landfill application through the control of the selected geomembrane roughness and asperities where possible. Furthermore, the asperity volume developed and validated herein enables the influence of surface asperities on interface strength to be estimated for a preliminary study.

GMB/GTX interfaces were tested at applied normal stresses of 25, 50, 100, 200, and 400 kPa. The interface shear strength, peak displacement, and friction angle were recorded for each interface. Based on the data collected, the following summary regarding the geosynthetics interfaces was drawn:

- Although an average increase of 5 kPa in interface shear strength was recorded as asperity shape changed, there was no significant difference in interface friction angle. This

suggests that not all changes in asperity changes result in friction angle improvement. Thus, the decision by manufacturers to change asperity shape should be made based on quantified experimental data.

- In geotechnical applications where GMB-S are interfaced against GTX, the type of GTX-polymer does not make a significant difference on the recorded peak and LD shear strength. Therefore, GTX selection should be made based on cost, availability, and the site anticipated chemical condition. Also, for GMB-S interfaces, the displacement required to develop peak shear stress rose gradually with applied normal stresses, where GTX-PP exhibited greater peak displacement than GTX-PET. Based on this behaviour, GTX-PP, together with GMB-S could be utilized in the top liner instead of GTX-PET, as it requires a longer period to experience strain softening, thus, increasing design durability.
- In applications involving GMB-T, geotextile-polymer contribute immensely to the development of interface shear. For most instances, GTX-PET, due to its fibre-structure and arrangement, exhibited higher shear strength than GTX-PP, thus, increasing stability against sliding particularly at the side-slope lining. Also, the magnitude of shear strength change is dependent on the asperity height and density, as well as applied normal stresses.
- As asperity height was increased by 70 %, a maximum increase in the displacement required to mobilize peak shear of 24 % was observed. It should be noted that the increase in peak displacement was limited to 8 % as asperity height was increased above 1.8 mm. Therefore, based on this behaviour, it was considered that the properties of the geotextiles such as; thickness and mass-density, should be considered before selecting higher asperities for usage at GMB/GTX interface, as the asperities could deform the fibres instead of contributing to durability or strength. On the contrary, a maximum 100 % increase in asperity density produced a 24 % increase to the displacement needed to develop peak shear. Hence, this observation suggests that in order to improve peak displacement, increasing asperity height is more effective than increasing asperity density.
- In addition, with respect to the displacement required to mobilize peak shear at textured geomembrane interfaces, where asperity height and density were increased, GTX-PP exhibited greater value than GTX-PET. Based on this behaviour, GTX-PP should be used

instead of GTX-PET at the basal-liner of landfill. This selection would delay the occurrence of strain-softening.

- Considering the effects of asperities on GMB/GTX frictional resistance, 20 %, 70 % and 12 % increase in asperity height resulted in 8 %, 25 %, and 10 % increase in peak friction angles, respectively. Whereas, doubling asperity density (100 % increase) at fixed asperity height led to an increase of 11 % to the peak friction angle. Also, 0 %, 20 % and 4 % increase in LD friction angles were produced by an asperity height increase of 20 %, 70 %, and 12 %, respectively. While doubling asperity density led to an increase of 12 % to the LD friction angle. Therefore, based on this observation regarding frictional resistance, the increase in asperity height is more effective than GMB asperity density increase.
- Provided the selected geosynthetics are similar to those considered in this investigation, the optimum asperity volume (product of asperity height and density) which should produce the maximum frictional resistance would be approximately 370 mm^3/mm^2. The estimation could be useful for material selection and preliminary design.
- With regard to cover liners subjected to relatively lower stresses of 25 & 50 kPa, GMB along-asperities roughness should be considered during geomembrane selection for the GMB/GTX interface. On the contrary, at the bottom and side-slope liners subjected to relatively higher stresses of 100, 200, and 400 kPa, both roughness parameters especially between-asperities roughness of the geomembrane, must be properly selected in order to achieve optimum frictional resistance. This is because between-asperity roughness with large undulating trend was anticipated to result in excessive geotextile-fibre pulling and breakage, and eventually result in reduced frictional resistance. Also, the critical surface roughness provided in Table 4-10 of this study could be used in selecting the appropriate geomembrane, provided the geotextile-type and asperities properties are very similar. Therefore, it is recommended that landfill liner designers should consider geomembrane roughness characteristics provided by geomembrane manufacturers during material selection and frictional resistance estimation.
- Additionally, along-asperities roughness often governs geomembrane-asperities damage and geotextile filament pulling wear mechanisms; however, both along-asperities and between-asperities roughness contribute to the geotextile-fibre breakage wear

mechanism. Therefore, geosynthetics degree of roughness is an important parameter that should be considered when selecting landfill geosynthetics and conducting landfill-liner stability analysis.

- In landfill stability analysis, particularly the slope liner, the computed factor of safety (FoS) value obtained through the limit equilibrium analysis method (LEM see example in Table A-4) and parameters presented in Table A-3, is an estimate of the tendency of sliding failure to occur at the weakest interface, which in this scenario was the GMB/GTX interface (see equations in Section 2.5.3). According to Qian et al. (2003), the minimum recommended FoS for peak and large displacement (LD) stability calculation were 1.5 and 1.0, respectively.
- Considering the effects of asperities on peak and LD FoS (see Table A-5), it was observed that FoS vary as the geomembrane asperities were altered, especially the asperity height. Also, it was observed that an increase in asperity height until 1.81 mm height resulted in a corresponding rise in peak and LD FoS. After which, a subsequent increase in asperity height led to little or no increase in the recorded FoS, where GMB-T5 and GMB-T7 produced the highest peak and LD FoS values (twice the recommended minimum FoS). An apparent reason for the little increase in FoS at high asperity height could be related to the asperity damage and fibre breakage.
- Also, the type of geotextile-polymer used at the interface affects the FoS, where for all tested GMB/GTX interface, GTX-PET resulted in greater FoS than GTX-PP. Therefore, GTX-PET is more preferred for a landfill liner designed according to LD shear parameters. Therefore, obtaining optimised shear strength parameters (i.e. friction angle and adhesion) which in turn produces the liner stability factor, is hinged on selecting the appropriate geotextile type and geomembrane asperity properties at the critical GMB/GTX interface.

5. CONCLUSIONS AND RECOMMENDATIONS

5.1. Introduction

In this work, interface shear tests were carried out on the geomembrane/geotextile (GMB/GTX) interface using the ShearTrac-III large direct shear apparatus of 305 mm x 305 mm box dimension. The geosynthetics interface tests were performed to examine the influence of asperity height, density, shape, volume as well as roughness on the shear strength characteristics. The test program was implemented to include geomembranes with relatable asperity properties.

The testing methods developed in this work enabled the study of responses such as shear stress against horizontal displacement, peak displacement against normal stress, shear stress versus normal stress, and asperity volume versus friction angle. The analysis of the results supplied crucial information about the preferential use of one geomembrane instead of the other. The preferences relate directly with the geomembrane asperity and roughness, as the surface properties influence the criticality of the geosynthetics interface in landfill liner. Thus, this chapter provides conclusions obtained from this research, thereafter areas for further research efforts are motivated and presented.

5.2. Conclusions of the study

The following conclusions emerging from this study are presented below;

1. Test results considering effects of asperity parameters on the GMB/GTX interface revealed that asperity height, as well as asperity density, shape and volume, affects the geosynthetics interface shear characteristics, i.e. friction angle and apparent adhesion are dependent on the geotextile interaction with the asperity features. Most importantly, asperity height was observed to be a major determinant of the interface shear strength, as relatively higher asperity surface often mobilizes greater peak shear stress even at relatively low asperity density.
2. In all GMB/GTX interfaces tests conducted, the “pre-peak” curvature of the shear stress – horizontal displacement curve exhibited typical geosynthetics shear stress behaviour with non-linear features, irrespective of the geotextile- polymer type, asperities properties and applied normal stresses. However, during the “post-peak” phase of the curve, undulations and shear reductions were noticed which were dependent on the geotextile-

polymer property, asperities parameters, and confining stress. Particularly, the shear behaviour after the peak stress was observed to be controlled by asperity density and shape. In addition, the undulation patterns were seen to increase with a corresponding increase in normal stresses.

3. The use of polyester geotextile (GTX-PET) at the geomembrane/geotextile interfaces tests generally resulted in greater shear stress and lesser fibre deformations and fractures than polypropylene geotextile (GTX-PP). The observed GTX-PET characteristics were caused by the superior interaction between GMB asperities and GTX-PET thin and tightly clustered fibres. This behaviour makes GTX-PET more preferred than GTX-PP as liner materials in landfills designed according to the ultimate limit criterion.
4. Generally, due to the presence of asperities, GTX-PP exhibited higher strains than GTX-PET, as GTX-PP possesses more ductility and tensile strength in its fibre constituent. Thus, for landfills design according to serviceability limit criterion, GTX-PP is more preferred because relatively greater shearing displacement is required to mobilise peak shear strength.
5. As asperity height was varied at constant asperity density, the obtained shear strength characteristics revealed that a 70 % increase in asperity height produced a peak friction angle improvement of 25 %, whereas a 100 % increase in asperity density at constant height resulted in an average increase of 25 % in the measured peak interface friction angle. Therefore, both asperity height and density affect the interface peak friction angle, with the asperity height being more significant than asperity density.
6. A further increase in asperity height above 1.81 mm was observed to produce little or no improvement on the GMB/GTX shear characteristics. Also, a high concentration of geomembrane asperity negatively affects the LD shear strength, as it influences extreme shear reduction. Furthermore, the dynamic of the asperity height and density interaction was evaluated through the quantified asperity volume, and based on the research findings, an optimal asperity volume of 370 mm^3/mm^2 was recorded.
7. Change in asperity shape (conical to “cone with hook”) when other asperity parameters were fixed did not produce significant changes in the peak and LD friction angle though minimal improvement in shear strengths was observed. Also, the GMB-T3/GTX (hooked asperities) interfaces produced more “undulations” than GMB-T1/GTX (conical

asperities), where the level of undulations was dependent on the interfaced geotextile-polymer.

8. The common wear mechanisms at the geomembrane/geotextile interface were geosynthetics polishing, geotextile filament pull-out, geotextile filament breakage, and geomembrane asperities damage, and were due to the micro-scale load-induced materials deformation at the shear interface. It was considered that the along-asperities roughness often governs geomembrane-asperities damage and geotextile filament pulling shear mechanisms. Whereas, both along-asperities and between-asperities roughness contribute to the geotextile-fibre breakage shear mechanism.
9. Along-asperities roughness influence interface shear characteristics at lower normal stresses (25 and 50 kPa), while both along-asperities and between-asperities roughness would interact with the interfaced geotextile at high normal stresses (100, 200 and 400 kPa). Furthermore, the friction angles were influenced by the interfaced geotextile and increase gradually as R_a values increases until a critical value was attained and then remains fixed or tapered off. The highest peak and LD friction angle for all interfaces is 35° and 19°, respectively.

5.3. Recommendations

The following are the recommendations for future research:

1. The use of geotextiles with high mass-density (> 400 g/m^2) and geomembranes with higher ranges of asperity height (> 2 mm) and density (> 663 spikes per 10000 mm^2) at the geomembrane/geotextile interface to investigate the effects of asperities on shear characteristics.
2. Additional asperity shapes effects on the geomembrane/geotextile interface should be considered.
3. Studies on the effects of asperities parameter on other recognized single critical landfill interfaces such as GMB/GCL and GMB/GCD should be considered.
4. Conducting direct shear tests on multi-interface to investigate the effects of asperities on the multi-interface liner shear characteristics as well as computing the corresponding stability factor could be a potential research area.

5. As the geotextile used in this study were extensible, real-time monitoring of displacement mobilization at the geomembrane/geotextile interface during shearing to evaluate the geosynthetics interaction behaviour is a viable area for further research.

REFERENCES

Adeleke, D; Kalumba, D; & Oriokot, J. 2019. Asperities effect on polypropylene & polyester geotextile-geomembrane interface shear behaviour. In E3S Web of Conferences. V. 92. 5. DOI: 10.1051/e3sconf/20199213017.

Adesokan, D. & Blond, E. 2018. Asperity height or asperity concentration : what matters more for interface shear resistance on textured polyethylene (PE) geomembranes ? *Proceedings of the 11th International Conference on Geosynthetics*, 16-21 September 2018, Seoul, Korea.

AGRU. 2020. *AGRU America's Innovative Geomembrane Liners*. Available: https://agruamerica.com/company/ [Accessed February 20 2020].

AKS. 2018. *AKS Lining Systems*. Cape Town.

AKS Lining Systems. 2020. *Co-Extruded Geomembrane application*. Available: http://www.aks.co.za/co-extruded-aks/ [Accessed February 24 2020].

Alzahrani, S. 2017. Effect of time on soil-geomembrane interface shear strength. MSc Dissertation submitted to the University of Dayton, Ohio.

ASTM D4439. 2018. Standard Terminology for Geosynthetics. *ASTM International*. 1(May): pp 1–4. DOI: 10.1520/D3878-15.2.

ASTM D5321. 2014. Standard Test Method for Determining the Shear Strength of Soil-Geosynthetic and Geosynthetic-Geosynthetic Interfaces by Direct Shear. *ASTM Int'l*. 14(1): pp 1–11. DOI: 10.1520/D5321.

ASTM D7466. 2015. Standard Test Method for Measuring Asperity Height of Textured Geomembranes. *ASTM International*. i(Reapproved):4. DOI: 10.1520/D7466.

ASTM D7702 - 14. 2014. D7702 / D7702M - 14. Standard Guide for Considerations When Evaluating Direct Shear Results Involving Geosynthetics. *ASTM International*.: pp 1–11. DOI: 10.1520/D7702.

Aza-Gnandji, R; Kalumba, D; & Gbaguidi, V. 2019. Modelling the geomembrane – fly ash interface behaviour. *Proceedings of the 17th European Conference on Soil Mechanics and Geotechnical Engineering*, 1 - 6 September 2019, Reykjavik, Iceland.

Bacas, M; Canizal, J; & Konietzky, H. 2015a. Shear strength behaviour of geotextile/geomembrane interfaces. *Journal of Rock Mechanics & Geotech Eng*. 7(6): pp 638–645. DOI: 10.1016/j.jrmge.2015.08.001.

Bacas, M; Canizal, J; & Konietzky, H. 2015b. Frictional behaviour of three critical geosynthetic interfaces. *Journal of Geosyn Int'l*. 22(5): pp 1–11. DOI: 10.1680/gein.15.00017.

Bacas, M; Konietzky, H; Canizal, J; & Sagaseta, C. 2011. A new constitutive model for textured geomembrane/geotextile interfaces. *Journal of Geotextiles and Geomembranes*. 29(2): pp 137–148. DOI: 10.1016/j.geotexmem.2010.10.014.

Berardino, S. Di. 2017. Municipal solid wastes Landfilling and composting. *LNEG*, pp 1-70.

Bergado, D; Ramana, V; Sia, I; & Varun. 2006. Evaluation of an interface shear strength of composite liner system and stability analysis for a landfill lining system in Thailand. *Journal of Geotextiles and Geomembranes*. 24(6): pp 371–393. DOI: 10.1016/j.geotexmem.2006.04.001.

Bhatia, S.K. & Kasturi, G. 1996. *Comparison of PVC and HDPE geomembranes (interface friction performance)* A Report for PVC Geomembrane Institue, Syracuse University.

Blond, E. & Elie, G. 2006. Interface shear-strength properties of textured polyethylene geomembranes, *Proceedings of the Sea to Sky Geotechnique 2006*, Quebec, Canada, pp 898–904.

Bouazza, A. 2002. Geosynthetic clay liners. *Journal of Geotextiles and Geomembranes*. 20(1): pp 3–17. DOI: 10.1016/S0266-1144(01)00025-5.

Buthelezi, S. 2017. Comparison of shear strength properties of textured polyethylene geomembrane interfaces in landfill liner systems. MSc Dissertation submitted to the University of Cape Town, South Africa.

Byrne, R.J., Kendall, J. & Brown, S., 1992. Cause and mechanism of failure Kettleman Hills landfill B-19, phase IA. In Stability and Performance of Slopes and Embankments II (pp. 1188-1215). ASCE.

Carlson, G.. 2002. *Experimental Errors and Uncertainty,* Report Section.

Cen, W-J; Wang, H; & Sun, Y-J. 2018. Laboratory investigation of shear behavior of high-density polyethylene geomembrane interfaces. *Journal of Polymers*. 10(734): pp 1–14. DOI: 10.3390/polym10070734.

Chai, J.-C. & Saito, A. 2016. Interface Shear Strengths Between Geosynthetics and Clayey Soils. *International Journal of Geosynthetics and Ground Engineering*. 2(3): pp 1–9. DOI: 10.1007/s40891-016-0060-8.

Chandrappa, R. & Bhusan Das, D. 2012. Solid Waste Management: Principles and Practice. First ed. R. Allan, U. Förstner, & W. Salomons, Eds. New York: Springer. Available: http://www.springer.com/series/3234.

Chenggang, B. 2005. Study on the interaction behaviour of geosynthetics and soil in China. *Ningbo Institute of Technology, Zhejiang University, China*. pp 104–115. Available: ftp://75.151.72.21/eng/terratech/GRS documents/19 GeoAsia04Chenggang.pdf.

Choudhary, A.K. & Krishna, A.M. 2016. Experimental Investigation of Interface Behaviour of Different Types of Granular Soil/Geosynthetics. *International Journal of Geosynthetics and Ground Engineering*. 2(1): pp 1–11. DOI: 10.1007/s40891-016-0044-8.

Chrysovergis, T. 2012. Laboratory investigation of the effects of temperature and moisture on interface shear strength of textured geomembrane and geosynthetic clay liner. MSc Dissertation submitted to California Polytechnic State University, San Luis Obispo.

CSIR. 2000. Guidelines for Human Settlement Planning and Design Volume 2. First ed. V. 2. Pretoria: CSIR Building and Construction Technology. DOI: 10.1108/eb045383.

Datta, M; Bhowmik, R; & Mahanta, A. 2018. Stability of two landfills against sliding along interfaces of geosynthetics in baselining systems. *Proceedings of the 11th International Conference on Geosynthetics*. 16-21 September 2018, Seoul, Korea.

Dejong, J.T. 2001. Investigation of particulate-continuum interface mechanisms and their assessment through a multi-friction sleeve penetrometer attachment. PhD Dissertation submitted to Georgia Institute of Technology, USA.

Dove, J. & Frost, J.. 1999. Peak friction behaviour of smooth geomembrane-particle interfaces. *Journal of Geotech and Geoenvironmental Eng*. 125(7): pp 544–555.

Dove, J.E. & Frost, J.D. 1996. A Method for Measuring Geomembrane Surface Roughness. *Journal of Geosynthetics International*. 3(3): pp 369–392. DOI: 10.1680/gein.3.0067.

DWAF. 1998a. *Minimum Requirements for Waste Disposal By Landfill*. Second edition. C.B. Printers, Ed. Cape Town: Department of Water Affairs and Forestry Republic.

DWAF. 1998b. Minimum Requirements for the Handling, Classification and Disposal of Hazardous Waste: Waste Management Series. Second edition. Printers CTP Book, Ed. Cape Town: Department of Water Affairs and Forestry.

Eid, H.T. 2011. Shear strength of geosynthetic composite systems for design of landfill liner and cover slopes. *Journal of Geotextiles and Geomembranes*. 29(3): pp 335–344. DOI: 10.1016/j.geotexmem.2010.11.005.

Fibertex. 2017a. Fibertex Geotextiles. *Geosynthetics Engineering Course Lecture note*. First ed. V. 01. J. Oriokot, Ed. University of Cape Town. pp 1-100.

Fibertex. 2017b. Fibertex Geotextiles - Product Data Sheet. V. 01. Cape Town: Fibertex. 1–2.

Fleming, I-R; Sharma, J-S; & Jogi, M-B. 2006. Shear strength of geomembrane-soil interface under unsaturated conditions. *Journal of Geotextiles and Geomembranes*. 24(5): pp 274–284. DOI: 10.1016/j.geotexmem.2006.03.009.

Fowmes, J; Dixon, N; Fu, L; & Zaharescu, C. 2017. Rapid prototyping of geosynthetic interfaces: Investigation of peak strength using direct shear tests. *Journal of Geotextiles and Geomembranes*. 45(6): pp 674–687. DOI: 10.1016/j.geotexmem.2017.08.009.

Fox, P.J. & Stark, T.D. 2004. State-of-the-art report: GCL shear strength and its measurement. *Journal of Geosynthetics International*. 11(3): pp 141–175. DOI: 10.1680/gein.2004.11.3.141.

Fox, P.J. & Stark, T.D. 2009. State-of-the-art report: GCL shear strength and its measurement. *Journal of Geosynthetics International*. 11(3): pp 141–175. DOI: 10.1680/gein.2004.11.3.141.

Fox, P.J. & Stark, T.D. 2015. State-of-the-art report: GCL shear strength and its measurement–ten-year update. *Journal of Geosynthetics International*. 22(1): pp 141–175. DOI: 10.1680/gein.2004.11.3.141.

Fox, P.J. & Thielmann, S.S. 2014. Interface Shear Damage to a HDPE Geomembrane. II: Gravel Drainage Layer. *Journal of Geotech and Geoenvironmental Eng*. 140(8):12. DOI: 10.1061/(ASCE)GT.1943-5606.0001120.

Fox, P., Stark, T. & Swan, R. 2008. Laboratory Measurement of GCL Shear Strength. *Advances in Geosynthetic Clay Liner Technology: Journal of ASTM International*. 92-109. DOI: 10.1520/stp12200s.

Fox, P.; Rowland, M.; Scheithe, J.; Davis, K.; Supple, M.; & Crow, C. 1997. Design and Evaluation of a Large Direct Shear Machine for Geosynthetic Clay Liners. *Geotechnical Testing Journal*. 20(3): pp 279–288.

Foye, K. 2011. Armored geomembrane cover engineering. *International Journal of Environmental Research and Public Health*. 8(6): pp 2240–2264. DOI: 10.3390/ijerph8062240.

Fronti, S. 1994. Solid waste management. *Chapter 7 of Emergency Sanitation Manual*. pp 105–120.

Frost, J.. & Lee, S.. 1990. Microscale study of geomembrane-geotextile interactions. *Journal of Geosyn Int'l*. 8(6): pp 577–597.

Frost, J.; DeJong, J.; & Recalde, M. 2002. Shear failure behaviour of granular–continuum interfaces. *Journal of Engineering Fracture Mechanics*. 69: pp 2029–2048. DOI: 10.1016/S0013-7944(02)00075-9.

Frost, J; Kim, D.; & Lee, S-W. 2012. Microscale geomembrane-granular material interactions. *KSCE Journal of Civil Engineering*. 16(1): pp 79–92. DOI: 10.1007/s12205-012-1476-x.

Geocomp. 2012. *ShearTrac-III User's Manual*. Nagog Park.

Geocomp. 2018. *Large ShearTrac III -Technical Specifications*.

Giroud, J.; Darrasse, J.; & Bachus, R. 1993. Hyperbolic expression for soil-geosynthetic or geosynthetic-geosynthetic interface shear strength. *Journal of Geotextiles and Geomembranes*. 12(3): pp 275–286. DOI: 10.1016/0266-1144(93)90030-R.

Goodman, R. 1989. *Introduction to rock mechanics*. 2nd edition. V. 33. New York: John Wiley & Sons.

Greenwood, J.H. 2015. *Durability of geosynthetics*. A report by CUR Building & Infrastructure. Netherlands.

Hardie, P. 2018. Introduction to Geosynthetics in Containment applications. *Geosynthetics Engineering Course Lecture note*. 1st ed. University of Cape Town. pp 1-120.

Hebeler, G.; Frost, J.; & Myers, A. 2005. Quantifying hook and loop interaction in textured geomembrane-geotextile systems. *Journal of Geotextiles and Geomembranes*. 23(1): pp 77–105. DOI: 10.1016/j.geotexmem.2004.06.002.

Hillman, R.P. & Stark, T.D. 2001. Shear strength characteristics of PVC Geomembrane-Geosynthetic interfaces. *Journal of Geosynthetics International*. 8(2): pp 135–162. DOI: 10.1680/gein.8.0190.

Hsuan, B.Y.G. & Koerner, R.M. 1998. Antioxidant Depletion Lifetime in High Density. *Journal of Geotechnical and Geoenvironmental Engineering*. 124(6): pp 532–541.

Jeon, H. & Kim, H.K. 2018. Review of specification and regulation of geomembranes for waste landfill application. *Proceedings of the 11th International Conference on Geosynthetics*. 16-21 September 2018, Seoul, Korea.

Jianxia, S. 2012. Durability Design of Concrete Hydropower Structures. *Comprehensive Renewable Energy*. (January, 1):377–403. DOI: 10.1016/B978-0-08-087872-0.00619-3.

Jorge, Z. & Christopher, B.R. 1999. Geosynthetics. *The Handbook of Groundwater Engineering*. CRC Press LLC. pp 1 - 32.

Kalumba, D. 1998. Effect of grading and grain size on the friction characteristics of a sand/geotextile interface. MSc Dissertation submitted to the University of Cape Town, South Africa.

Karademir, T. 2011. Elevated temperature effects on interface shear behavior. PhD Dissertation submitted to Georgia Institute of Technology, USA.

Keyence. 2020. *VR-3100 Wide-area 3D measurement system sensor head*. Available: https://www.keyence.com/.

Kim, D. 2006. Multi-Scale Assessment of Geotextile- Geomembrane Interaction. PhD Dissertation submitted to Georgia Institute of Technology, USA.

Kiptoo, D., Aschrafi, J., Kalumba, D., Lehn, J., Moormann, C. & Zannoni, E. 2017. Laboratory investigation of a geosynthetic reinforced pavement under static and dynamic loading. Journal of Testing and Evaluation. 45(1):76–84. DOI: 10.1520/JTE20160170.

Koerner, R.M. 2005. *Designing With Geosynthetics*. 5th edition. New Jersey: Pearson Prentice Hall.

Koerner, R.M. & Koerner, G.R. 1999. Rationale and Background for the GRI-GM13 Specification for HDPE Geomembranes. *Proceedings of the Geosynthetics Conference '*. V. 1. (GRI White Paper). Folsom: IFAI. 385–400.

Lajevardi, S.; Shaykhi, P.; & Briancon, L. 2018. Determine geotextile-geomembrane interface frictional properties using inclined plane test. *Proceedings of the 11th International Conference on Geosynthetics*. 16-21 September 2018, Seoul, Korea.

Martinez, A. & Frost, J.D. 2017. The influence of surface roughness form on the strength of sand–structure interfaces. *Proceedings of Géotechnique Letters*. 7(1): pp 104–111. DOI: 10.1680/jgele.16.00169.

McCartney, J.; Zornberg, J.; & Swan, R. 2002. Internal and Interface Shear Strength of Geosynthetic Clay Liners (GCLs). Geotechnical Research Report submitted to the University of Colorado, USA.

McCartney, J.; Zornberg, J.; & Swan, R. 2005. Effect of Geomembrane Texturing on GCL-Geomembrane Interface Shear Strength. *Waste Containment and Remediation. ASCE Geotechnical Special Publication*. 1(142):1–11.

McCartney, J.; Zornberg, J.; & Swan, R. 2009. Analysis of a Large Database of GCL-Geomembrane Interface Shear Strength Results. *Journal of Geotechnical and Geoenvironmental Engineering*. 135(2): pp 209–223. DOI: 10.1061/(ASCE)1090-0241(2009)135.

Mitchell, K.; Seed, R.; & Seed, B. 1990. Kettleman Hills Waste Landfill Slope Failure. II: Stability Analyses. *Journal of Geotech Eng*. 116(4): pp 669–690. DOI: 10.1061/(ASCE)0733-9410(1990)116:4(669).

Mosawi, M. 2013. Effect of viscoelasticity on soil-geomembrane contact surfaces. MSc Dissertation submitted to the University of Dayton, Ohio.

Nanak, G. 2012. Reinforced Soil and Geosynthetic Engineering. *Proceedings of the One day International Workshop on Reinforced Soil and Geosynthetic Engineering*. Guru Nanak Dev Engineering College, Punjab. pp 1–30.

Orebowale, P.B. 2006. Investigating the Stability of Geosynthetic Landfill Capping Systems. PhD Dissertation submitted to Loughborough University, UK.

Oriokot, J. 2018. Introduction to Geosynthetics. *Geosynthetics Engineering Course Lecture note*, University of Cape Town. pp 1-63.

Oriokot, J., 2014. Reinforcement of pavement subgrade using granular fill and a geosynthetic layer. MSc Dissertation submitted to the University of Cape Town, South Africa.

Osano, S. 2009. Direct Shear Box and Ring Shear Test Comparison: Why Does Internal Angle of Friction Vary. *ICASTOR Journal of Engineering*. 5(2): pp 77–93.

Osswald, T.A. 2003. *Materials science of polymers for engineers*. 2nd edition. Munich: Hanser Publishers.

Prashanth, V.; Krishna, A.; & Dash, S. 2016. Pullout Tests Using Modified Direct Shear Test Setup for Measuring Soil–Geosynthetic Interaction Parameters. *International Journal of Geosynthetics and Ground Engineering*. 2(2):1–10. DOI: 10.1007/s40891-016-0050-x.

Qian, X. & Koerner, R.M. 2004. Effect of Apparent Cohesion on Translational Failure Analyses of Landfills. *Journal of Geotechnical and Geoenvironmental Engineering*. 130(1):71–80. DOI: 10.1061/(asce)1090-0241(2004)130:1(71).

Qian, X.; Koerner, R.; & Gray, D. 2003. Translational failure analysis of landfills. *Journal of Geotechnical and Geoenvironmental Engineering*. 6(129): pp 506–519.

Rawal, A. & Saraswat, H. 2011. Pore size distribution of hybrid nonwoven geotextiles. *Journal of Geotextiles and Geomembranes*. 29(3):363–367. DOI: 10.1016/j.geotexmem.2010.12.006.

Robbe-Valloire, F.; Progri, R.; & Botelho, T. 2018. Theoretical Analysis of the Influence of Asperity's Dimensions Affected by a Scale Factor on the Mixed Lubrication between Parallel Surfaces. Advances in Tribology. 2018(3702324):11. DOI: 10.1155/2018/3702324.

Romano Disposal Services. 2018. *How Much Time Does Waste Take to Decompose in a Landfill?* Available: https://romanodisposal.com/blog/how-much-time-does-waste-take-to-decompose-in-a-landfill/ [Accessed July 12 2019].

Ross, J.D. 2009. Static and dynamic shear strength of a geomembrane/geosynthetic clay liner interface. MSc Dissertation submitted to Ohio State University, USA.

Rouncivell, W. 2007. Experimental Investigation Of the Shear Strength Characteristics of a Geosynthetic Clay Liner and its Application. MSc Dissertation submitted to the University of Cape Town, South Africa. Available: thesis_ebe_2007_rouncivell_wesley.pdf.

Russell, D.; Jones, V.; & Dixon, N. 1998. Shear strength properties of geomembrane/geotextile interfaces. *Journal of Geotextiles and Geomembranes*. 16(1):45–71. DOI: 10.1016/S0266-1144(97)10022-X.

SANS 10228. 2012. *The identification and classification of dangerous goods for transport by road and rail modes*. 6th edition. Groenkloof.

Shamrock, J. & Jabulile, M. 2014. HDPE Geomembrane Specification and Performance Implications.

Shukla, S. & Yin, J. 2006. *Fundamentals of Geosynthetic Engineering*. 1st edition. V. 39. Taylor & Francis, Ed. London: Taylor & Francis Group.

Sikwanda, C.; Kalumba, D.; & Nolutshungu, L., 2019, "Comparison of Single and Multi-Interface Strengths for Geosynthetic/Geosynthetic", Proceedings of the 17th African Regional Conference: Soil Mechanics and Geotechnical Engineering (XVII ARCSMGE), Cape Town, South Africa, 6–9 October 2019, pp. 77–81.

Sikwanda, C. 2018. An Investigation of the Effects of Specimen Gripping Systems on Shear Stress at the Geosynthetic-Geosynthetic Interface. MSc Dissertation submitted to the University of Cape Town, South Africa.

Sikwanda, C.; Kalumba, D.; & Nolutshungu, L. 2018a, "An Investigation of the Effects of Specimen Gripping Systems on Shear Stress at the Geosynthetic-Geosynthetic Interface", Proceedings of Indian Geotechnical Conference: Sustainability and Geoenvironmental Engineering, Bangalore, India, 13–15 December 2018.

Sikwanda, C.; Buthelezi, S.; & Kalumba, D. 2018b, "Review of effects of poor gripping systems in geosynthetic shear strength testing", Proceedings of GeoShanghai 2018 International Conference: Ground Improvement and Geosynthetics, Shanghai, China, 27–30 May 2018, pp. 420–429.

Stark, T.D. 1999. Stability of waste containment facilities. *Proceedings of Municipal and Industrial Solid Waste Disposal Technology WasteTech Conference. 1-3 February 1999, New Orleans, Louisiana,* pp 1-23.

Stark, T.; Willamson, T.; & Eid, H. 1996. HDPE Geomembrane - Geotextile Interface Shear. *Journal of Geotech and Geoenvironmental Eng*. 122(3):9. DOI: https://doi.org/10.1061/(ASCE)0733-9410(1996)122:3(197).

Stark, T.; Niazi, F.; & Keusher, T. 2015. Strength Envelopes from Single and Multi Geosynthetic Interface Tests. *Journal of Geotechnical and Geological Engineering*. 33(5): pp 1351–1367. DOI: 10.1007/s10706-015-9906-4.

Textile Center of Excellence. 2019. *Textile Innovation Knowledge Platform*. Available: http://www.tikp.co.uk/knowledge/market-sectors/geotextiles/applications/ [Accessed July 11 2019]

Thiel, R. 2001. Peak vs. residual shear strength for landfill bottom liner stability analyses. *Proceedings of the 15th GRI Conference*. pp 40–70.

Thomas, T. 1999. *Rough surfaces*. 2nd edition. Sweden: Imperial College Press.

Triplett, E. & Fox, P. 2001. Shear Strength of HDPE Geomembrane / Geosynthetic Clay Liner Interfaces. *Journal of Geotechnical and Geoenvironmental Engineering*. 127(6): pp 543–552. Available: https://doi.org/10.1061/(ASCE)1090-0241(2001)127:6(543).

Uesugi, M. & Kishida, H. 1986. Frictional Resistance at Yield Between Dry Sand and Mild Steel. *Journal of Japanese Society of Soil Mechanics and Foundation Engineering*. 26(4):139–149. Available: https://www.jstage.jst.go.jp/article/sandf1972/26/4/26_4_139/_pdf.

United States Environmental Protection Agency. 1994. *Test Methods for Evaluating Solid Waste*. Third edition. Volume. 87. Washington.

Xuede, Q. 2008. Critical interfaces in geosynthetic multilayer liner system of a landfill. *Journal of Water Science and Engineering*. 1(4):22–35. DOI: 10.3882/j.issn.1674-2370.2008.04.003.

Yesiller, N. 2005. Core thickness and asperity height of textured geomembranes : a critical review Experimental case study. *GFR Engineering Solutions*. 23(4): pp 4–7.

Zaharescu, C.A. 2018. Wear Quantification of Textured Geomembranes using Digital Imaging Analysis. PhD Dissertation submitted to Loughborough University, UK.

Zornberg, J.G. & Christopher, B.R. 2007. Geosynthetics. *The Handbook of Groundwater Engineering*. pp 1–36.

Zornberg, J.G. & McCartney, J.S. 2009. Internal and interface shear strength of geosynthetic clay liners. *Geosynthetic Clay Liners for Waste Containment Facilities*. Book section, pp 143–168.Available:http://ceae.colorado.edu/geotech/mccartneyfiles/GCL_2009_CRC_Chapter.pdf.

APPENDICES

Table A-1: Summary of the peak and LD strength obtained from all GMB/GTX interface test

Geosynthetics Material				Normal applied stress									
				25 kPa		50 kPa		100 kPa		200 kPa		400 kPa	
GMBs	Asperity		GTX	Peak	LD	Peak	LD	Peak	LD	Peak	LD	Peak	LD
	Height	Density											
GMB-S	0	0	PP	8.9	6.4	16.5	10.2	31.9	18.1	61.6	33.3	113.3	65.2
			PET	8.8	6.2	16.3	10.1	30.9	17.9	61.1	34.6	121.5	61.3
GMB-T1	0.70	332	PP	20.7	13.9	29.5	26.6	48.3	28.7	92.3	69.4	173.1	91.1
			PET	11.3	9.3	34.3	19.4	65.1	34.8	112.9	59.3	199.7	98.9
GMB-T2	0.70	663	PP	24.0	16.3	38.3	20.1	80.6	33.0	139.8	57.5	236.2	97.3
			PET	22.0	16.4	45.6	31.3	84.5	48.9	140.6	80.0	245.9	122.8
GMB-T3	0.73	337	PP	16.5	14.9	31.6	18.5	53.7	30.3	102.0	52.6	172.0	90.3
			PET	15.6	11.3	27.9	18.1	59.3	30.3	105.0	60.9	216.0	112.0
GMB-T4	0.85	337	PP	17.3	13.2	37.9	19.8	63.5	32.6	112.8	57.2	216.3	102.7
			PET	15.5	13.8	36.6	24.5	68.2	38.9	122.9	65.0	220.7	104.5
GMB-T5	1.20	306	PP	22.5	15.1	46.8	21.4	78.6	35.9	146.0	62.9	252.8	119.7
			PET	26.4	15.0	45.9	24.1	97.9	43.5	160.3	69.1	286.7	120.6
GMB-T6	1.81	211	PP	25.5	13.9	44.2	31.9	76.4	48.3	143.9	90.9	238.1	121.9
			PET	22.6	16.6	48.0	28.7	78.5	49.1	143.1	86.2	261.1	145.1
GMB-T7	2.02	217	PP	21.3	17.0	42.7	27.9	80.8	44.4	149.0	77.6	289.1	131.6
			PET	24.5	15.2	38.6	25.6	82.2	48.5	143.7	84.9	253.0	150.0

Table A-2: Summary of GMB asperity volume effects on GMB/GTX interface friction angle

GMB	GTX	Asp. height (mm)	Asp. density (knobs per 10000mm^2)	Asp. Volume (mm^3/mm^2)	δ (°)	
					Peak	LD
GMB-S	PP	0	0	0	15.6	8.9
	PET				16.8	8.6
GMB-T1	PP	0.70	332	232	27.5	13.2
	PET				26.5	13.7
GMB-T2	PP	0.70	663	464	29.5	12.4
	PET				30.3	15.4
GMB-T3	PP	0.73	337	246	27.5	13.0
	PET				26.5	15.1
GMB-T4	PP	0.85	337	286	29.7	13.4
	PET				28.3	13.3
GMB-T5	PP	1.20	306	366	31.2	17.1
	PET				35.2	17.7
GMB-T6	PP	1.81	211	382	29.5	16.8
	PET				32.1	18.7
GMB-T7	PP	2.02	217	438	35.3	17.6
	PET				31.4	19.1

Table A-3: Recommended liner system design parameter

Property	Symbol	Units	Magnitude
Front slope angle	$\boldsymbol{\alpha}$	°	14
Back slope angle	$\boldsymbol{\beta}$	°	18.4
Solid waste unit weight	γ_{sw}	$k\ N/m^3$	10
Landfill cell subgrade angle	θ	°	1.1
Internal friction angle of solid waste	Δ_{sw}	°	33
Waste mass top width	B	m	20
Height of back slope	H	m	30

Table A-4: Typical geosynthetics interface design calculation

Interface	**Formula** (Qian *et al*., 2003; Qian & Koerner, 2004)	**Output**	**Remarks**
GMB-S/GTX-PET	For $B < \frac{H}{tan\beta}$		
	$C_A = c_a.\frac{H}{sin\beta}$	$C_A = 0$	c_a is assumed to be 0
	$W_A = 0.5.\gamma_{sw}.\frac{H^2}{tan\beta} - 0.5.\gamma_{sw}.\left[\frac{H}{tan\beta} - B\right]^2.tan\alpha$	$W_A = 7386.93$	
	$C_P = c_p\left[\left(H - \frac{H}{tan\beta} + B.tan\alpha\right) + (cos\theta.tan\alpha - sin\alpha)\right]$	$C_P = 0$	c_p is assumed to be 0
	$W_P = 0.5.\gamma_{sw}.\left[\left(\frac{H}{tan\alpha} - \frac{H}{tan\beta} + B\right)^2.\frac{tan\alpha.tan\theta}{tan\alpha - tan\theta} + \left(\frac{H}{tan\alpha} - \frac{H}{tan\beta} + B\right)^2.tan\alpha\right]$	$W_P = 3398.10$	
	$a = W_A.sin\beta.cos\theta + W_P.cos\beta.sin\theta$	$a = 2393.15$	
	$b = (W_A.tan\delta_p + W_P.tan\beta).sin\beta.sin\theta - (W_A.tan\delta_a + W_P.tan\delta_p).cos\beta.cos\theta - C_A.cos\theta - C_P.cos\beta$	$b = -3066.84$	
	$c = -\left[(W_A.cos\beta.sin\theta + W_P.sin\beta.cos\theta).tan\delta_a.tan\delta_p + C_A.sin\theta.tan\delta_p + C_P.sin\beta.tan\delta_a\right]$	$c = -109.88$	
	$FoS_{min} = \frac{-b \pm \sqrt{b^2 - 4.a.c}}{2.a}$	$FoS_{min} = 1.32$	$1.3 < 1.5 = FoS_{min}$, *not ok*

Table A-5: Changes in GMB/GTX peak and LD FoS as GMB asperity was varied

Interface	GMB	GTX	Peak		LD	
			δ (°)	FoS	δ (°)	FoS
GMB/GTX	GMB-S	PP	15.6	1.21	8.9	0.68
		PET	16.8	1.31	8.6	0.66
	GMB-T1	PP	27.5	2.27	13.2	1.02
		PET	26.5	2.17	13.7	1.06
	GMB-T2	PP	29.5	2.47	12.4	0.96
		PET	30.3	2.55	15.4	1.20
	GMB-T3	PP	27.5	2.27	13.0	1.01
		PET	26.5	2.17	15.1	1.18
	GMB-T4	PP	29.7	2.49	13.4	1.04
		PET	28.3	2.35	13.3	1.03
	GMB-T5	PP	31.2	2.64	17.1	1.34
		PET	35.2	3.08	17.7	1.39
	GMB-T6	PP	29.5	2.47	16.8	1.32
		PET	32.1	2.73	18.7	1.48
	GMB-T7	PP	35.3	3.09	17.6	1.38
		PET	31.4	2.66	19.1	1.51